EFFECTS OF CuF_2 NANO-PARTICLE INCLUSION ON MgB_2 SUPERCONDUCTOR

BY

ESAM GUNAID ABDO AL-NAHARI

A Dissertation Presented to the
DEANSHIP OF GRADUATE STUDIES

KING FAHD UNIVERSITY OF PETROLEUM & MINERALS

DHAHRAN, SAUDI ARABIA

In Partial Fulfillment of the
Requirements for the Degree of

DOCTOR OF PHILOSOPHY

In

PHYSICS

MARCH 2018

KING FAHD UNIVERSITY OF PETROLEUM & MINERALS

DHAHRAN- 31261, SAUDI ARABIA

DEANSHIP OF GRADUATE STUDIES

This thesis, written by **ESAM GUNAID ABDO AL-NAHARI** under the direction of his thesis advisor and approved by his thesis committee, has been presented and accepted by the Dean of Graduate Studies, in partial fulfillment of the requirements for the degree of **DOCTOR OF PHILOSOPHY IN PHYSICS.**

Khalil Ziq

Dr. Khalil Ali Ziq
(Advisor)

I. Nasser

Dr. Ibraheem M.A. Nasser
(Member)

Dr. Abdullah A. Al-Sunaidi
Department Chairman

Md. Shahabuddin

Dr. Mohammed Shahabuddin
(Member)

Dr. Salam A. Zummo
Dean of Graduate Studies

8/5/18

Date

A. Makki

Dr. Abdelkarim Mekki
(Member)

Ayman Sharf El-Said

Dr. Ayman Sherif El-Said
(Member)

I dedicate this dissertation with all of my love

to my parents, my family and my brothers

ACKNOWLEDGMENTS

First and foremost, thanks to Allah Almighty who gave me strength, patience and ability to accomplish this work.

I would like to express my appreciation to my thesis advisor Dr. Khalil A. Ziq for his guidance and patience through dissertation, his continuous support and his encouragement. I would like to thank the committee members Dr. Abdelkarim Mekki, Dr. Ayman Sherif El-Said, Dr. Ibraheem M.A. Nasser and Dr. Mohammed Shahabuddin for their constant support and cooperation

Thanks are due to the Chairman of the Physics Department for providing all available facilities. Particular thanks go to Mr. Mohammed Al-Saeed for analyzing our samples by XRD and XPS.

I am also grateful to all members of our superconductivity and magnetism group, we go a long way back. We had endless descussions, often stayed many long ours working on perfecting our experimental setup. M Abo Baker, M. Hamad, R. Hamad and F. Obad thank you all. To all my friends at KFUPM and elsewhere, your help and encouraged during this work shall always be cherished and remembered.

Acknowledgment is due to King Fahd University of Petroleum & minerals for supporting this work.

I also would like to thank my home institution, Al-Hodeidah University, for giving me the opportunity for completing my Ph.D. degree in KFUPM.

TABLE OF CONTENTS

LIST OF TABLES

LIST OF FIGURES

LIST OF ABBREVIATIONS

T_c : Critical temperature

H : Magnetic Field

M : Magnetization

H_c : Thermodynamic Critical Field

H_{c1} : Lower Critical Magnetic Field

H_{c2} : Upper Critical Magnetic Field

J_c : Critical Current Density

F_p : Pinning Force

λ : Penetration Depth

ξ : Coherence Length

H_p : Full Penetration Field

H_{irr} : irreversible magnetic field extracted from the pinning force curve

H_{irr}^{K} : irreversible magnetic field extracted from Kramer plot.

ABSTRACT

Full Name : [Esam Gunaid Abdo Al-Nahari]

Thesis Title : [Effects of CuF2 Nano-Particle Inclusion on MgB2 Superconductor]

Major Field : [Physics]

Date of Degree : [March 2018]

In this work, we studied the effect of CuF_2 nanoparticle inclusion on the structural, transport and magnetic properties of $MgB_2/(CuF_2)_x$ superconductor for $0 \leq x \leq 0.1$. The samples were annealed at 750ºC and 850ºC and then investigated by different techniques such as XRD, Ac- susceptibility measurement, resistivity measurement and VSM (magnetic measurement). XRD results showed a significant reduction of MgO commonly found at the grain boundaries in the MgB_2 superconductor. Moreover, CuF_2 inhibited the formation of boron oxides B_2O and B_2O_3 leading to single phase of MgB_2. The resistivity measurements confirmed that the grain connectivity is improved by CuF_2. These measurements indicate that the optimal CuF_2 concentration is close to 2%, and the optimal annealing temperature is 750ºC. The critical current density, J_c and pinning force, F_p were calculated from the hysteresis loop using Bean's Model. The optimal sample ($MgB_2/(CuF_2)_{0.02}$) has the highest critical current density (J_c) *and* the maximum pinning force (F_p) amongst all the annealed samples.

The normalized volume pinning forces have been analyzed at different temperatures and CuF_2 concentrations. Fietz-Webb scaling law procedure has been used to fit the normalized pining force and normalized field H/H_{irr}^{K} where we used Kramer's plots to obtain the irreversibility field H_{irr}^{K}. The normalization procedure revealed three different temperature ranges where pinning force curves follow universal behavior: low temperature(4-15K), intermediate temperature(20-25K) and high temperature(30-32K). The results indicate different dominant pinning mechanisms in each region; single vortex pinning, grain boundary pinning and normal point pinning for low, intermediate and high ranges of temperature mentioned, respectively.

The grain boundary pinning is found to be the dominant pinning mechanism in all the doped and undoped samples. The peak field enhances with the increase of doping level which embodies the suppression of anisotropy from clean to dirty limit.

ملخص الرسالة

الاسم الكامل: عصام جنيد عبده النهاري

عنوان الرسالة: تأثير تضمين حبيبات فلوريد النحاس النانومترية على بورايد الماغنيسيوم الفائق التوصيل

التخصص: فـــــــــيزيـــــــاء

تاريخ الدرجة العلمية: مارس 2018

نستقصي في هذه الرسالة آثار تضمين حبيبات CuF_2 النانومترية على الخصائص الهيكلية والانتقالية والمغناطيسية للموصل الفائق $(CuF_2)_x / MgB_2$ لـ $0 \le x \le 0.1$ عند تسخين العينات عند 750 و850 درجة مئوية. قمنا باستخدام تقنيات مختلفة مثل جهاز مطياف الأشعة السينية للحيود وجهاز قياس القابلية المغناطيسية المترددة ومقياس المقاومة وجهاز اهتزاز العينة المغناطيسي لأجل دراسات الخواص المختلفة للعينات. أظهرت نتائج جهاز مطياف الأشعة السينية للحيود إنخفاضا كبيراً في MgO الموجود عادة بين حبيبات الموصل الفائق MgB_2 .وعلاوة على ذلك، وجد أن CuF_2 يثبط تشكيل أكاسيد البورون B_2O و B_2O_3 وينقي MgB_2 من الشوائب وأكدت قياسات المقاومة أن CuF_2يحسن الاتصال بين حبيبات MgB_2. أشارت هذه الدراسات أن تركيز2% من CuF_2 هو التركيز الأمثل وأن درجة حرارة التسخين المثلى 750 درجة مئوية.

كما قمنا بحساب كثافة التيار الحرج J_c، وقوى التثبيت F_p باستخدام منحنى التخلف المغناطيسي مع نموذج بينز وقد وجد أن العينة المثلى $(CuF_2)_{0.02}$/ MgB_2 لديها أعلى كثافة تيار حرجة وأقصى قوى تثبيت بين كل العينات المعدة.

وقد تم تحليل ومعايرة قوى التثبيت والمجال المغناطيسي باستخدام بارمتران معايرة هما قوة التثبيت العظمى $F_{p,max}$ والمجال غير العكسي H_{irr}^{K} على التوالي عند درجات حرارة مختلفة وتركيزات متنوعة من CuF_2 وقد تم استخدام إجراءات قانون فيتز- ويب لمواءمة كل من قوى التثبيت والمجال المغناطيسي التي اظهرت وجود ثلاثة انواع مختلفة من مراكز قوى التثبيت في ثلاثة نطاقات مختلفة من درجات الحرارة: درجة حرارة منخفضة(4-15) كلفن، ودرجة الحرارة المتوسطة (20-25) كلفن، ودرجة حرارة عالية (30-32) كلفن.

كما أظهرت نتائج الموائمة أن التعزيز السائد لمراكز قوى التثبيت تم من خلال عيوب حدود حبيبات السطوح في كل العينات المشوبة والنقية وأن ذروة المجال تعززت مع زيادة مستوى الإشابة في العينات.

CHAPTER 1

INTRODUCTION

In 1911, the Dutch physicist H. Kamerlingh Onnes discovered the superconductivity in a mercury sample while investigating the resistance of metals at a low temperature. He observed that the resistance of the mercury sample dropped abruptly to zero near 4K.

He called this unexpected phenomenon ‘superconductivity’; the temperature at which this the resistance vanishes is called the critical temperature T_c. The materials are known as superconductors.

Later on, superconductivity was discovered in many elements such as Ti, Al, Sn, etc. Surprisingly, the noble conductors; Cu, Ag, Pt and Au, did not show any signs of superconductivity down to very low temperatures.

In 1933, W. Meissner and R. Ochsenfeld studied an effect of the magnetic field on Lead (Pb) element. They cooled down Lead below its critical temperature and then applied magnetic fields. They found that Pb completely expelled weak magnetic field from its interior whereas the strong magnetic fields destroyed superconductivity and Pb became normal conductor below Tc.

The Meissner-Ochsenfeld effect cannot be interpreted by Maxwell’s equations. After two years from the discovery this effect H. and F. London offered an electrodynamics equation of the superconductor which explained the Meissner-Ochsenfeld effect. The London brothers concluded that the applied magnetic field H penetrates the superconductor surface for very small distance due to a “super-current” circulating the surface and screens the applied magnetic field from the interior of the superconductor. The penetration distance is denoted by the penetration depth λ_L .The applied magnetic field decays exponentially during this length and thus no magnetic field is inside the superconductor. The London equation yield that the penetration depth λ_L depends on the density of the superconducting electrons (n_s) as shown in the following equation:

$$\lambda_L = \left(\frac{mc^2}{4\pi\, n_s e^2}\right)^{1/2}$$

where m, e and c are the electron mass, charge, and the speed of light respectively.

According to this equation the magnetic field can fully penetrate the superconductor when its superconducting state vanishes at the transition temperature Tc where the all Cooper pairs separate into single electrons ($n_s = 0$)..

In addition to the penetration depth λ_L parameter there is another parameter has been introduced by Pippard in 1950; the coherence length (ξ). This length has been shown by the BCS theory to represent the effective distance between the Cooper pairs[1].

In 1950 Ginsburg-Landau (GL) introduced a treatment based on the shortcomes of the London theory taking in account the quantum effects. The GL theory described the the superconducting electron density n_s by a wave function ψ as an order parameter, given as:

$$n_s = |\psi|^2$$

The theory considered that the superconducting transition (without an applied magnetic field) is a second order transition in which both the free energy and its first derivative as functions of temperature are continuous.

The new theory introduced the dimensionless parameter κ $\left(\kappa = \frac{\lambda}{\xi}\right)$which is known as G-L parameter which is used to distinguish type I and type II superconductor; namely:

$$\kappa < \frac{1}{\sqrt{2}} \quad and \quad \kappa > \frac{1}{\sqrt{2}}$$

for types I & II respectively. However this theory has some weakness which was treated later by BCS theory of superconductivity[2].

In 1957, Abrikosov described type II superconductor by the solution of G-L equation of $\kappa > \frac{1}{\sqrt{2}}$ and showed that this type of superconductor possesses properties that differ from type I. In this type, the superconducting state reduces gradually with increasing the magnetic field starting from a point represents a lower critical field H_{c1} until vanishes completely at an upper critical field H_{c2}. Whereas in type-I; superconductivity vanishes abruptly at a certain critical magnetic field H_c and become normal as shown in Fig. 1.1.

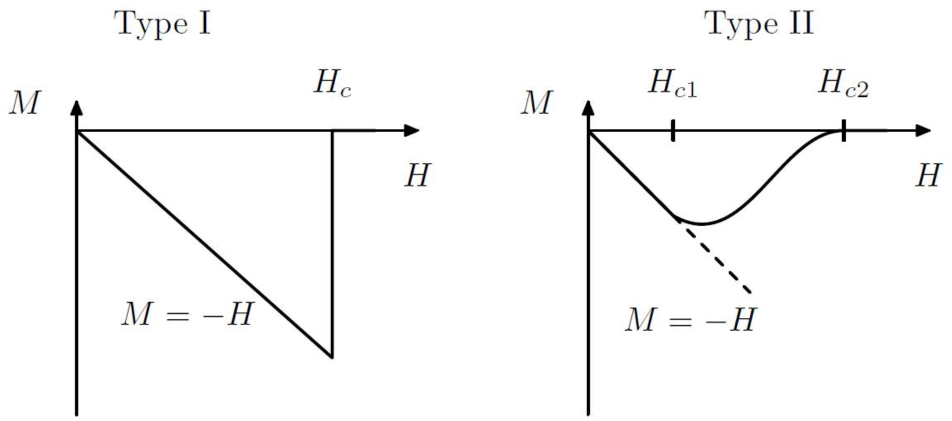

Fig. 1.1 Magnetization (M) vs. magnetic field (H) applied in superconductors, type I and type II

In type II superconductors; when the applied magnetic field value is between H_{c1} and H_{c2}; is in a mixed state of normal and superconducting states (vortex state) [3].

1.1 BCS theory

In 1957 John Bardeen, Leon Cooper, and John Robert Schrieffer published their BCS theory of superconductivity that successfully explained why the material resistance vanishes when the material is cooled below the critical temperatures.

The BCS theory is based on the condensation of the electrons in one quantum ground state. The electrons are coherent in pairs such that the momentum and spin of each pair is equal to zero and all pairs have the same energy level. Electron pairs carry the current in the superconducting state. The BCS proposed that the lattice vibrations (phonons) are directly responsible for the formation of the electron pairs. When the electron passes through the lattice, the positive ions interact attractively toward the electron and accumulate about its path as shown in Fig. 1.2

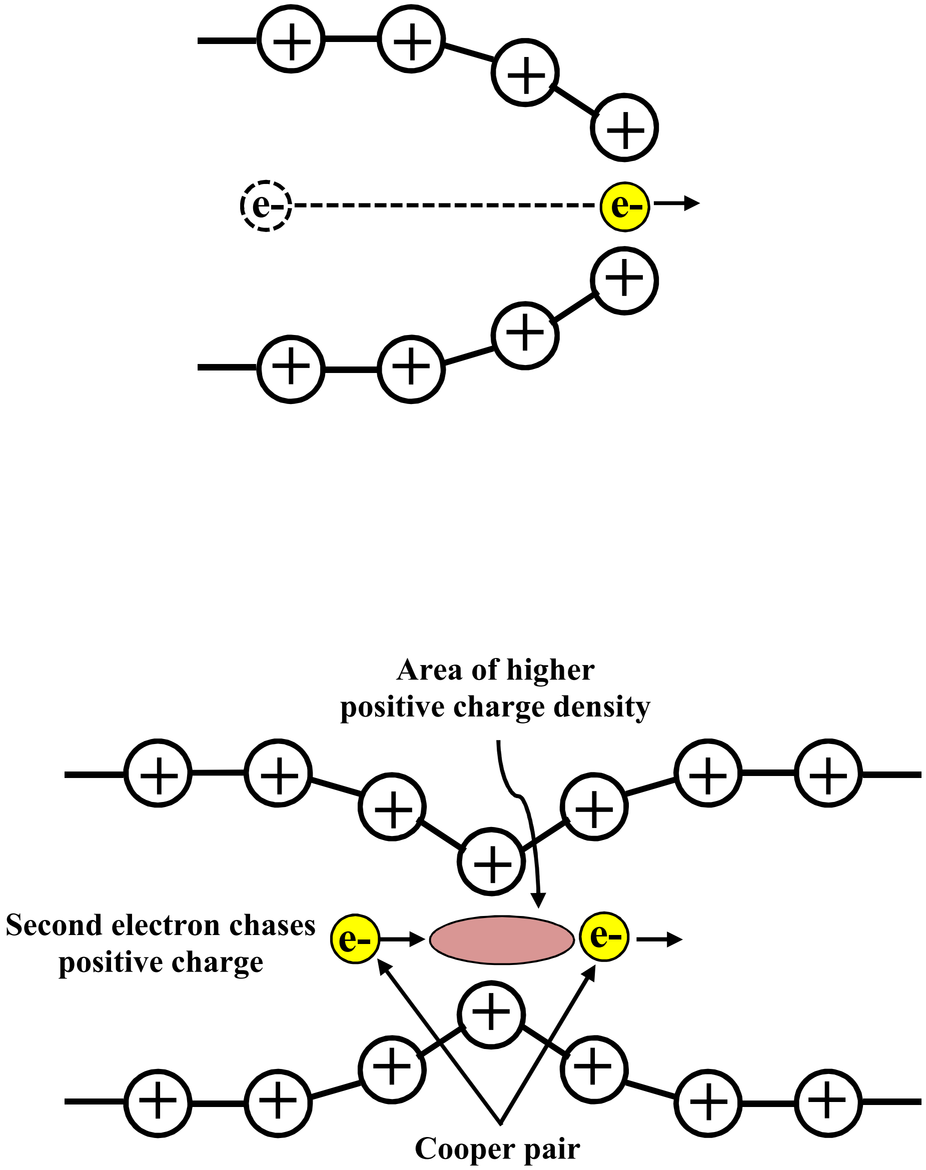

Fig. 1.2 Cooper pair formation [77]

The collective ions attract another electron close to the first electron. The distance between two electrons reduces effectively and forms electrons coupling (pairs) before returning ions to their normal positions in the lattice. Once the electron pair pass the region, the positive ions go back to their original positions due to the repulsive force among these ions. The two electrons are known as "Cooper pair ". These pairs are not permanently pined together but, they break and reform continuously and constantly.

A Cooper pair travels through the crystal lattice. Oscillating lattice makes the Cooper electron pair moves through the lattice without collisions with atoms or the other electrons.

The material remains in the superconducting state as long as it is maintained below the critical temperature Tc. The BCS theory also provided a connection between two important superconducting properties; the transition temperature Tc and the energy ga p Eg;

$$\mathrm{Eg} \approx 3.528 k_B T_c \ (1)$$

Where k_B is the Boltzmann’s constant[2-3].

1.2 Mixed state in type II superconductor

The mixed state appears when the external magnetic field H which exceeds H_{c1} starts partly penetrating the superconductor sample. The threaded regions become normal state regions (normal cores) surrounding by superconducting state. Thus, because of the field threading, currents arise in the superconducting regions and circulate around the normal cores forming vortices known as (Abrikosov vortices) as in Fig. 1.3[4].

Fig. 1.4 shows the structure of the vortices in the superconductor under the applied magnetic field H. The superconducting electrons density is zero at the vortex center whereas the density increases gradually moving away from the center to the edge of the vortex. The radius of the vortex core equals the coherence length ξ. As it can be seen that the applied magnetic field can go into the interior of the superconductor for a certain distance equals the penetration depth λ_L then the magnetic field decays by the screening currents of the vortex that generate an opposite magnetic field[5].

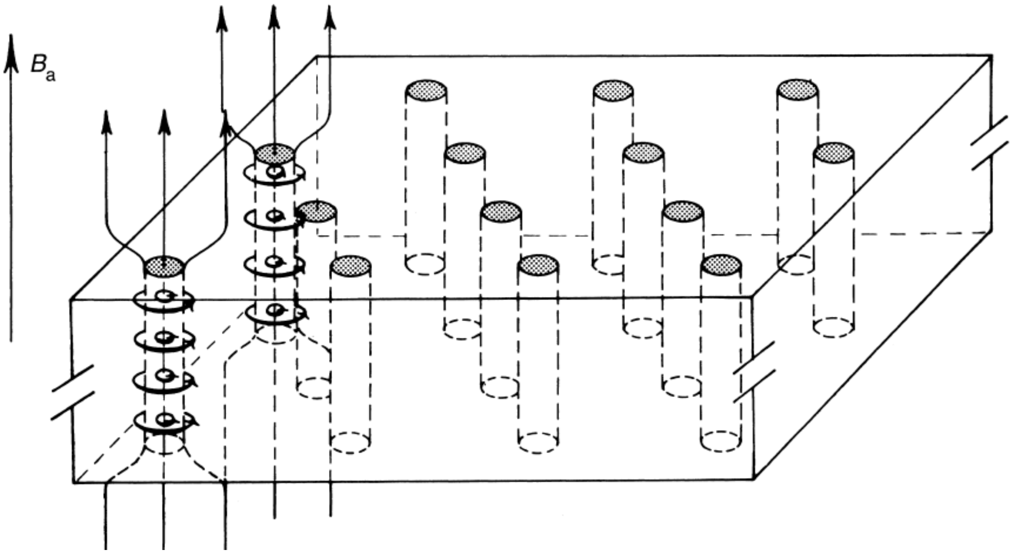

Fig. 1.3 Abrikosov vortices in type II superconductor

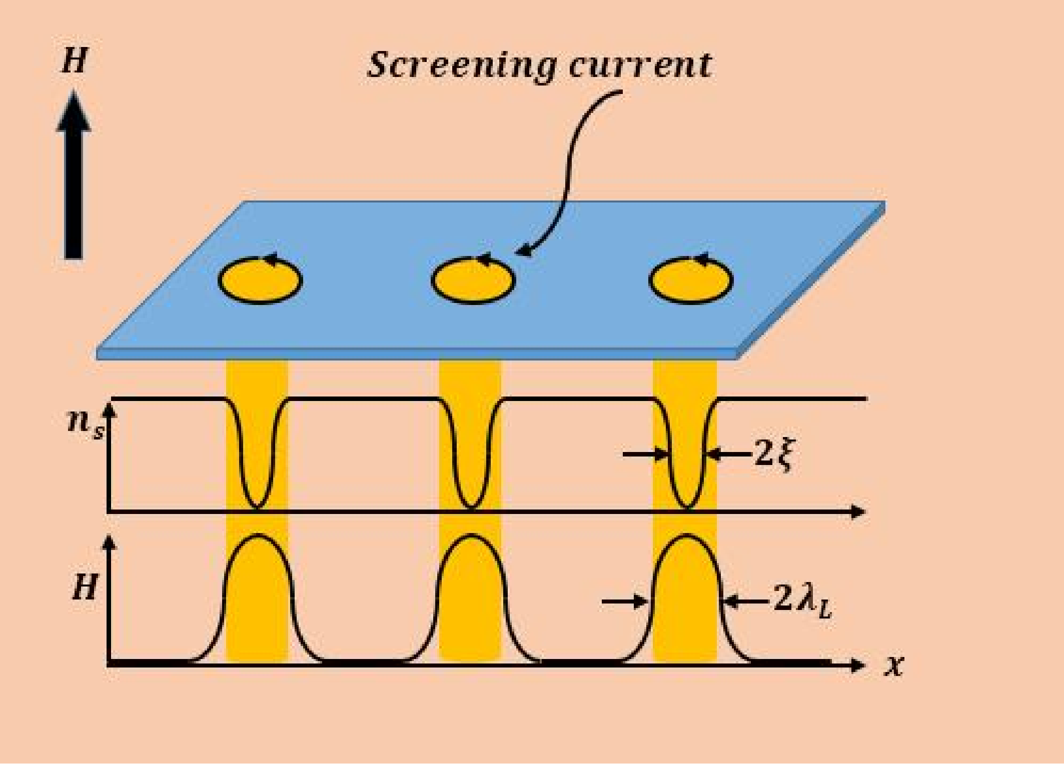

Fig. 1.4 The vortex structure

Forming the vortices are necessary for minimizing the free energy of the type II superconductor and thus the superconductor allows the magnetic field to thread its interior producing a large number of vortices. The vortices are distributed in the superconductor and parallel to the applied magnetic field in a triangular lattice form. This arrangement is as result of the lowest free energy of the superconductor. The surface boundary area of vortices is maximum if their volume is very small such that the ratio of the surface area to volume of the superconductor is high. The magnetic field flux density is maximum at the normal cores center while it decreases to a small value away from the center. The magnetic field flux density then becomes zero at distance above the penetration depth λ_L. The currents from the all vortices form the total current that circulates in the perimeter of the superconductor sample.

Abrikosov prediction was verified using neutron diffraction and real space images of the mixed state was obtained by Essmann and Trauble using a decoration technique as shown in Fig. 1.5

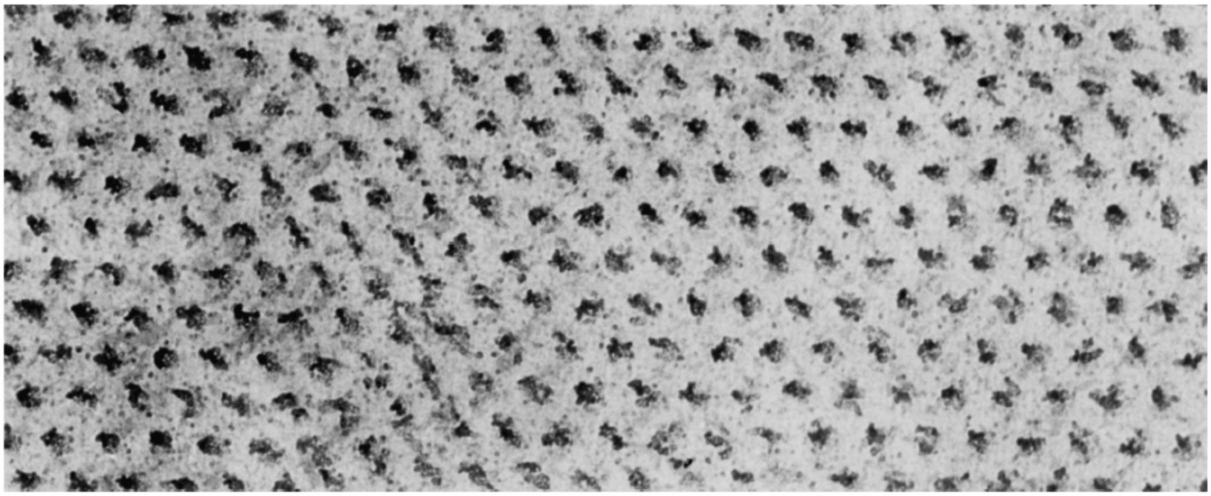

Fig. 1.5 Confirmation for Abrikosov vortices [9]

1.3 Irreversible Magnetization

An ideal (defects free) Type-II superconductor exhibits a perfect reversible magnetization the increasing and the decreasing magnetization curves are the same. However, real superconductors (with defects and pinning centers) have an irreversible magnetization where the magnetization curves versus the increasing and decreasing field have certain width. The presence of these centers hinders the reversible motion of the vortices as shown Fig. 1.6. Magnetization curve 1 for increasing the applied magnetic field starts from zero until almost H_{c2} whereas the magnetization curve 2 of decreasing the applied magnetic field is shifted above curve 1. At $H=0$; the magnetization has non zero value M_r which known as the remnant magnetization due to the trapped flux inside the superconductor.

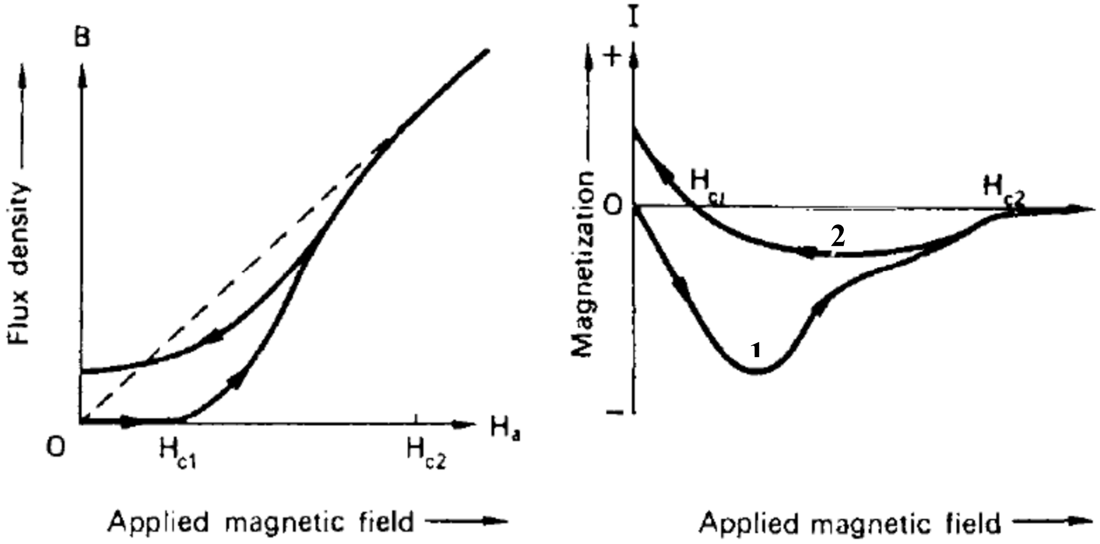

Fig. 1.6 Irreversible magnetization of Type II superconductor

The remnant magnetization is produced by the trapped flux and is due to pinning the normal cores in the mixed state by imperfections such as dislocations, defects and chemical impurities. The imperfection dimensions are larger than the coherence length of normal cores. The hysteresis loop is used to obtain various irreversible properties of the superconductor such as the irreversible magnetic field, H_{irr}, the critical current density, J_c and pinning forces, F_p [6].

The maximum current that can pass through a superconductor before breaking down the superconducting state is known as the critical current. The critical current density J_c behaves in a similar manner as the critical magnetic field strength H_c , both depend on the temperature and vanish at the transition temperature T_c[6].

1.4 MgB_2 Superconductor

Research in type II superconductor continues to include many compounds and fabricates new materials which have the superconducting properties such as Cu-based, Fe-based and MgB_2 superconductors[7- 9]. MgB_2 is a known material since 1950's, but the discovery of its superconducting behavior was found late in 2001 [10] at a remarkably high critical temperature close to 40K. The discovery revived an interest in possible applications of these materials at elevated temperatures using closed cycle or pulsed tube refrigerators that do not need liquid Helium to operate [11-13].

Since the discovery of superconductivity at 39K in MgB_2 [14], major efforts have been devoted towards understanding basic superconducting and normal state properties of this binary inter-metallic compound. However, the substitution chemistry in MgB_2 has proven not to be so simple. Limited substitution on either the Mg or B sites has been achieved for only a few elements-for examples, Al on the Mg site or C on the B site. Chemical substitution has been found to affect various superconducting and normal state properties of MgB_2 material.

MgB_2 has a hexagonal structure that is like AlB2 prototype crystal structure with a p6/mmm space group. The crystal structure is shown in Fig. 1.7

The boron atoms localize as a hexagonal lattice structure and the Mg atoms occupy the centers for this hexagonal structure. The lattice parameters of MgB_2 structure are a = 0.3084 nm and c = 0.3524 nm [9], [15-16].

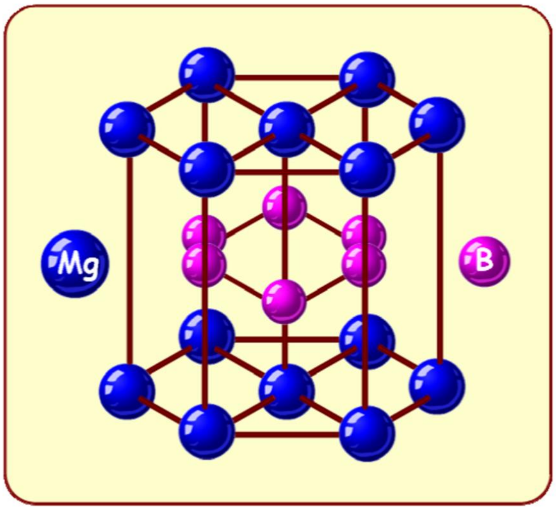

Fig. 1.7 MgB2 Crystal structure

MgB_2 has many attracting properties that made it one of the best candidates for possible applications; its low cost, abundance and the simple hexagonal structure, high T_c, large coherence lengths ξ, high critical current densities and fields and simplicity of preparations. MgB_2 has been synthesized in different forms for example; bulk, single crystals, thin films, tapes and wires [17]

In addition to that, superconducting properties such as the pinning force (F_p), the critical current density (J_c), the critical field (H_c), and irreversibility field (H_{irr}) can be enhanced using various methods and techniques.

MgB_2 has high transport critical current densities at low temperatures that can be controlled by many factors such as fabrication methods, heat treatment process. In a ddition to this the grain boundaries of MgB_2 create weak links and therefore the connectivity and J_c might be affected by these boundaries. In order to improve J_c properties, many experimental procedures, like chemical doping, irradiation, magnetic field annealing, and ball milling methods have been utilized[18].

The critical field is an important property defined in a type II superconductor. It is considered as phase boundary between the superconducting and normal states.

The upper critical field H_{c2}, lower critical field H_{c1}, and irreversibility field H_{irr} are important parameters to characterize the superconductivity. For many potential applications, it is desired to enhance all critical fields in these materials, H_{c1}, H_{c2} and H_{irr} [19]. Typical values of these fields are: $H_{c1} \sim 50$ mT, $H_{c2} \sim 15\text{-}20$T and $H_{irr} \sim 6\text{-}12$T [20–24]. Low values of the irreversibility field mean that J_c will degrade rapidly at high fields leading limitation in the temperature and field ranges.

1.5 Doping of MgB_2 Superconductor

Doping process is a method for enhancing weak grain boundary effects of MgB_2 which in turn will reflect positively on vortex pinning centers, the critical current density J_c and the upper critical field H_{c2}. Many elements, such as Ti, Al, Mn, Cu, Sc, Ag, C, Zr, Mn ,Y ,etc. have been used in an effort to improve several properties of MgB_2 by their substitution into Mg or B atoms sites. In addition to these elements, several compounds have also been used as dopants or inclusions as nano-sized materials in MgB_2, such as SiC, Y_2O_3, TiO_2, SiO_2, ZrB_2, etc[2],[25]. Nanomaterial inclusion has occupied a distinct effect in enhancement of MgB_2 properties.

CHAPTER 2

LITERATURE REVIEW

2.1 MgB_2 Synthesis

Due to unique MgB_2 properties and its important practical applications most researches have interested with preparing MgB_2 in a high purity using optimal conditions. However, its synthesis encounters two major issues; the first is attributed to the low melting point of magnesium Mg (~ 651˚C) and the high melting point of boron B (~2076 ˚C). Therefore, during synthesis of MgB_2 some Mg will evaporate and be lost from MgB_2 matrix, leading to the presence of secondary phases. A reasonable excess of Mg added to the starting materials is enough for compensatation of the lost Mg and reduction of the secondary phases.[26-27].

The second issue is ascribed to fact that Mg interacts highly with oxygen forming MgO. Magnesium oxide often surround the grain boundaries, in small amount it helps producing grain boundary pinning centers but may lead an increase in the normal state resistance and may completely isolate the superconducting grains from each other. Magnesium oxide (MgO) may also reduce the MgB_2 superconducting volume fraction.

For removal or reduction of MgO from MgB_2 samples, all Mg amount has to be reacted with B. Several practical methods have been adopted in this regard such as the wrapping the sample with a metal foil such as Ta and sealing in a metallic tube such as Fe, Ta or Nb etc and sintering in an argon gas environment and high temperature [26].

Another problem in MgB_2, occurred when exposed to air for 8-10 hours, it interacts with moisture forming complete insulating layers [28] and gradually degrade the superconducting state of MgB_2.

Sintering conditions of MgB_2 have been extensively studied, J. Ishiwata et al, studied the effect of sintering time and the optimal synthesis condition in MgB_2. They found that the sintering time enhanced the critical current density (J_c) of the bulk MgB_2 superconductor. Samples were prepared from Mg and B powders and each mixture was pressed, warped with Ta sheet, sintered at 775°C for 3hours into an argon gas environment and cooled down to room temperature. The samples were re-sintered at 660°C for 24, 45, 72 and100 hours. X-ray diffraction results exhibited a single phase and homogenous samples. The magnetization measurements showed a sharp drop at temperature ~ 37 K. The re-sintering time at 660°C improved the critical current density (J_c) of samples. Porosities or cracks were effectively absent, these cracks may reduce the current density of the superconducting regions [29].

A. Berenov and his team synthesized pure and doped MgB_2 in two sets: in the first powders were mixed according to their stoichiometry and pressed as pellets. Each pellet was covered with a mixture of the powder from which was prepared and warped in Ta foil. The pellet with extra Mg rods were put together into a tubular oven in a 1% of H_2/N_2 environment. Finally, the samples were annealed at 900°C for 15 min

The second set was formed from the Mg, B, and Al powders. The powders were pressed as capsules. Some Mg turnings were added to the capsules, and all were wrapped with Ta sheet then placed into a tube furnace for annealing at 900°C for one hour under a high pure Ar flow. The sample was cooled to 500°C by 0.5°C/min and then cooled to room temperature. XRD results showed Mg and MgO impurities within MgB_2. Very little amount MgO was observed in all the samples[30].

M Mustapić and co-workers studied “Enhancing superconducting properties of MgB_2 pellets by an addition of amorphous magnetic Ni-Co-B nanoparticles”. Synthesized MgB_2 samples showed sizable improvement in the critical current density (J_c) especially at high magnetic fields. The samples were prepared with different Ni-Co-B nanoparticles concentrations using the solid-state reaction method. The samples were put into iron tubes, then annealed at 650, 770, 850 and 950 °C for 30 min in Ar gas environment and cooled down to room temperature. Moreover, the optimal temperature for obtaining the maximum J_c was 850 °C. XRD patterns showed a minor amount of MgO in all prepared samples. The results obtained from samples showed a smaller grain size (~10 nm) for samples annealed at 650 °C comparing with samples annealed at 850°C[31].

Wang et al. reported the influence of citric acid on the critical current density J_c and the upper critical field H_{c2} in MgB_2 superconductor. They mixed Mg and B powders with 10% wt of the citric acid. The mixture was ground, pressed and annealed at different temperatures (650, 750, 850 and 950ºC) for half of an hour with heating rate of 5ºC/ min in a high pure Argon gas. The XRD results showed that the dominant phase was MgB_2 with very small amount of MgO. They also observed a reduction in grain size with increasing annealing temperature. The citric acid addition had good effects for decreasing the reduction in grain size leads to an improvement in J_c and the irreversible magnetic field (H_{irr}). The improvement in H_{irr} and H_{c2} may be caused by the C-atoms substituting B atoms into the MgB_2 lattice. As it was observed that T_c decreased with the addition of the citric acid and higher annealing temperature T_c[32].

Fabrication of MgB_2 at low temperaures have been tried at 450, 500, 550ºC for 5 days, 2 days and 16 hours then quenched to room temperature. XRD analysis showed a single phase of MgB_2 obtained for samples at annealed at 550ºC. MgO and Mg were found in samples annealed at 500ºC. No superconducting MgB2 phases were obtained in the samples annealed at 450ºC. The susceptibility measurements exhibited a high magnetization with very sharp drop at T_c for annealed samples at 550ºC compared to annealed samples at 500ºC whereas annealed samples at 450ºC did not show any superconducting behavoir[33].

Gupta and Sahni reported the synthesy of two MgB_2 samples by the solid state reaction with different starting materials. The first sample was prepared from Mg and B powders whereas the other was syntheized from Mg flakes and B powder. Both samples were pelletized then warpped by a tantalum foil contains Mg flakes. The pellets were annealed in an environment of a pure Ar gas for 2 hours at 650ºC and 4 hours at750ºC followed by 950ºC for 2 hours. Finally, the samples were quenched using liquid N_2. Characterization of the samples was achieved by XRD and XPS techniques. XRD results showed that the first sample had a XRD pattern of MgB_2 with unreacted B where a small amount of Mg was lost due to the high evaporation of Mg at 650ºC. The second sample was better than the first sample where the XRD pattern just indicated MgB_2 phase. There was small amount of Mg losses. They noted that Mg powder melts and evaporates faster than Mg flakes due to increasing the surface to the volume ratio in the powdered samples leading to more Mg losses. Thus, Mg flakes should find an enough time to diffuse into B forming a single phase of MgB_2.

Resistivity measurements showed the onset transition temperature at 36 K for the first sample whereas the second sample showed two onset transition temperatures at temperatures ~39.5 K and~36K. The transition width of the second sample was wider due to the presence of more than one phase. The critical current density J_c was higher in the second sample especially. XPS results showed an influence of the moisture on MgB_2 superconducting properties and morphology, structure and chemical changes. These samples were put into deionized water for different times (up to 72 h) and then dried at~28°C and relative humidity >70%. The resistance of exposed samples rose up and T_c remained ~ 39.7 K, but the transition was wider and with a long tail. XPS results revealed that B 1s spectrum has two peaks belong to MgB_2 and B_2O_3. The MgB_2 amount decreased after exposing to the moisture for B_2O_3. Similarly, Mg 2p the amount of Mg reduced for carbonate or hydroxide under the moisture effect. Both O_2 and C contributed to formation of MgO, B_2O_3, $MgCO_3$ and Mg $(OH)_2$ according to the following equations [28]:

$$MgB_2 + 2H_2O \rightarrow Mg(OH)_2 + 2B + H_2$$

$$Mg(OH)_2 + CO_2 \rightarrow MgCO_3 + H_2O$$

$$4B + 3O_2 \rightarrow 2B_2O_3$$

Singh et al studied the of MgO impurity on the superconducting properties of MgB_2". Two bulk MgB_2 samples were synthesized by the solid-state route. One was prepared in the ambient atmosphere whereas the second was produced in a glove box saturated by Ar gas. Both the samples were formed as pellets, sealed under vacuum, annealed at 750°C for time of 2.5 h and left to be cooled normally to room temperature.

XRD characterization proved that MgO reduced significantly (7.3% of MgO) in the second sample if compared to the first sample (39.6% of MgO). As that Dc magnetization measurement also exhibited a wide transition for the first sample while the second appeared very sharp transition. The wide transition indicated an existence of several phases while the sharp transition indicated a single phase. MgO layers reduce the volume fraction of the superconducting regions and the grains connectivity due to MgO layers isolated grains then the resistance of MgB_2 increased[34].

Zongqing Ma and Yongchang Liu reported the mechanism of sintering which affects the properties of MgB_2 as superconductor. Using Differential Thermal Analysis (DTA) they found that the formation of MgB_2 phase starts at above 550ºC and continues until 750ºC with heating rates 20ºC min^{-1} or 5ºC min^{-1}. Fig. 2.1 shows the exothermic peak located at temperature below 650ºC where the melting point of Mg is.

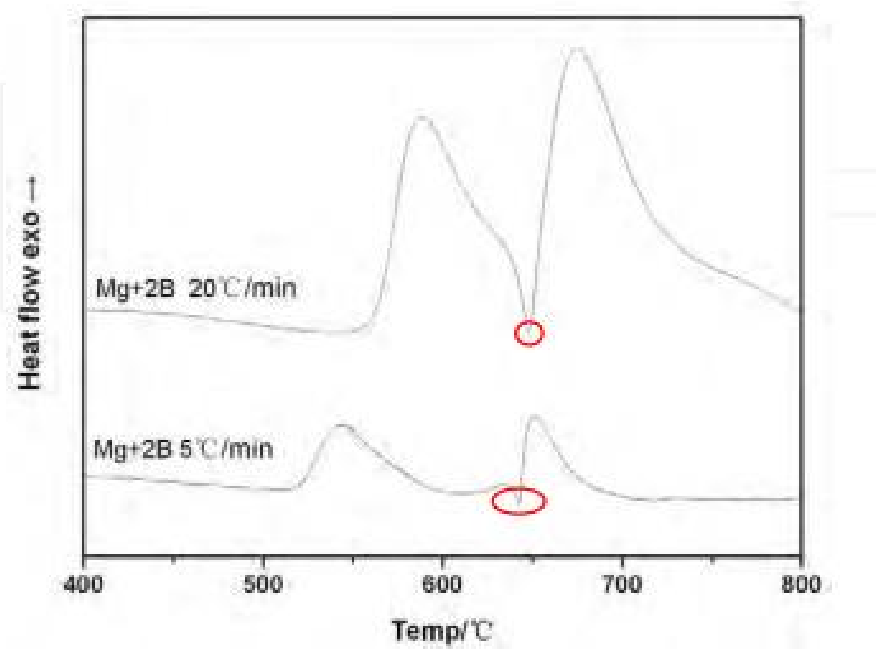

Fig. 2.1 Differential Thermal Analysis (DTA) for the synthesis

The formation of MgB_2 starts at 550ºC by the solid-solid interaction between Mg and B as shown Fig. 2.2. At 650ºC, the solid-liquid interaction starts where Mg melts and a little amount of MgB_2 forms by the diffusion of Mg into B sites producing a single phase of MgB_2. The complete diffusion is followed by the liquid precipitation and grain growth shown in Fig. 2.3. Small grains of MgB_2 are more soluble into the liquid phase than large grains and then precipitate on the large grains of MgB_2 giving rise to increasing the growth of the grains.

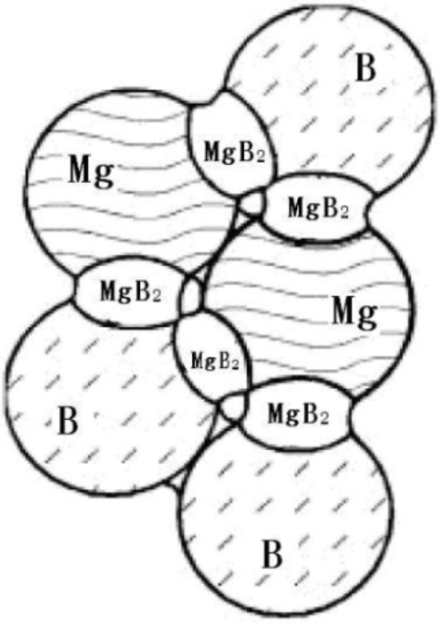

Fig. 2.2 Solid - solid interaction between Mg and B elements

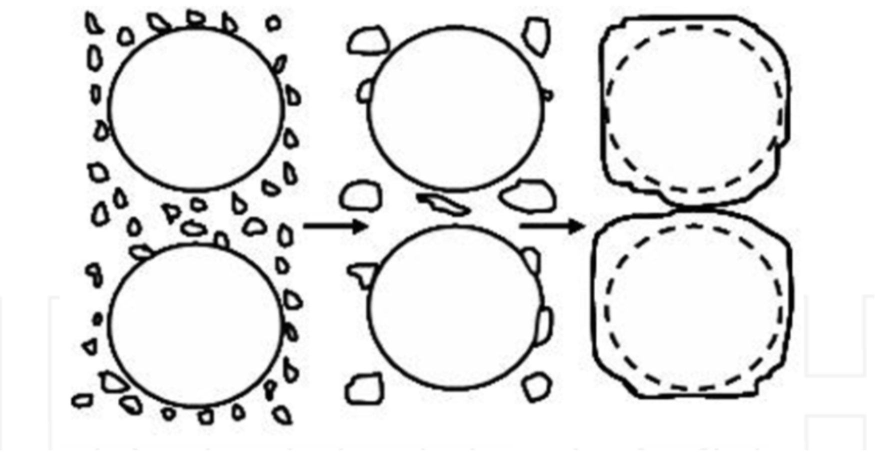

Fig. 2.3 The liquid precipitation and grain growth

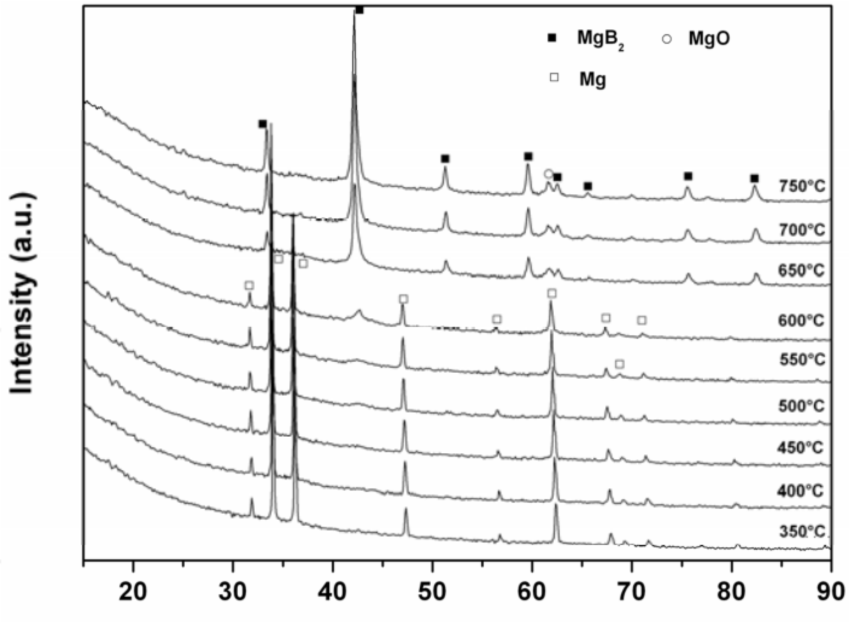

Fig. 2.4 XRD patterns shows the sintering temperatures at which MgB_2 forms.

XRD results confirmed the previous three stages as it is shown in Fig. 2.4. At temperature is less than 650°C Mg is available with MgB_2 phase due to an incomplete interaction Mg with B. Also, the intensity of MgB_2 peaks are very low comparing with the intensity of MgB_2 peaks at higher temperatures above 650°C. The essential problem with high temperature is the MgO formation. MgO has a negative influence om MgB_2 phase where it forms insulator layers between and on MgB_2 grains leading destroy of superconducting and transport MgB_2 properties. The standing challenge is how to remove or at least reduce the MgO phase during synthesis of MgB_2 phase. New studies tried to synthesize MgB_2 at low temperature for reducing or removing MgO by increasing the sintering time for long time such as 16 hours and 240 hours for 550ºC and 600ºC respectively. This method produces a pure and dense MgB_2 and improves the connectivity among MgB_2 grains and reduces MgO phase.

A very new method includes two stages of sintering method has been used by Maeda et al [35].The first stage is sintering at high-temperature (1100 °C) for a short time followed by the next stage which requires reducing sintering temperature to low temperature. This route produces unique small grains with a high connectivity of the MgB_2 phase. The critical current density J_c is higher than the critical current density J_c produced by the single stage method. But this two stages way cannot be applied for fabrication of MgB_2 wires.

Hishinuma et al [36] reported that a very small additive of Cu to MgB_2 is enough to reduce the MgO ratio within MgB_2. They thought that Mg-Cu liquid forms initially through a eutectic interaction and the oxidization of Mg drops dramatically

B. B. Sinha and his team in their work reported the efficient role of the excess magnesium in formation of MgB_2 superconductor. This role is important for several reasons. First; reducing loss of Mg though the fabrication process and keeping MgB_2 stoichiometry. Second; improving the connectivity and decreasing the insulation layers between grains and enhances the critical current density. They prepared pelletized MgB_2 samples with stoichiometry as follows M1 (1:2), M2 (1:1) and M3 (1.5:1) via the solid-state reaction. Then the samples were covered with extra Mg, sealed into a stainless-steel tube of ~30 cm with a pure environment of Ar gas and inserted into a furnace at 900ºC for 3 hours. XRD analysis exhibited the main phase for MgB_2 followed by Mg phase and little traces of MgO phases in all samples. It was also noticed that extra Mg increases the intensity of MgB_2 and MgO peaks.

The electrical transport measurements exhibited a very sharp transition in M1 sample whereas the transition became wider in M2 and M3 due to Mg and MgO phases. Transition temperature for M1 did not decrease because Mg does not infiltrate into MgB_2, but it localizes at grain boundaries. For M2 and M3, Mg penetrated MgB_2 grains giving rise to decrease of the transition temperature. The solubility of Mg into MgB_2 stopped at certain value and the crystal structure of M1 was not affect by the addition of extra Mg. The dc susceptibility measurements showed a sharp transition for M1 and M3. Transition temperature decreased for M3 to 35.5 K. This decrease is attributed to excess Mg. It was noticed that the irreversibility field H_{irr} increases in M3 sample indicating Mg excess played a significant role in enhancing H_{irr} and the critical current density[27].

D.G. Hinks et al. investigated the non-stoichiometry which may occur in Mg_xB_2 where x represented different concentrations of Mg. They produced four samples of MgB_2 at

850°C for different annealing time (0-8 hours). They found by XRD technique that MgB_4 phase can be found in samples which have $x<1$ while Mg was found in samples which have $x>1$. When $x=1$ the MgB_2 phase is dominant. The increase of annealing time helped in minimizing MgB_4 phase, and Mg phase appeared at more than 2 hours. It appears that 2 hours annealing is an optimal for synthesizing MgB_2 at 850ºC. The magnetic ac susceptibility measurements showed that the transition temperature is larger for the sample annealed for two hours [37].

2.2 Doping Process

There are limited number of elements that can be incorporated in the structure of MgB_2. Cava et al. report that the modification in the structural MgB_2 properties by the chemical substitution is difficult. For successful MgB_2 modification, the chemical substitution should be compatible with the chemistry of MgB_2. All substitutions were not successful except three; Al, C and Mn[38].

Zhao et al.[39] synthesized Ti-doped MgB_2 samples by solid-state reaction at an ambient pressure with different concentrations of doping. The J_c of the samples had remarkably changes with different concentrations of Ti. In addition, some fine particles (with sizes from 10 to 100 nm) are distributed by Ti doping into the MgB_2 matrix may play an important role in a flux pinning enhancement.

Mudgel and his team, [40] synthesized MgB_2 doped with nano-carbon ($MgB_{2-x}C_x$). A set of superconductivity parameters such as transition temperature T_c, upper critical field H_c, critical current density J_c, irreversibility field H_{irr} and flux pinning F_p have been studied with increasing doping up to x = 0.20. Carbon has been found to substitute boron atoms in the structure which lead to improved H_{irr} and J_c. However, T_c showed a continuous decrease with increasing carbon contents. Increase in the irreversibility field values H_{irr} to about 11.0 T and 13.4 T at x = 0.08 for 5 and 10K has been achieved respectively. The critical current density (J_c) of the nano-carbon-doped sample (x = 0.08) rose up by a factor of 24 at 10 K and 6 T field.

C. Cheng and Y. Zhao[41] prepared $Mg_{1-x}(Ho_2O_3)_xB_2$ by solid state reaction and found that very little effects on flux pinning behavior, the crystal structure, T_c, and H_{c2}. However; J_c and H_{irr} have been significantly enhanced.

H.L. Xu et al.[42] synthesized nano-Al powder doped $Mg_{1-x}Al_xB_2$ samples(x = 0.00, 0.01, 0.02, 0.05, 0.08) by using solid-state reaction in a flow of high purity argon. Nearly Al atoms substituted Mg atoms in the lattice structure of MgB_2. Thus, the lattice parameters and critical temperature of MgB_2 are lowered with increasing Al concentration. Values of J_c for the doped samples were slightly larger than those of the un-doped samples. Optimal J_c properties of MgB_2 bulk have been obtained at the concentration of x = 0.02 and the temperature less than 20 K and a magnetic field above 6 T.

C.H. Cheng et al.[43] have doped MgB_2 bulks with iron. Doping has been achieved using Fe-nano- and micro-size powder. The easy doping into MgB_2 crystalline structure was by nano-iron with low solid solubility limit while the doping into the MgB_2 by micro-iron faced some difficulties and caused a reduction in both T_c and J_c.

I. A. Ansari et al. [44] studied the doping effect of ZnO-nanoparticles on the superconducting properties of MgB_2. The 2% nano-ZnO doped MgB_2 was excellent for enhancement of J_c and H_{irr} at all temperatures and magnetic fields amongst the doped and undoped sample. Also, the lattice parameter-c increased to a higher value at 2% ZnO doped MgB_2 sample. This indicated clearly a strain on the lattice parameter in doped samples. Very slight variation in T_c is observed from the temperature dependence of resistivity plot of nano-ZnO doped MgB_2. It was also observed through M (H) curves that vortices have suffered instabilities at 2% and 4% doped samples.

2.3 Objectives

In our work we propose to synthesize MgB_2 with CuF_2 nanoparticles inclusion. We aim to reduce MgO and improve the superconducting properties of MgB_2 . We expect that MgO content into MgB_2 will reduce because F_2, due to its high electronegativity, will reject O_2 from MgO and then Cu will deposite on the grains and improve the grains connectivity. In addition to that, the nano-size of CuF_2 ensures a uniform distribution of CuF_2 particles on MgB_2 grains.

We intended to measure the ac-susceptibility using an improved design of ac-susceptibilities set up with the following new features:

1. Improved sensitivity in measuring both real and imaginary part of the susceptibility.
2. Improved phase sensitive detection.
3. Improved zero level correction.

The main objectives of this project are:

1. To investigate various methods to achieve optimal conditions for inclusion of CuF_2 nano particles in MgB_2 superconductors.

2. To investigate the corresponding effects on the critical current and pinning forces.

3. To apply various scaling techniques on pinning forces and critical currents in MgB_2.

4. To study grain boundary effects in MgB_2 superconductors.

CHAPTER 3

EXPERIMENTAL WORK

3.1 Experimental Technique

Since discovery of Magnesium boride (MgB_2) in 2001 in polycrystalline form, , single crystals, thin films, tapes and wires have been prepared using various techniques[17]. Bulk MgB_2 was prepared by different methods such as Combustion method[45], SHS method [46], hot deformation, high pressure sintering, and mechanical alloying of Mg and B powders with subsequent hot compaction[47], solid state method[48],[30].

In our work we select the solid-state method in preparing MgB_2 (pure and doped) because it is fairly easy to handle, cheap and fast to obtain good quality samples [58].

3.2 Samples Preparation

This process is a very important step especially for preparation of MgB_2. Generally, the synthesis passes through several steps:

- Selection of Precursor materials. MgB_2 can be produced from its initial elements Mg and B or used Mg and B compounds. In our case, we use two methods: readymade MgB_2 and preparation from the elements Mg and B. In both cases we used the nanomaterial CuF_2 compound as a modifier with various concentrations. Desired amounts of the precursor materials are weighted by an advanced digital balance with 10^{-4}g accuracy.

Table 3.1 The chemical properties of the precursor materials

Material	Melting point	Boiling point	Molar mass
Mg	830 ºC	1091 ºC	24.3050 g /mole
B	2075 ºC	4000 ºC	10.811 g /mole
MgB_2	830 ºC	---	45.93 g / mole
CuF_2	836 ºC	1676 ºC	Anhydrate 101.543 g/mole or Dihydrate 137.573 g/mole

- Grinding process: The mixture must be homogenous to ensure an efficient reaction between components. Precursor with smaller particle sizes are more active due to the high surface to volume ratio.
- Pressing process: The well grinded mixture is pelletized by a hydraulic pressing machine. The pellet is a cylindrical shape with diameter and thickness 10 mm and 4 mm respectively. The pressure exerted on the sample was about 4 tons/in^2.
- Sealing process: For achieving the reaction between the contents, the sample must be isolated from the air (O_2, moisture, C, etc.). For this reason, the samples are sealed in a quartz tube under partial Ar-pressure.
- Annealing process: For our samples, we annealed the samples at different annealing temperatures of 750ºC and 850ºC for 2 hours and left the samples to cool down to room temperature. The sample are divided into small pieces for different investigation measurements.

Table 3.2 List of all prepared samples of MgB_2 (pure, doped, un annealed and annealed) by the solid-state method at 750°C and 850°C

Label	The sample description	Annealing temperature/Time
MB00	Pure MgB_2	No
MB26	Pure MgB_2	750°C/2 hours
MB27	MgB_2 +10% Mg	750°C/2 hours
MB30	MgB_2 + 1% CuF_2	750°C/2 hours
MB28	MgB_2 + 2% CuF_2	750°C/2 hours
MB29	MgB_2 + 5% CuF_2	750°C/2 hours
MB31	MgB_2+ 1% CuF_2 +10% Mg	750°C/2 hours
MB8R	MgB_2+ 2% CuF_2 +10% Mg	750°C/2 hours
MB21	MgB_2+ 5% CuF_2 +10% Mg	750°C/2 hours
MB01	Pure MgB_2	850°C/2 hours
MB23	MgB_2 +10% Mg	850°C/2 hours
MB32	MgB_2 + 1% CuF_2	850°C/2 hours
MB24	MgB_2 + 2% CuF_2	850°C/2 hours
MB25	MgB_2 + 5% CuF_2	850°C/2 hours
MB33	MgB_2+ 1% CuF_2 +10% Mg	850°C/2 hours
MB10	MgB_2+ 2% CuF_2 +10% Mg	850°C/2 hours
MB22	MgB_2+ 5% CuF_2 +10% Mg	850°C/2 hours

3.3 Characterization techniques

3.3.1 X-Ray Diffraction

This technique is used in the investigation of bulk properties of the materials for instance, the identification of the crystal structure, the lattice parameters and measurement of grain size. In this dissertation, we investigated the crystalline structure of all MgB_2 with various concentrations of CuF_2 nanoparticle inclusions and under several annealing temperatures. Shimadzu 6000 X-ray diffractometer with a Cu K_α radiation wavelength equals $\lambda = 0.154$ nm, operated at 40 kV and 30 mA has been used in this investigation.

3.3.2 Vibrating Sample Magnetometer (VSM)

A vibrating sample magnetometer (9Tesla 4500PAR-VSM) in its operation is based on Faraday's Law of Induction. It is used for studying a sample magnetic property such as hysteresis loops. The sample vibrates between two oppositely winded sensing coils. Any changes in the magnetization of the sample will be detected as an electromagnet force (emf) in the sensing coils. The sensitivity of the system is about 10^{-5} emu, a large stability of 10^{-3}. The magnetic moment is calibrated using Ni-standard sample.

3.3.3 AC Susceptibility Measurement

AC susceptibility measurement is used for characterizing the magnetization dynamics of the superconductor. as the high sensitivity and the simple design made it possible to build our improved design of the susceptometer [49].

There are several designs for the ac susceptometer, but the working principle is basically the same. The configuration of the design is based on the sample geometry and magnetic properties being measured of materials [49- 51].

The ac magnetic susceptibility consists of two parts; a real part of the susceptibility (χ') which is in phase with magnetic field applied on the sample and an imaginary part of the susceptibility (χ'') which is out of phase with the applied magnetic field.

$$\chi = \chi' + i\,\chi''$$

The imaginary susceptibility is related to the energy losses. Both parts χ' and χ'' can be expressed in term of the magnitude of the total susceptibility χ and the phase difference ϕ between input signal to and output signal from the coil[52].

$$\chi' = \chi \cos \phi \quad \leftrightarrow \quad \chi = \chi'^2 + \chi''^2$$

$$\chi'' = \chi \sin \phi \quad \leftrightarrow \quad \phi = \arctan(\chi'' / \chi').$$

In the following section we present our design of the ac-susceptometer. The susceptometer has been used extensively to investigate several magnetic and superconducting materials in our lab.

3.3.3.1 AC Susceptometer Design

Ac magnetic susceptibility or Ac susceptometer is very useful experiment technique to extract various magnetic properties of superconductors such as the critical current density.

The Ac susceptometer consists of two identical secondary coils with opposite winding and connected in series and surrounded by a primary coil. The secondary coils have the same number of the turns. Any current passes in the primary coil will generates a magnetic field which in turn induces an *emf* in both secondary coils. The induced *emf* cancel each other out when there is no sample available in any of the coils. When a sample is introduced into one of secondary coils, the magnetization of the sample changes the inductance of hosting secondary coil. This will result in net *emf* that can be easily detected by a lock-in-Amplifier.

The design of the ac susceptometer is shown in Fig. 3.1. The coils of the susceptometer is made from Vespel (polyimide-based plastics) material which is suitable for low temperature measurements and does not have any magnetic effects[53]. Two grooves for the secondary coils and then the primary coil covers the secondary coils. There is an axial hole along the susceptometer center for insertion of the sample to one of the secondary coils. The sample volume should be convenient to the hole of the secondary coil[49]. The detailed dimensions of the coil are shown in Fig. 3.1. The magnetic field can be calculated using the number of turns in the primary coil and from the following formula [49]

$$B = \mu_0 NI/l$$

B, N, I, l and μ_0 being the magnetic field, the number of turns, the current, the length of susceptometer and the permeability ($4\pi \times 10^{-7}\ N/A^2$) respectively.

After machining the coil, we cleaned it by acetone to remove any contaminations and obstacles and checked for any crack under wide angle microscope. Next, we use a copper wire of 0.04 mm in radius and wind each secondary coil into its groove by a winding machine, starting from its first point to the final point along the groove length. This winding process was monitored via the optical microscope for ensuring the regular distribution of the turns without any spaces or overlaps of these turns. After finishing the first layer of the secondary coil, we add GE-varnish to fix the turns to each other and prevent any vibrations that may be caused by the passing the ac-current in the coil. This step is very important to reduce noise and fluctuations in the output signal. The GE-varnish should be left to dry before winding the next layer. The process continues until the layers fill the groove. The terminals of the secondary coil must be long, each is about half meter that might be needed for connections and balancing. The secondary coils are covered by thin Teflon layer with GE-varnish. Each secondary coil consists of 11 layers with a total of 440 turns. By the same way, we wind 6 layers of the primary coil with total of 990 turns. The resistances of both secondary and primary coils are 80.3 Ω and 129.3 Ω respectively.

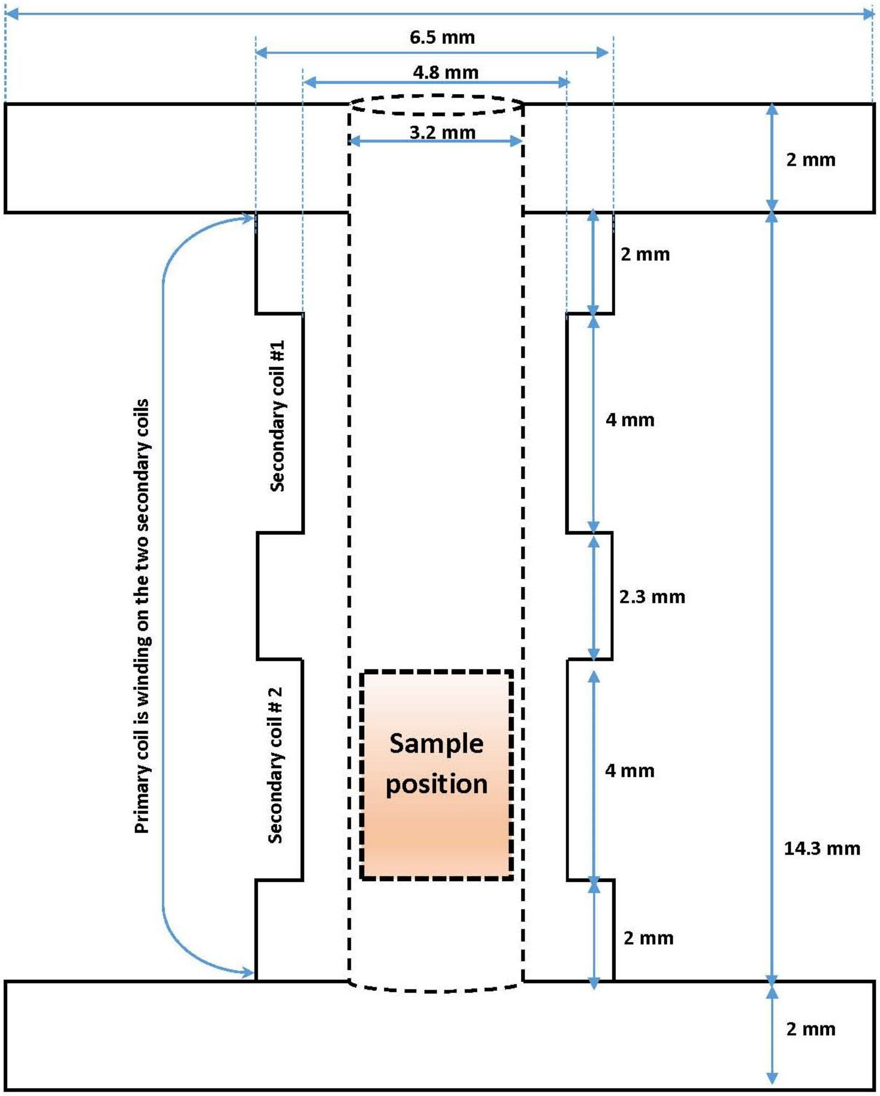

Fig. 3.1 Schematic of the ac susceptometer

3.3.3.2 Balancing the susceptometer

We connect the ac susceptometer to SR850 Lock In Amplifier. The primary coil is connected to sine out outlet and the secondary coil is connected to A-signal outlet. The important step is to adjust the susceptometer measurement where χ' is maximum and χ'' is minimum. Lock In amplifier readings for the real and imaginary susceptibility must be of nano -order. This is achieved by increasing or decreasing some turns of the primary coil and adjusting the frequency, phase difference, time constant and the gain as shown in Table 4.1 and then we fix the connecting pins. The balance of the ac susceptometer must be occurred far away about any magnetic source such as ferromagnetic materials [54],[50]. The ac susceptometer is fixed on a base made of a red copper for obtaining high thermal conductivity between the susceptometer and the surrounding environment. We often add a very large resistance ~ 10KΩ in series with the primary coil to eliminate the eddy current which may be produced and affects the sample signal. The sample is inserted into the hole to be located into one of the secondary coils. A temperaure sensor (CGR-1000) is connected to the position of the sample to read the temperature of the sample during the experiment by temperature controller. The data of the susceptibility and temperature are collected by the LabView program (Version.8).

Table 3.3 The operation conditions of Lock In amplifier for optimal susceptibility measurements.

Frequency	Time constant	Difference phase	Gain
887 Hz	1 sec	125.598°	50 μvolts

The system used for investigation of the ac susceptibility is the cryostat(JANIS) shown in Fig. 3.2 with the following components:

- The closed cycled refrigerator(Sumitomo-RDK-408D2).
- Lock In Amplifier (STANDFORD RESEARCH SYSTEMS-SR850 DSP) which is used in detection and measurement of very small AC signals reach a few nanovolts. This instrument can be adjusted at a required frequency for discriminating a special signal if the noise background is very high. (reaches many thousands of times of the signal).
- The temperature controller (LAKE SHARE 336) is used for measurement of the sample temperature along the temperature range.
- The analysis system (LabVIEW program-version 8.).

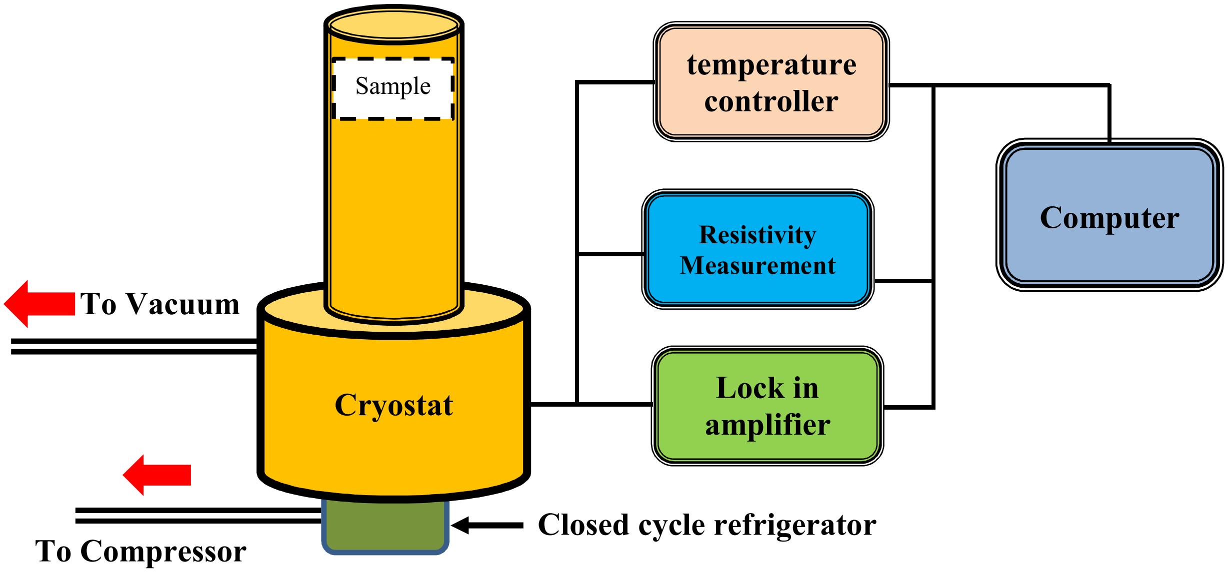

Fig. 3.2 The system used for susceptibility measurements

3.3.4 Resistance vs temperature

Measurement of the resistance of superconductor materials is one of methods for characterization of the superconductor behavior. It is well known that some materials become superconductors when they lose abruptly their resistances at a very low temperature range below the critical temperate T_c. However, the decline in the resistance may be slow due to some impurities present in the superconductor sample. The resistance of the superconductor can be measured by the two-probe method. But the situation will be different if the sample resistance is very much small such that the resistance reading is not easy to be estimated due to the contact points of the sample with the reading device produce an additive resistance to the sample resistance. For that, the four-probe method is an accurate method in a measurement of the resistance. Fig. 3.3 shows the four-probe method, the probes 1 and 4 are connected for the current measurement while the voltage drop is measured across the probes 2 and 3. The wires are connected to the sample by silver-based glue. The ac signal is used instead of the dc signal for removing the capacity which generates between the wire contact points and the sample surface[55]. The resistivity measurement is performed by the system shown in Fig. 3.2. The measurements are taken for the superconductor resistivity versus the temperature.

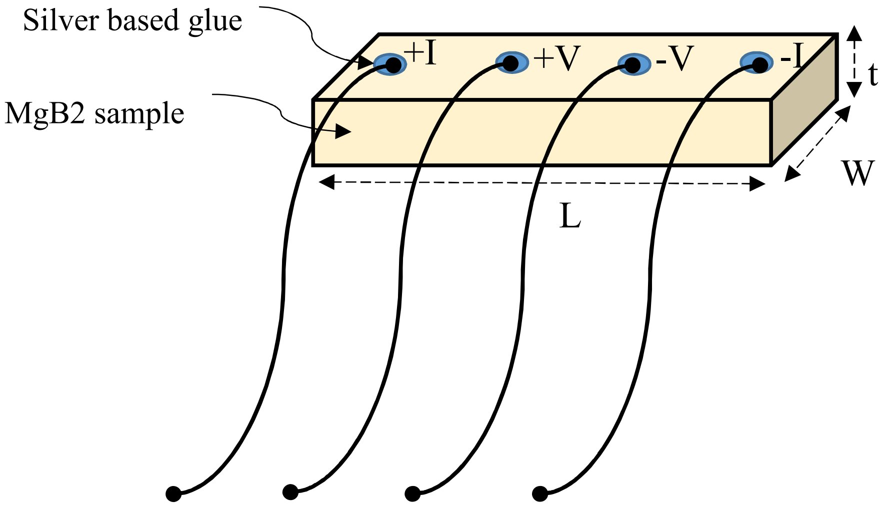

Fig. 3.3 Four probes method for resistivity measurements

CHAPTER 4

CHARACTERIZATION AND DISCUSSION

4.1 XRD Characterization

In this section we report the XRD analysis for all samples investigated in this thesis. To enhance the contribution of the low intensity peaks coming from the impurity phases, we represent the intensity of the scattered X-ray as squre root on the y-axis ($I^{0.5}$ vs. 2θ).

Nanoparticle size of CuF_2: first we confirm the nano-particle nature of CuF_2 used in sample preparation. The Scherrer equation is often used to evaluate the particle or crystallites size. The broadening of the diffraction peaks is directly related to the particle size. Fig. 4.1 shows XRD pattern of CuF_2 structure. The grain size of CuF_2 using Scherrer equation:

$$g = \frac{0.9\ \lambda}{\beta \cos\theta}$$

where g is the average size of the grain, λ is the wavelength of x-ray radiation source, β being the full width of half maximum. The full width of half maximum(FWHM) is determined from the maximum peaks of 27.5°, 31.6° and 33.6° as in shown Fig. 4.1. The average of grain size was estimated to be about~ 40 nm.

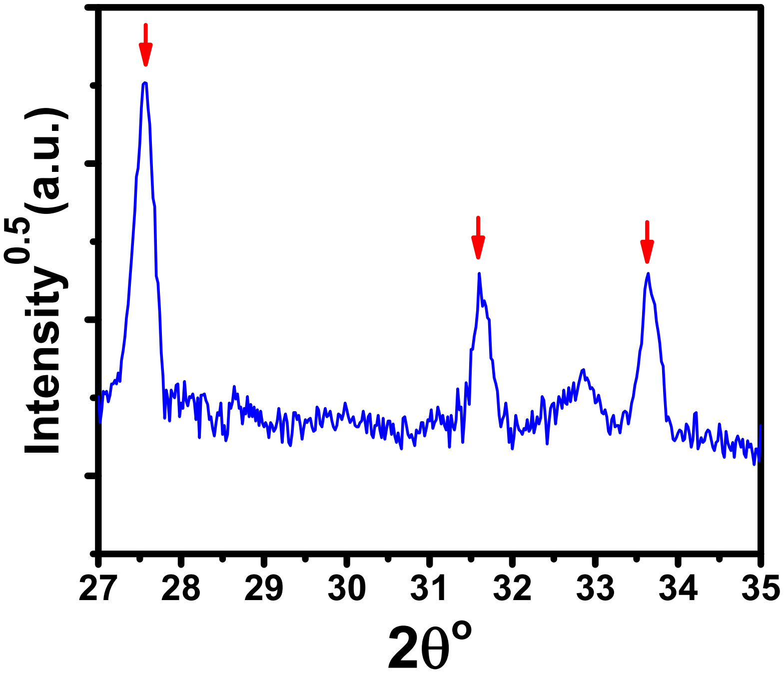

Fig. 4.1 XRD pattern for CuF_2 used as doping material for MgB_2.

We prepared two groups of pure and doped MgB_2 samples by the solid-state method as shown in Table 4.1. The first and second groups were annealed at two different temperatures; 750°C and 850°C for two hours, respectively. We investigated the XRD patterns of all samples in both groups, in order to screen the optimal preparation conditions that prodeuces improved magnetic and superconducting properties of MgB_2.

- **Annealing of the pure samples (MB00, MB26 and MB01)**

Fig. 4.2 shows three patterns of XRD for pure MgB2 samples, MB00(as is), MB26 (annealed at 750ºC) and MB01 (annealed at 850ºC). It can be observed that the MgB_2 phase of MB00 contains the MgO peak.As soon as Mg is exposed to air during preparations, it interaction readly with O_2 available in air as we mentioned before. Similarly, MB26 and MB01 samples exhibit a clear appearance of other impurities beside MgO phase such as Mg, B_2O, B_2O_3 and SiO_2. The latter phase results from interaction sample with the quartz tube which resulted in decomposition of MgB_2, producing Mg, B_2O and B_2O_3.It can be also observed that XRD pattern of MB26 (annealed at 750°C) has several impurities peaks more than any of the other sample in Fig. 4.2.

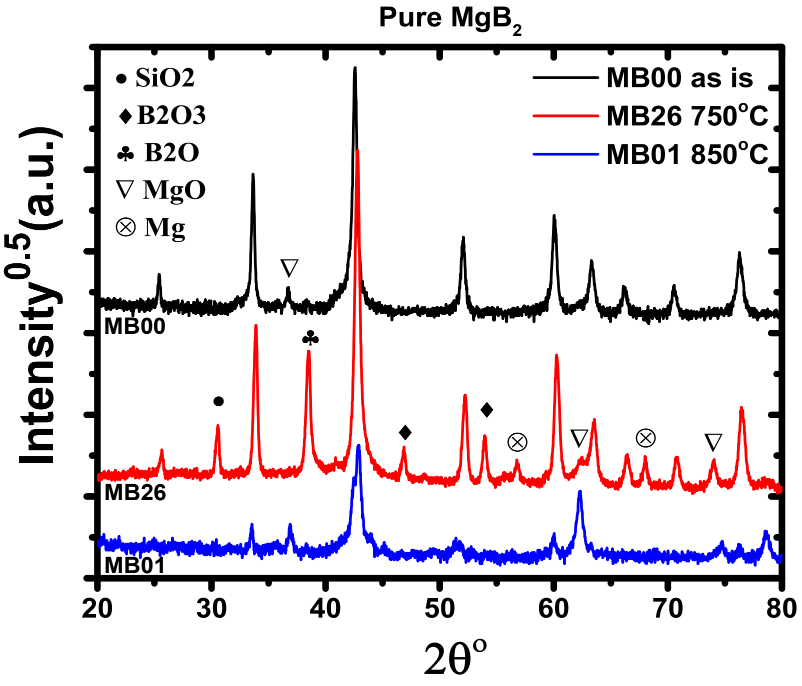

Fig. 4.2 XRD patterns for MgB_2 samples, un annealed (as is), annealed at 750°C and annealed at 850°C.

- **Excess of Mg-during preparation**

Fig. 4.3 exhibits XRD patterns of two samples, MB27 and MB23, of (MgB_2 + 10%Mg) annealed at 750°C and 850°C respectively. The aim of the Mg extra is to compensate for Mg losses during annealing. The XRD patterns revealed a similar behavior shown in Fig.

4.2. MgB_2 phase shows more deterioration and this indicates that Mg extra is not efficient in enhancement of MgB_2 phase and reducing MgO content.

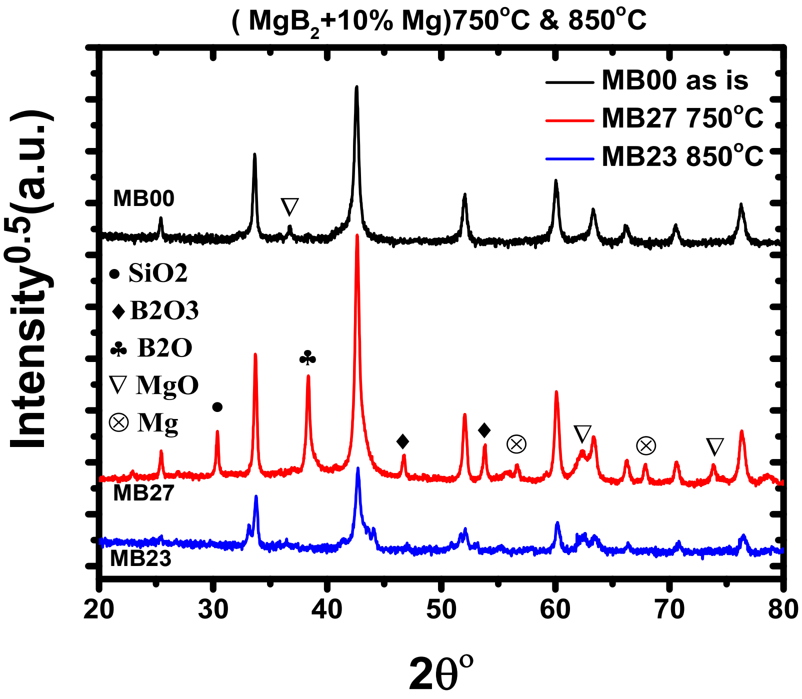

Fig. 4.3 XRD patterns for MgB_2 samples, un annealed (as is) (MB00), (MgB_2+10 %Mg) annealed at 750°C (MB27) and (MgB_2+10 %Mg) annealed at 850°C(MB23).

- **Effects of CuF_2 nanoparticles inclusion**

Similarly, Fig. 4.4 shows three samples of MgB_2 doped only with 1, 2, and 5% of CuF_2(MB30, MB28 and MB29) annealed at 750°C. MgO, Mg, B_2O, B_2O_3 and SiO_2 are also found within MgB_2 phase. In Fig. 4.5, three samples of MgB_2 doped only with 1, 2, and 5% of CuF_2 (MB32, MB24 and MB25) annealed at 850°C. In both figures Fig. 4.4 and Fig. 4.5, 1% of concentration of CuF_2 enhances the impurities peaks while the 2% and 5% concentrations degrade MgB_2 structure. A slight improvement can be seen in the samples annealed at 850C as compared with the previous figures.

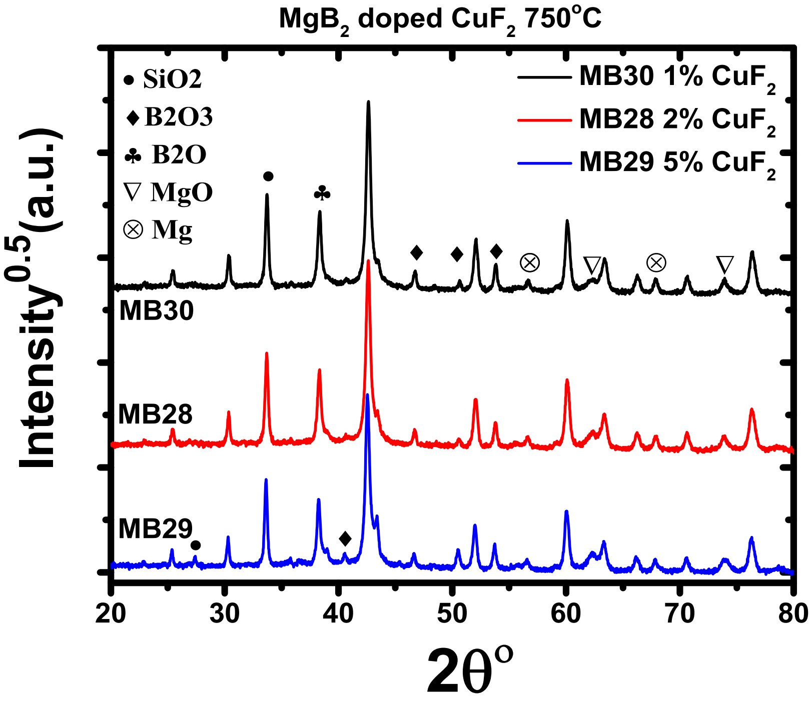

Fig. 4.4 XRD patterns for MgB_2 samples doped with 1, 2 and 5% for (MB30),(MB28) and (MB29) respectively and annealed at 750°C.

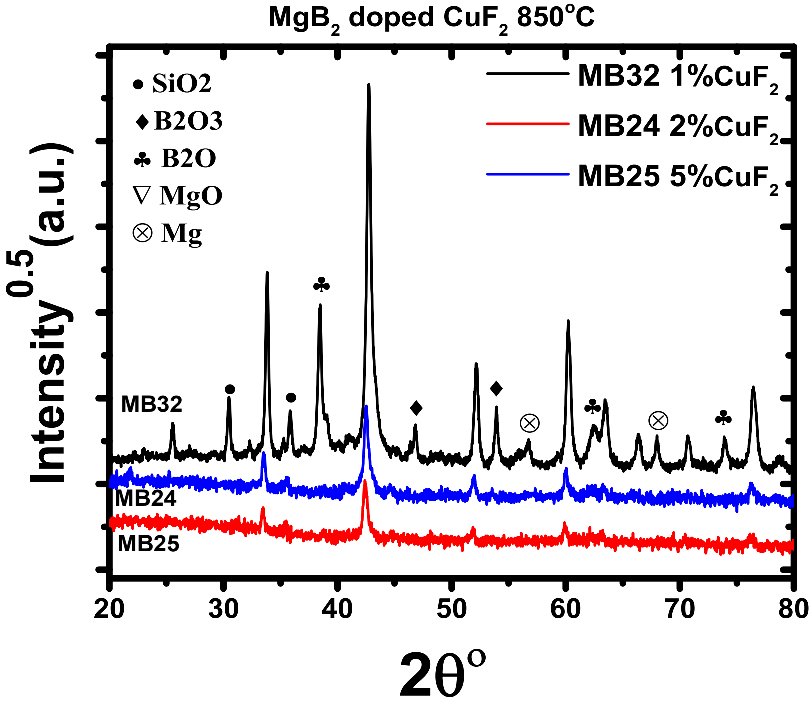

Fig. 4.5 XRD patterns for MgB_2 samples doped with 1, 2 and 5% for (MB32), (MB24) and (MB25) respectively and annealed at 850°C.

- **Effects of CuF_2 and excess of Mg**

Fig. 4.6 and Fig. 4.7 show (MgB_2+10%Mg) samples doped with 1, 2, and 5% of CuF_2 (MB31, MB8R and MB21) and (MB33, MB10 and MB22) annealed at 750ºC and 850ºC respectively. The results of XRD patterns are supersizing; 1% of concentration of CuF_2 is not sufficient to remove or prevent the formations of various oxides at both annealing temperatures. However, 2% concentration showed only a single phase of MgB_2 in MB8R prepared at 750ºC while a trace of MgO phase can be seen in MB10 prepared at 850ºC. For samples with 5%CuF_2 concentration, the XRD patterns revealed deterioration in the structure and re-emerging of impurity phses(MB21 and MB22 samples) as shown in Fig. 4.6 and Fig. 4.7, respectively. The impurities have been partially reduced in MgB_2 as shown Fig. 4.6 but also caused some damage to MgB_2 structure as in Fig. 4.7.

We conclude that MB8R sample (MgB_2+2%CuF2+10%Mg) at 750ºC is the best sample MgO and other contaninations almost disapprear and the only dominent phase belongs to MgB_2. This achievement leads to improvement of magnetic properties of MgB_2 phase.

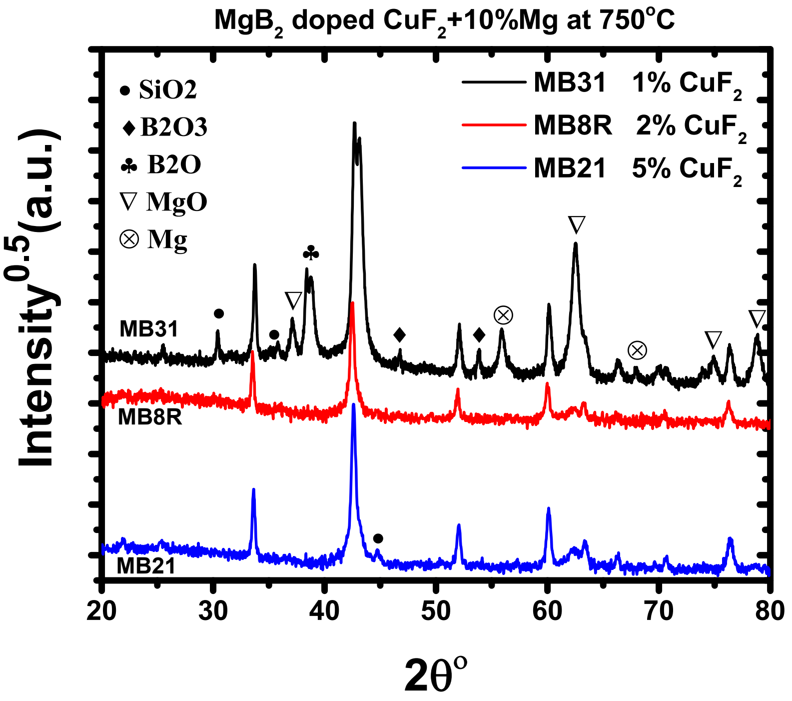

Fig. 4.6 XRD patterns for(MgB2+10%Mg) samples doped with 1, 2 and 5% for (MB31), (MB8R) and (MB21) respectively and annealed at 750°C.

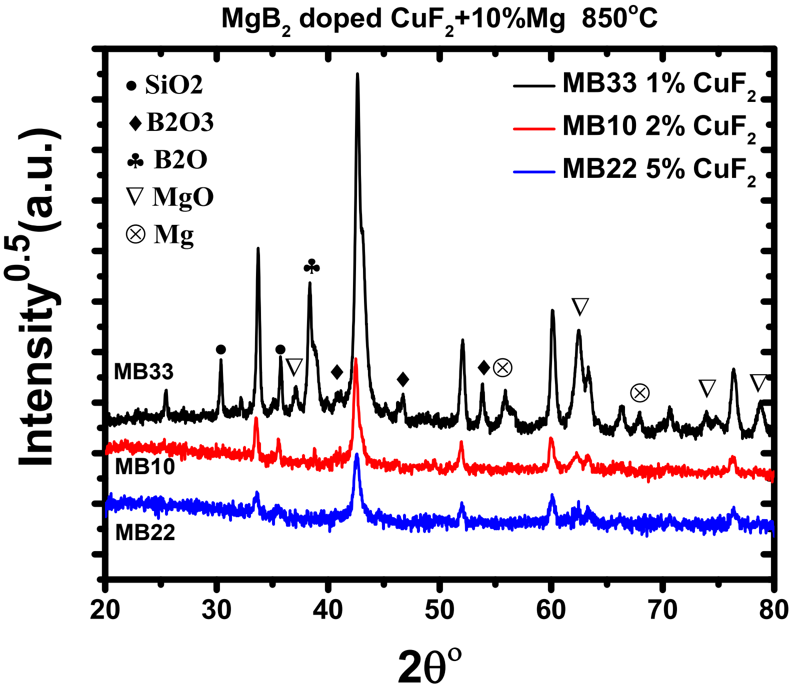

Fig. 4.7 XRD patterns for MgB2 samples doped with 1, 2 and 5% for (MB33), (MB10) and (MB22) respectively and annealed at 850°C

4.2 Resistivity Measurements

Fig. 4.8 shows the normalized resistivity measurements versus temperature for (as is) sample and samples prepared at 750°C. The measurements were carried out for a range from 30 K to 45 K in zero magnetic filed. It can be seen the normalized resistivity of MB8R sample (MgB_2+10%Mg+ 2% CuF_2) drops sharply down at the onset of transition temperature $T_{c,onset}$ of 38.6° which is the highest transition among all investigated samples. Moreover; the transition width, ΔT, is very small indicating sharper for MB8R and MB21(ΔT~2K) as shown in Table 4.1. The sharpness of the transition curves can be attributed to good quality of the samples and good grain connectivity in MB8R and MB21 whereas the as is sample (MB00) displays a wider width (ΔT=7.7K) can be ascribed to the contamination of MgO which is localized on the grain boundaries of MgB_2 and isolates MgB_2 grains. The MB26 (750ºC annealing with no Mg extra) sample exhibits non conducting behavior with very high resistance at low temperature. This indicates that the grain are completely isolated with MgO layerThis non-conducting behavior in further supported by the oxide impurity paheses seen in the XRD patterns (Fig. 4.1). The best sample (MB8R) also supports by the XRD results, conferming that doping MgB_2 with 2% CuF_2 as well as 10%Mg is enough for improvement of superconducting MgB_2 properties[56].

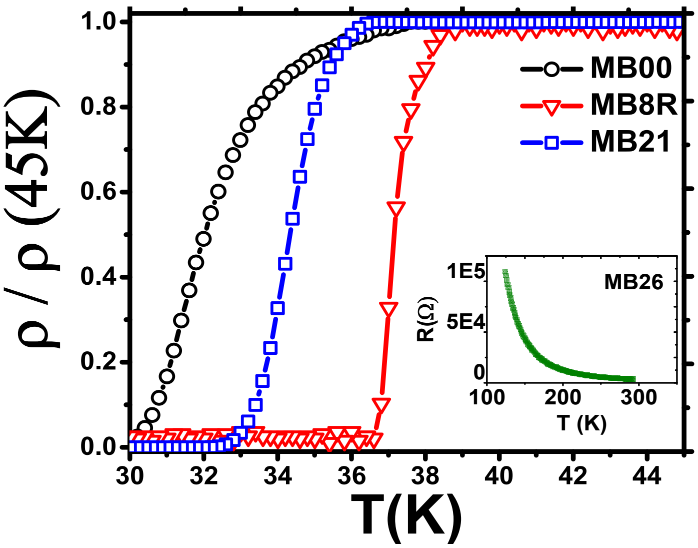

Fig. 4.8 Normalized resistivity vs temperature for undoped and doped MgB_2 at 750°C

Table 4.1 shows the variation of the transition temperature of Tc, onset , Tρ=0 and ΔT for resistivity measurements of samples annealed 750°C.

# sample	Tc(onset)K	Tc(ρ=0)K	ΔT K
MB00	37.6	29.9	7.7
MB26	---	----	∞
MB8R	38.6	36.6	2
MB21	36.4	32.4	2

Fig. 4.9 shows the normalized resistivity measurements versus temperature for all samples prepared at 850°C. The measurements were carried out for a range from 30 K to 45 K at zero filed mode. The transition temperature onset, $T_{c,onset}$ of MB25(MgB_2+5%CuF_2) and MB24(MgB_2+2%CuF_2) show the highest $T_{c,onset}$ (38.6K) and (37.8K), respectively. The width of the transition temperature is too wide.

Table 4.2. The data shows the width is wider than that for samples prepared at 750C. This could probably due to increasing MgO and Boron oxides at the MgB_2 grain boundaries. The MB22 sample (MgB_2+10%Mg +5%CuF_2) displays the least $T_{c,onset}$ (33.7K). The reduction may be attributed to formation of secondary phases (see XRD patterns in Fig. 4.7.

Samples MB23(MgB_2+10%Mg) and MB10(MgB_2+10%Mg+2%CuF_2) also show the transition temperature onset $T_{c,\ onset}$, at 36.7°C and 36.0°C, respectively and the transition width is ΔT=4.1K and 2K, respectively. This sharpness of transition curve in these samples indicates good connectivity among the MgB_2 grains by CuF_2 and Mg extra when compared with MB00 (MgB_2 as is with ΔT=7.7K).

To summarize, CuF_2 inclusions only as in MB24 and MB25 has a negative effect and causes deterioration in MgB_2 matrix and the formation of MgO and Boron oxides.. The addition of 10% Mg along with CuF_2 compensate for Mg losses and maintains MgB_2 phase and stoichiometry. MB10 is the optimized sample among all samples synthesized at 850°C, while MB8R (MgB_2+10%Mg+2%CuF_2) sample is the optimal sample prepared at 750°C. Overall, MB8R is better sample than MB10 due to its highest $T_{c,onset}$.

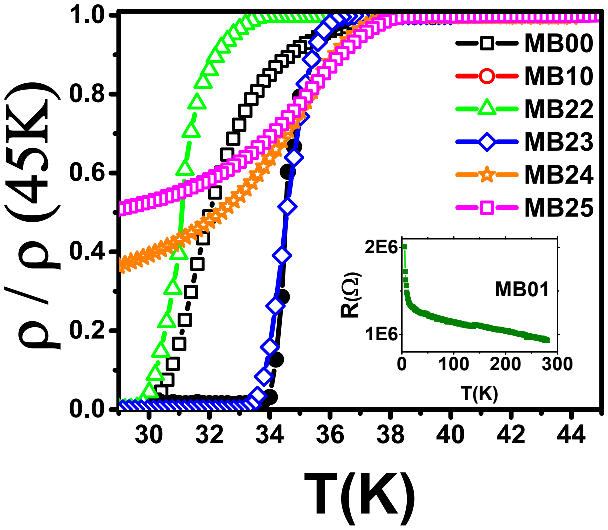

Fig. 4.9 Normalized resistivity vs temperature for undoped and doped MgB_2 at 850°C

Table 4.2 shows the variation of the transition temperature of Tc ,onset , Tc, ρ=0 and ΔT for resistivity measurements of samples annealed 850°C

sample	Tc(onset)K	Tc(ρ=0)K	ΔT K
MB00	37.6	29.9	7.7
MB23	36.7	33.1	3.6
MB24	37.8	---	Very wide
MB25	38.4	---	Very wide
MB10	36.0	34.0	2
MB22	33.7	29.6	4.1

4.3 Ac-Susceptibility Measurements

4.3.1 Phase Difference

The ac susceptibility represents the response of the sample to be magnetized by applying alternating magnetic field. Any changes in the magnetization due to temperature changes can be easily detected in the set of pick up coils and displayed by the lock-in-amplifier as a real and imaginary parts of the susceptibility and the phase angle between them. The real part refers to the real susceptibility, the imaginary part is linked to the energy losses associated with the changing magnetic field. The phase angle basically represents the lag angle begtween the applied magnetic field and the sample magnetization and also linked to the energy losses. Any changes in state of the sample will be reflected as changes in the magnetization and changes in the lag angle. Hence one can use the changes in the lag angle to detect phase transition.

- **Annealing of the pure samples (MB00, MB26 and MB01)**

In Fig. 4.10 we present the variation of the lag angle ($\Delta\theta$) phase difference of ac susceptibility measurements of the sample signal and reference signal versus temperature for the three pure samples of MgB_2, MB00(as is), MB26(750^{o}C), MB01(850^{o}C). The phase difference of the sample signal and reference signal in the normal state (above T_c) is very small and near to zero where the magnetization is almost zero. The imaginary part is also zero, and no losses in the normal state appears due to the ac-applied magnetic field.Below T_c, the sample is diamagnetic, its magnetization is out of phase with the applied magnetic field ($\Delta\theta$~180o), and no losses is observed in the superconducting state.

The phase difference changes dramatically to be reached 160° ~ 175°. This change occurs at the transition temperature at which the sample state transfers from normal to superconducting state. We extracted all transition temperatures for all samples and recorded into Table 4.3.

For pure samples MB00, MB26 and MB01, the annealing temperature of 750°C for MB26 leads to reduction of the transition temperature onset, $T_{c,onset}$ to 32.3K whereas T_c,onset of MB01sample increases to 39.9K by annealing at 850°C.

- **Excess of Mg-during preparation**

Fig. 4.12 shows the results ofthe annealed samples at 750°C and 850°C have similar effect on MB27 and MB23 samples with 10%Mg with transition at 35.7K and 39.7K respectively.

- **Effects of CuF_2 nanoparticles inclusion**

In Fig. 4.12 the same behavior with the samples of MgB_2 doped with 2% and 5% CuF_2 only (MB28 and MB29) and, (MB24 and MB25) is repeated where that the annealing temperature of 850°C enhances the $T_{c,\ onset}$ while 1% of CuF_2 for the two annealing temperatures of 750°C and 850°C does not enhance the $T_{c,onset}$ but reduces it to around ~35.7 and 35.9K, respectively. The samples of MB30 and MB32 (MgB_2+1%CuF_2+10%MgB_2) show reducing $T_{c,\ onset}$ to 34.8K and 35.8K for both annealing temperature of 750°C and 850°C respectively.

- **Effects of CuF_2 and excess of Mg**

From Fig. 4.13 the samples of MB8R and MB10 show opposite manner for $T_{c,\,onset}$ with the annealing temperatures. The annealing temperature of 750ºC improves $T_{c,onset}$ to 38.9K whereas 850ºC degrades the T_c, onset to 37.5K. The samples MB21 and MB22 represent no change in the $T_{c,onset}$ (40K and 39.4K). In addition to that 1% CuF_2 for samples (MB31) annealed at750ºC destroys partially the superconducting fraction volume of MgB_2 due to MB31 transition temperature is not sharp and so much wide. As well as reduction of the phase difference to be 150ºC.

Table 4.3 shows the variation of the transition temperature of Tc ,onset susceptibility measurements for samples using phase difference

mple	$T_{c,\,onset}$ (K)	Description/750ºC for 2 hours	Sample	$T_{c,\,onset}$ (K)	Description/850ºC for 2 hours
MB00	37.8	As is (no heat treatment)	------	-------	-------
MB26	32.3	Pure	MB01	39.9	Pure
MB27	35.7	10%Mg	MB23	39.7	10%Mg
MB30	35.9	1%CuF_2	MB32	35.7	1%CuF_2
MB28	35.7	2%CuF_2	MB24	38.2	2%CuF_2
MB29	35.5	5%CuF_2	MB25	40.0	5%CuF_2
MB31	34.8	1%CuF_2+10%Mg	MB33	35.8	1%CuF_2+10%Mg
MB8R	38.9	2%CuF_2+10%Mg	MB10	37.5	2%CuF_2+10%Mg
MB21	40.0	5%CuF_2+10%Mg	MB22	39.4	5%CuF_2+10%Mg

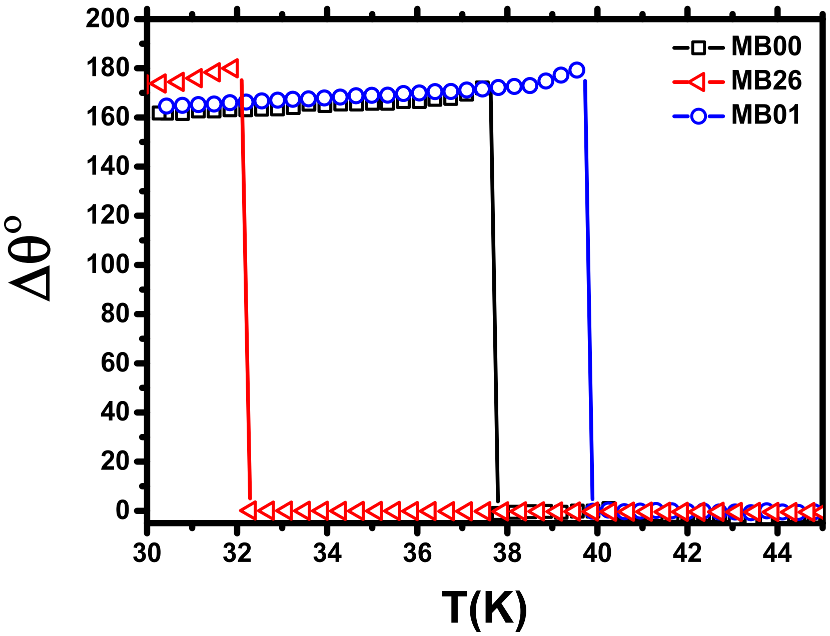

Fig. 4.10 The phase difference measurements for pure MgB_2 sample; MB00(as is), MB26 and MB01 annealed to750°C and 850°C respectively

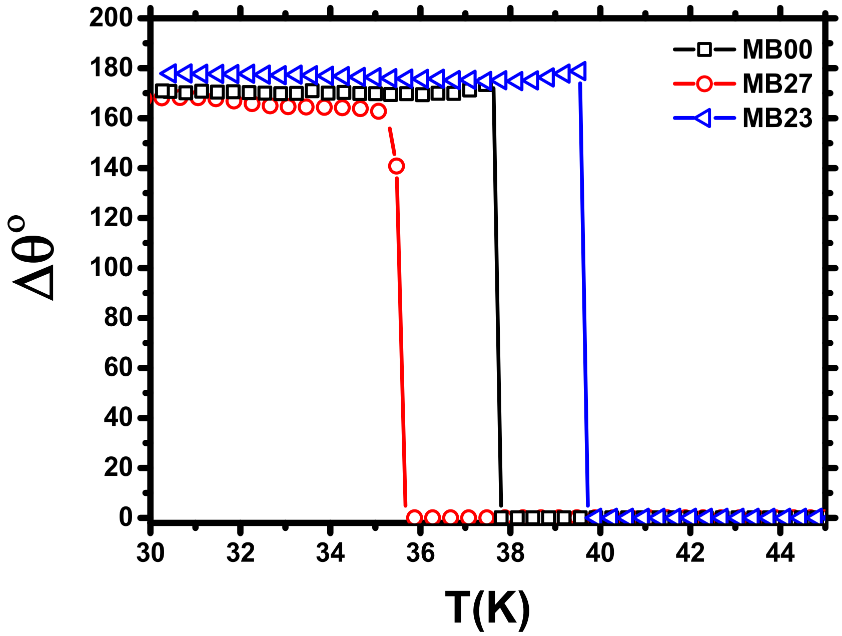

Fig. 4.11 The phase difference measurements for MB00 and (MgB_2 +10%Mg)samples;

MB27 and MB23 annealed to750°C and 850°C respectively

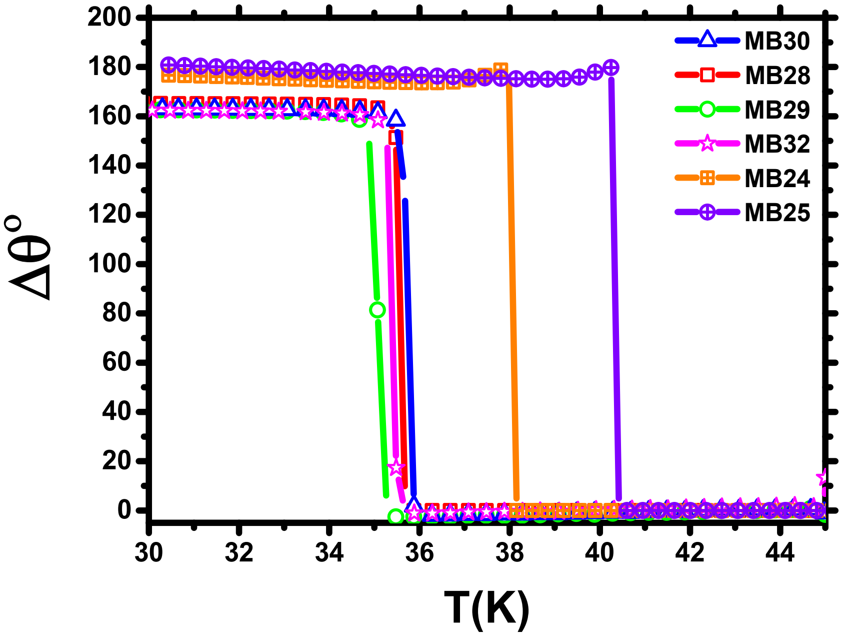

Fig. 4.12 The phase difference measurements for MgB_2 doped with 1, 2 and 5% CuF_2 at 750°C (MB30,MB28 and MB29) and at 850°C (MB32, MB24 and MB25), respectively

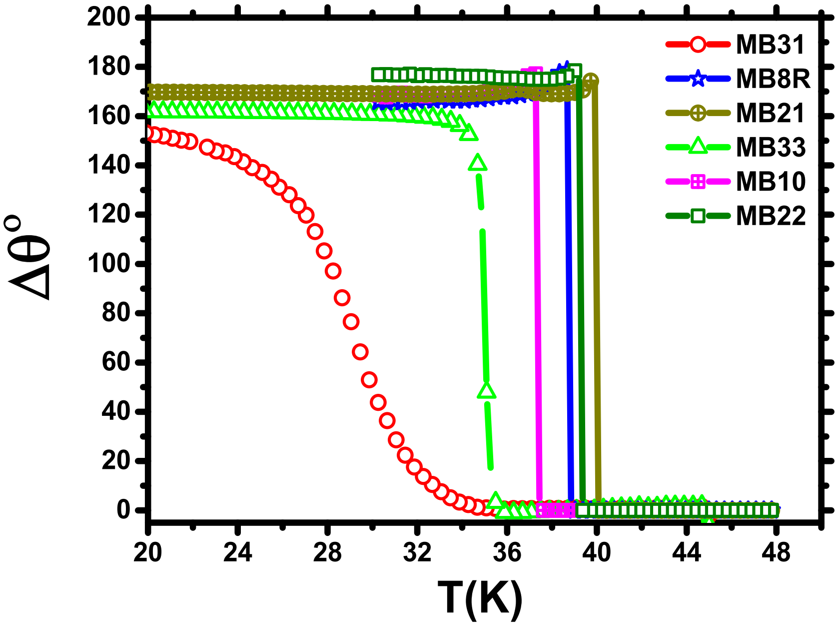

Fig. 4.13 The phase difference measurements for(MgB_2+10%Mg) doped with 1, 2 and 5% CuF_2) at 750°C (MB31,MB8R and MB21) and at 850°C (MB33, MB10 and MB22), respectively

.

4.3.2 Total Ac-Susceptibility

The ac-susceptibility measurements have been performed with temperature for all samples synthesized under annealing temperatures 750^{o}C and 850^{o}C. These measurements are displayed in Fig. 4.14, Fig. 4.15, Fig. 4.16 and Fig. 4.17

- **Annealing of the pure samples (MB00, MB26 and MB01)**

Fig. 4.14 shows the total susceptibility (χ_{total}) versus temperature for pure MgB_2 samples; MB00(as is), MB26 and MB01annealed to750^{o}C and 850^{o}C respectively. The transition temperature shifts to a lower and higher values in MB26 andMB01 respectively. This shift is attributed to the annealing temperature influence.

- **Excess of Mg-during preparation**

In Fig. 4.15, adding 10%Mg to pure MgB_2 at annealing temperature of 750^{o}C for (MB27) sample increases the susceptibility magnitude and transition temperature while the Mg addition with annealing temperature of 850^{o}C for (MB23) sample decreases the susceptibility magnitude and increases transition temperature if both samples are compared to MB00 sample (as is). As it is noticeable that the transition curve of MB27 has a second transition peak, is attributed to a secondary phase, may be residual Mg is not reacted during the annealing temperature of 750^{o}C. The secondary peak disappears in MB01 annealed at 850^{o}C.

- **Effects of CuF_2 nanoparticles inclusion**

In Fig. 4.16. the total susceptibility (χ total) meaurement versus temperaure for MgB_2 doped with 1, 2 and 5% CuF_2) respectively with samples(MB30,MB28 and MB29) annealed to750ºC and (MB32, MB24 and MB25) annealed 850ºC. It can be seen that MB28 sample(2%CuF_2 at 750ºC) represents the higher susceptibility magnitude and transition temeraurewhereas MB30(1%CuF_2 at 750ºC)displays the opposite behavior which in turn confirms the effeciency of 2% CuF_2 under 750ºC in enhanement of the MgB_2 susceptbility and the transition temperature. The rest samples show very low susceptibilty although that the transition temeraure is high.

- **Effects of CuF_2 and excess of Mg**

Fig. 4.17 exhibits the total susceptibility (χ) meaurement versus temperaure for (MgB_2+10%Mg) doped with 1, 2 and 5% CuF_2 respectively with samples (MB31,MB8R and MB21) annealed to750ºC and (MB31, MB10 and MB22) annealed 850ºC. MB31 sample (1%CuF_2 at 750ºC) does not show any suscepotibility magnitude (no magnitzed sample) followed by MB33 sample(1%CuF_2 at 850ºC) which displays a very weak susceptibility. Thus we can saying that 1% CuF_2 concentration is not effective in improvimg MgB_2 but leads to more destruction of MgB_2 superconductivity.

As well, samples MB21 and MB22 (MgB_2+10%Mg +5%CuF_2) annealed 750ºC and 850ºC respectively show weak susceptibility but the susceptibility of MB21 is larger and exhibits a second peak as happened with MB27(MgB_2+10%Mg) which is ascribed to a secondary phase may be residual Mg is not reacted during the annealing temperature of 750ºC.

The samples MB8R and MB10 which were synthesized from (MgB_2+10%Mg+2%CuF_2) and annealed at 750°C and 850°C respectively represents high susceptibility magnitude equals almost three times of susceptibility magnitude of MB00(as is) sample. MB8R sample exhibits susceptibility with higher and sharper transition temperature in Fig. 4.17.

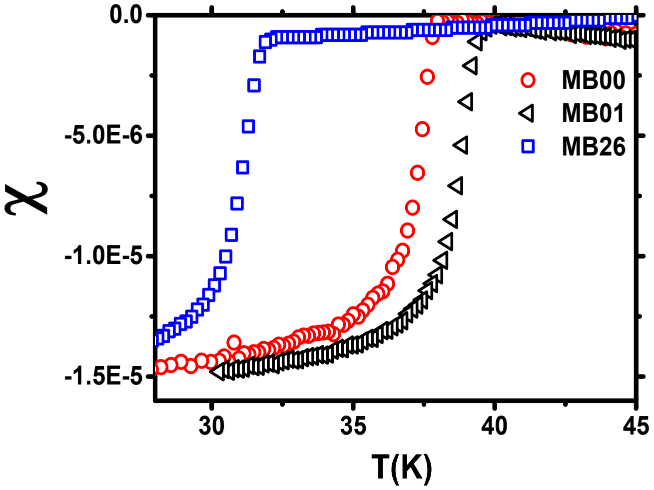

Fig. 4.14 The ac-susceptibility measurements for pure MgB_2 sample; MB00(as is), MB26 and MB01 annealed to750°C and 850°C respectively

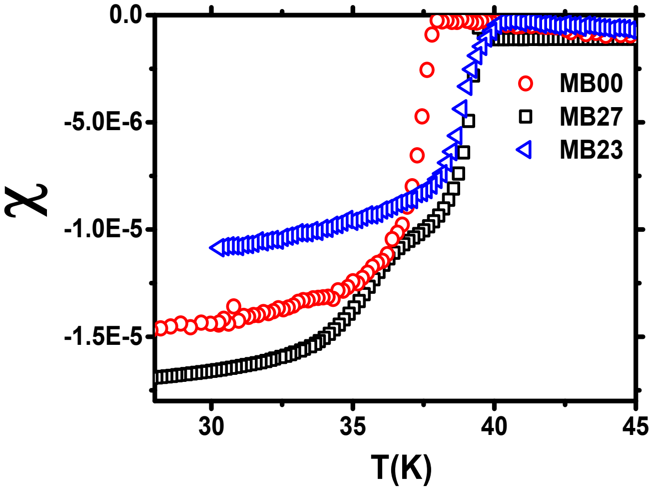

Fig. 4.15 The ac-susceptibility measurements for MB00 and (MgB_2 +10%Mg) samples; MB27 and MB23 annealed to750°C and 850°C respectively

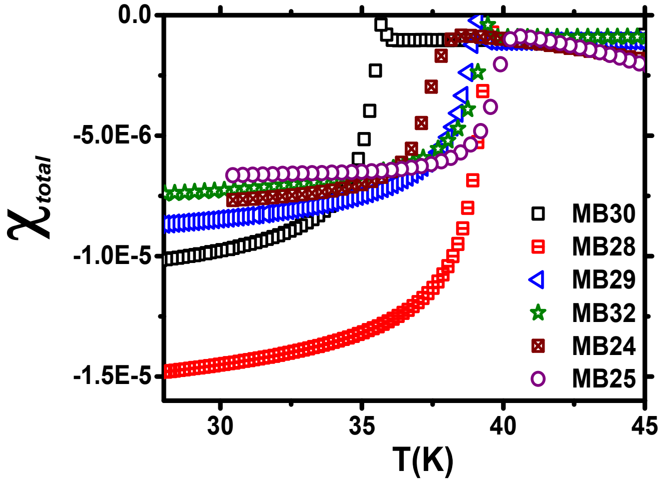

Fig. 4.16 The ac-susceptibility measurements for MgB_2 doped with 1, 2 and 5% CuF_2 at 750°C (MB30,MB28 and MB29) and at 850°C (MB32, MB24 and MB25), respectively

.

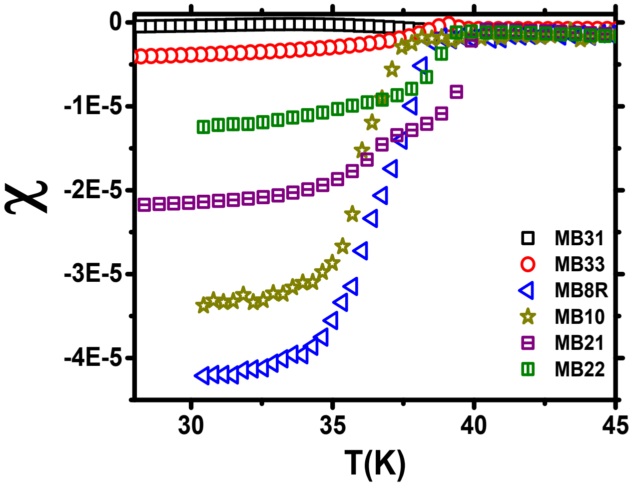

Fig. 4.17 The ac-susceptibility measurements for (MgB_2+10%Mg) doped with 1, 2 and 5% CuF_2 at 750°C (MB31, MB8R and MB21) and at 850°C (MB33, MB10 and MB22), respectively.

CHAPTER 5

MAGNETIC PROPERTIES OF MgB_2 SUPERCONDUCTOR

The magnetic properties of superconducting materials are essential for understanding various properties of superconductors. The magnetization curves can be used to obtain valuable information about the superconducting-magnetic state. The remnant magnetization, critical current density and other reversible and irreversible properties can be readily evaluated. The irreversible properties are largely attributed to irregularity and inhomogeneity, such defects or impurities in type II superconductor. These are commonly known as pinning sites and serves as traps for magnetic flux lines (vortices) [57]. The *M-H* magnetization curves of type–II superconductors usually form irreversible loops known as hysteresis loops as shown Fig. 5.1 The magnetization does not go back to zero when the applied field reduces to zero, but there is a remnant magnetization (M_r) in the superconductor. This remnant magnetization is proportional to the number of trapped vortices flux lines in the material. Other properties that can be obtained from the hysteresis loops include for example; critical current density J_c, pinning force F_p, irreversible fields H_{irr}, condensation energy and critical fields (H_{c1}, H_c and H_{c2}) [2].

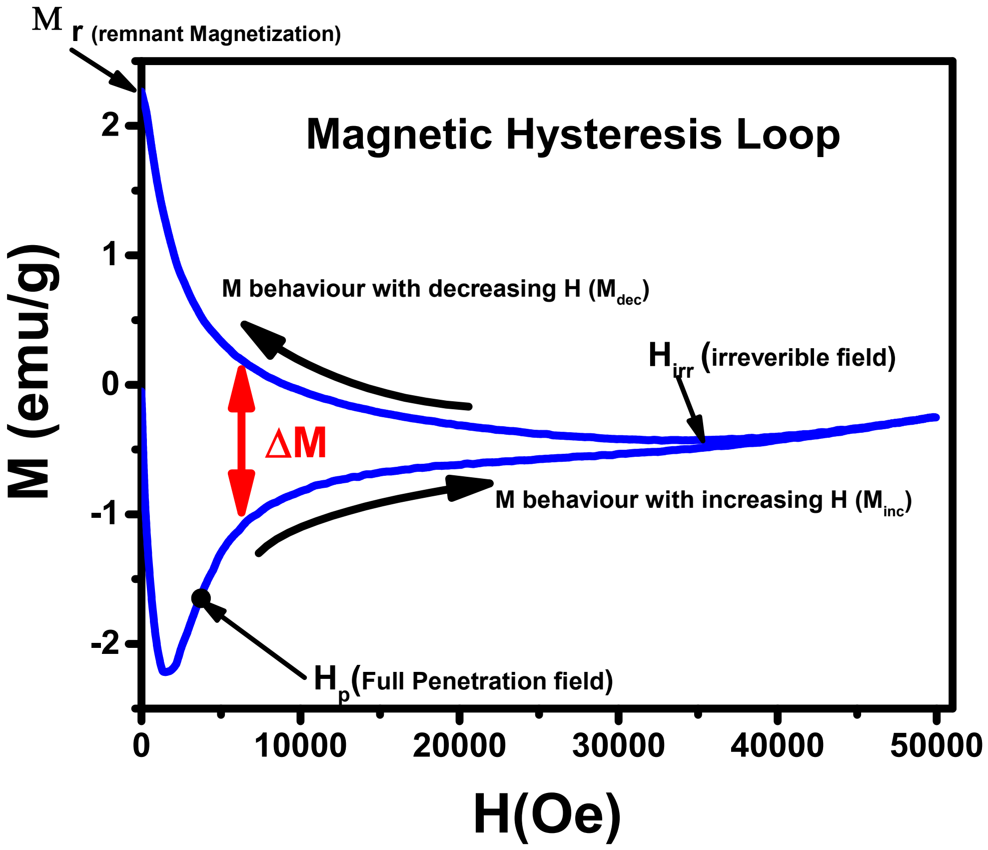

Fig. 5.1 Magnetic Hysteresis Loop of MgB_2 superconductor

5.1 Hysteresis Loops of the Investigated Samples

The magnetization M(emu/g) of each sample was measured using the vibrating sample magnetometer (VSM) vs the applied DC magnetic field H(Oe) at different temperatures from 4 to 32K. Fig. 5.2 shows the hysteresis loop for MB00 (as is) sample.

It is clear that the area of the hysteresis loops decreases with increasing temperature. In addition, the remnant magnetization (M_r) and the irreversibility field (H_{irr}) represent a clear decrease as temperature rises up. Using these hysteresis loops along with the Bean's model we can evaluate the critical current density (J_c), volume pinning force (F_p) and the irreversibility field (H_{irr}) as well as full penetration field HP can also be evaluated. The hysteresis loops of annealed pure and doped samples at 750ºC and 850ºC for 4K are shown in Fig. 5.3.

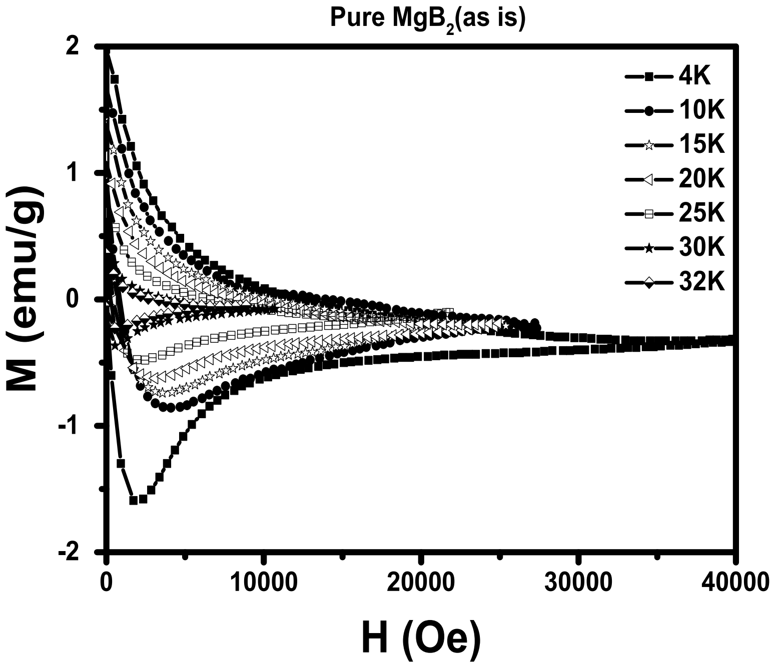

Fig. 5.2 The hysteresis loop for MB00 (as is) sample

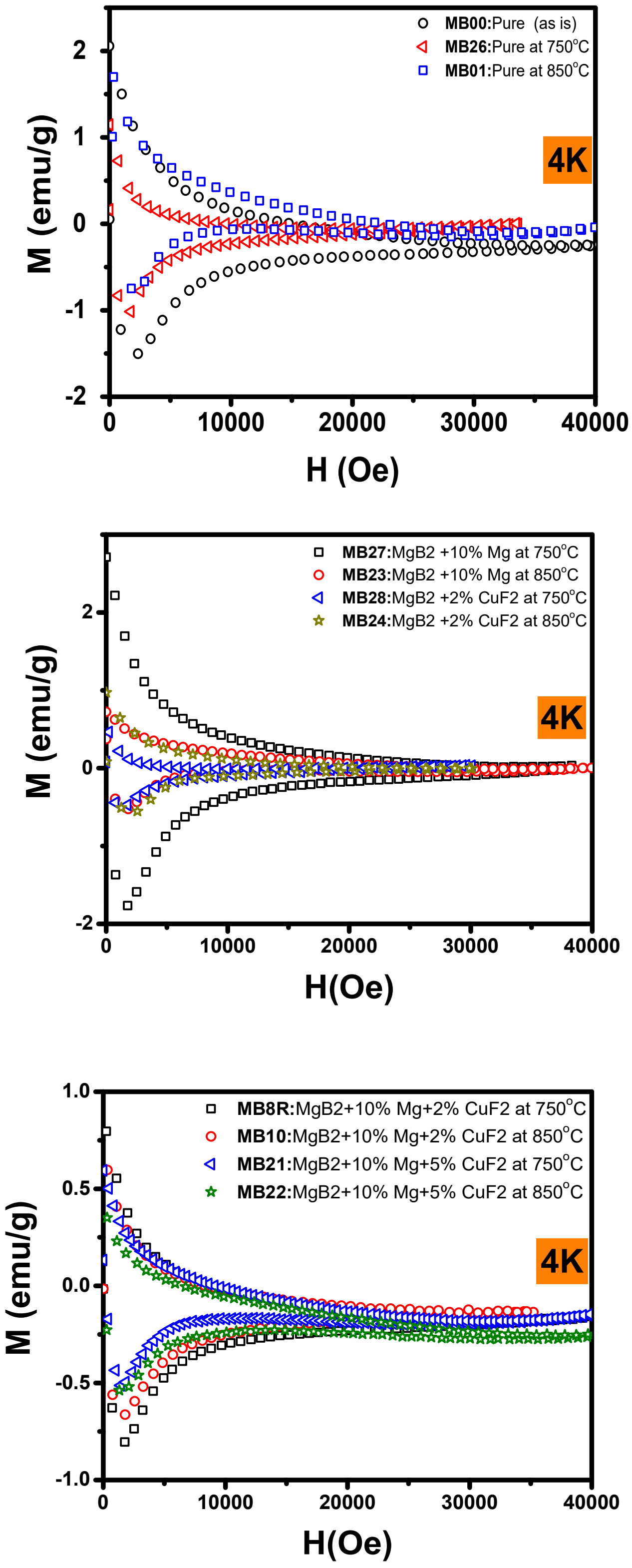

Fig. 5.3 The hysteresis loops for all pure and doped samples annealed at 750°C and 850°C for 4K.

5.2 Critical Current Density, J_c, Measurements

Transport measurements offer a direct method to evaluate the critical current density. The method is relatively simple for low current density, especially near the transition temperatures. However; at very low temperatures and for materials with high critical current densities, technical difficulties associated with high currents and heat dissipation become enormous and hinder using the transport method in evaluating the critical current density of superconducting material.

A much simpler method is provided by magnetic measurements. The critical current density J_c can be evaluated from the magnetic hysteresis loop of the sample. When the magnetic flux lines penetrate the sample in the mixed state, the circuiting currents are created around the magnetic flux lines. Each circulating current and the flux line form what is called a vortex. The flux line represents the normal core of the vortex with radius ξ while the circulating current forms the supercurrent with radius λ of the vortex. Both magnetic field H and the critical current density J_c drive the vortex to move through the sample bulk by Lorentz force resulting from $H \times J$. The Lorentz force reaches a maximum value if H is perpendicular to J.

In the absence of pinning, the vortices move freely along the force direction without any barriers prevent their motions. When the magnetic field reaches H_{c2} the superconductor becomes in the normal state. If the magnetic field is reverse from H_{c2} to zero, the magnetization curve is identical to the magnetization curve of increasing the magnetic field in reversible way and at $H=0$, the magnetization becomes zero. Thus, this sample does not carry any current due to the reversibility in the magnetization. For inhomogeneous sample with various pinning centers, the magnetization is not reversible and results in a sizable hysteresis loop. At H=0, there will be a remnant magnetization and trapped flux lines. The width of the magnetization curve is directly proportional to the density of the trapped flux lines. Irreversibility of the magnetization is attributed to the trapping of the flux lines by inhomogeneities such as dislocations, precipitates, impurity and grain boundaries which serve as a pinning force that inhibits a vortex motion. Bean speculated that the the current density (J_c) is directly proportional to the width of the hysteresis loop. In the following we discuss two main characteristic irreversible properties of the superconductor directly obtained from the hysteresis loops; the critical current density, J_c and the pinning force, F_p. [57]**.** The superconducting inhomogeneous sample can carry any amount of current density as long as Lorentz force does not exceed the pinning force, F_p. When the external magnetic field H increases the flux lines density increases leading to increasing Lorentz force. When Lorentz force equals the pinning force, the current density reaches its maximum value. In the following sections we will discuss the Bean's critical state model and apply it to the magnetic hysteresis loops to evaluate the critical current density and pinning force and their scaling behavior.

5.3 Bean's Critical State Model

Bean critical state model describes the magnetization of type II superconductor under varying external magnetic fields. The model presents a simple and effective method for evaluating the critical current density in the hard superconductor from the width of the hysteresis loops ΔM. The model is based on the following main assumptions:

- The critical state is associated with the irreversible magnetization.

- Above the full penetration field, the critical current density Jc is independent of the external magnetic field H.
- In any penetrated region of a superconductor, the critical current density is normal to the applied magnetic field.

Although that the Bean's model is a good model for calculating the critical current density, but it has some limitations:

- It does not consider Meissner effect.
- In most superconducting materials including high temperature superconductors (HTSC), J_c depends strongly on the applied magnetic field.
- No consideration for the critical current density origin[58].

The critical current density, J_c can be calculated directly from the width of the hysteresis loop ΔM as shown in Fig. 5.1 [10]. The magnetization of the sample varies according to the variation of the applied magnetic field H. The critical current density, J_c is directly proportional to the magnetization difference, ΔM. For example, for a cylindrical sample

$$J_c \sim \Delta M/r$$

where r being the sample radius and the field is applied perpendicular to r [59]

Bean's model can be expressed in a simple form; namely: [60]:

$$J_c = \frac{30\,\Delta M}{\langle d \rangle} = \frac{30\,(M_{dec} - M_{inc})}{\langle d \rangle}$$

where $\Delta M=(M_{dec} - M_{inc})$ (in emu/cm^3) is the width of hysteresis loop as shown in Fig. 5.1. and $\langle d \rangle$(in cm) is the average diameter of sample perpendicular to the applied field. Fig. 5.4 shows the variation of the critical current density, J_c with the magnetic field, H within the temperature rang (4-32) K in MB00 (as is) sample. It can be seen that the critical current density decreases with increasing the field and temperature from 4K to 32K.

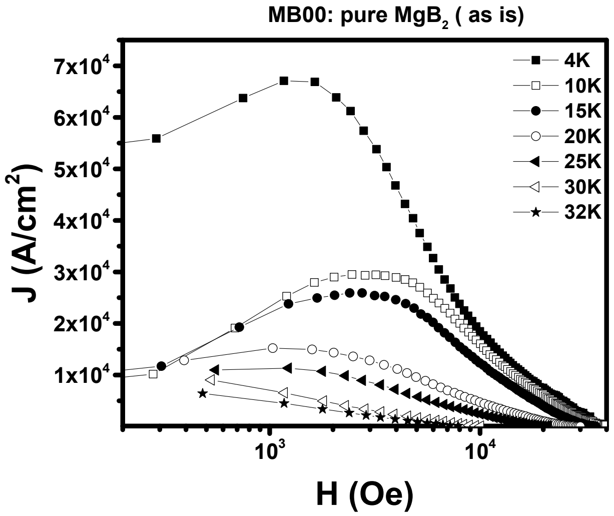

Fig. 5.4 The critical current density, J_c for MB00 (as is) sample.

In Fig. 5.5, we will study the variation of the critical current density for pure and doped samples at 4K as follows

- **Annealing of the pure samples (MB00, MB26 and MB01) for 4K**

Fig. 5.5 shows the critical current density, J_c (A/cm^2) measurement versus the applied magnetic field, H(Oe) on log scale for pure samples. MB00 sample produces the highest critical current density, J_c at 4K among all studied samples. However, it decreases rapidly in annealed samples MB26 and MB01 which may be due to improving MgO content into MgB_2 phase leading weak pinning and degradation of the connectivity between MgB_2 grains.

The critical current density J_c was estimated in MB00 sample for 4K at ~ 7x10^4 A/cm^2 while its value reduces to 1.5 x10^4 A/cm^2 in MB26 and MB01 samples. This indicates that annealing has negative effects and deteriorates the critical current density. XRD analysis of the treated samples revealed a large increase in MgO, B_xO, B_2O_3 indicating dissociations of the main MgB_2 phase.

- **Excess of Mg-during preparation for 4K**

It is common practice in preparing MgB_2 to use excess of Mg to compensate for Mg evaporating and losses. It has been suggested that excess Mg reduces Mg oxidation at the grain boundaries and hence helps in obtaining almost a pure MgB_2 single phase. Excess Mg may also play an important role in improving grain connectivity.

In this section, we investigate the effects of excess Mg on the critical current density in MgB_2. Fig. 5.5 shows the critical current density, J_c measurements with the applied magnetic field, H in log scale for pure MgB_2 mixed with 10% Mg for two samples of MB27 and MB23 annealed at 750°C and 850°C, respectively. The critical current density, J_c improves more in MB27 sample comparing with the critical current density, J_c of MB26 sample. We find that Mg extra provides an increase in J_c followed by MB23. We suspect that a large amount of Mg is lost or oxidized rapidly during annealing at 850°C. It seems that using excess Mg may be more effective at 750°C and improves the grain connectivity between the MgB_2 grains.

- **Effects of CuF_2 nanoparticles inclusion for 4K**

Also Fig. 5.5 shows the critical current density, Jc measurements with the applied magnetic field, H in log scale for MgB_2 samples MB28 and MB24 (MgB_2+2%CuF_2) annealed at 750°C and 850°C, respectively. It can be observed that doping by CuF_2 did not introduce any enhancement in the critical current density, J_c. The behavior of J_c is similar to its behavior of pure samples MB26 and MB01 annealed at 750°C and 850°C respectively

- **Effects of CuF_2 and excess of Mg for 4K**

Fig. 5.5 represents the critical current density, J_c measurements with the applied magnetic field, H in log scale for (MgB_2+10%Mg+2%CuF_2) samples MB8R and MB10 annealed at 750°C and 850°C. The critical current density, J_c in MB8R seems the higher followed by the critical current density in MB10. It is clearly observed that the critical current density of MB8R is enhanced if compared to MB26 sample (MgB_2 at 750°C). The annealing temperature effect of 850°C is shown in reduction of the critical current density unlike the annealing temperature of 750°C. Therefore we can notice that $750^{O}C$ is considered as suitable annealing temperature in enhancement of J_c[61].

For 5% concentration of CuF_2, (MgB_2+10%Mg+5%CuF_2) samples, MB21 and MB22, annealed at 750°C and 850°C, respectively exhibit the same behavior of MB8R and MB10 samples. But the 5% concentration of CuF_2 affects negatively the critical current density, J_c as in MB21 and MB22 samples if they are compared with MB8R and MB10 samples respectively. This suggests that 5% of CuF_2 is a high concentration of doping in MgB_2 and leads to deterioration of the superconducting state, ultimately affecting the pinning mechanism that we will present in the following section.

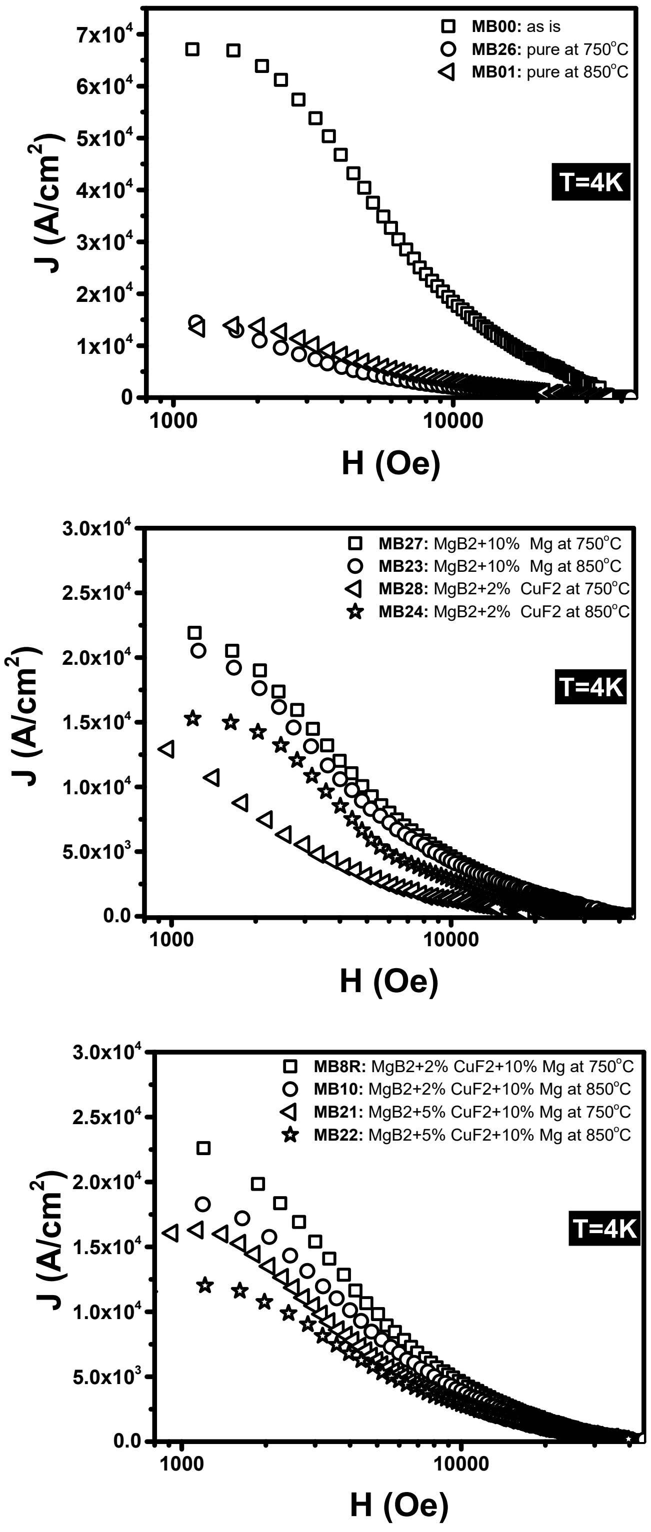

Fig. 5.5 The critical current density, J_c measurements for all pure and doped samples at 750°C and 850°C for 4K.

We present in Fig. 5.6 the variations of the critical current density, J_c against the applied magnetic field, H for MB00, MB26, MB8R, MB10 and MB21 samples for 25K. it is clearly seen that MB00 sample has the highest critical current density followed by MB8R while the other samples exhibit the lowest critical current density. However, the slope of MB8R sample is smaller than that of MB00 and this indicates a high stability of MB8R sample. We may attribute this to enhancement of the pinning centers by CuF_2 doping with extra Mg. MB26 and MB10 samples depict obviously the influence of annealing temperature on the critical current density, J_c if compared with MB00 and MB8R., respectively. Based on XRD results and resistivity measurements, the annealing temperature increases the contaminations ratio within the sample and then reducing the superconducting fraction volume and the connectivity among the grains. To investigate, the variation of the critical current density J_c with temperature at fixed applied magnetic field (3KOe), Fig. 5.7 the critical current density J_c curve of MB8R sample trends to be almost linear and smaller whereas the curve of MB00 suffers a high reduction in the low temperature range and becomes almost a straight line in the high temperature range. This is another evidence about the good effect of the doping MgB_2 by CuF_2 nanoparticles with the help of extra Mg.

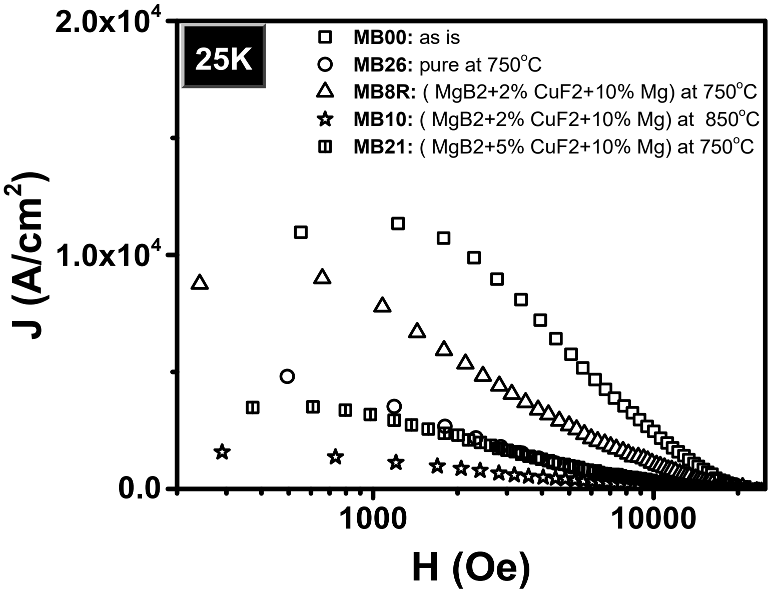

Fig. 5.6 The varaiation of the critical current density against the applied magnetic field for MB00, MB26, MB8R, MB10 and MB21 samples for 25K.

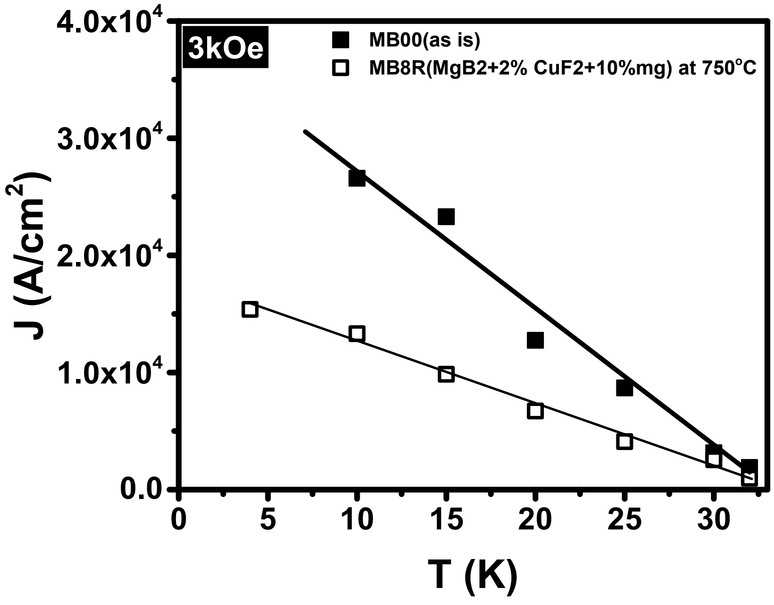

Fig. 5.7 The varaiation of the critical current density against the temperature for MB00 and MB8R at the magnetic field of 3kOe.

5.4 Kramer plots (the critical current density scaling)

Kramer plots relation $J^{0.5}$ $H^{0.25}$ versus H can be concluded from Fietz and Webb relation[62]: $f \propto h^p(1-h)^q$ (1)

and the pinning force is given by $F = Jc \times H$

$$\Rightarrow \frac{F}{F_{p,max}} = \frac{J_c}{J_{c,max}} \times \frac{H}{H^*} \text{ where } H^* \text{ is the field value at } F_{p,max}$$

$$\Rightarrow f = \frac{J_c}{J_{c,max}} \times \frac{H}{H^*} \Rightarrow f \propto Jc \times H \qquad (2)$$

by comparing (1)and (2)

$$\Rightarrow \quad Jc \times H \propto h^p(1-h)^q \qquad \text{where } h = \frac{H}{H_{irr}}$$

$$\Rightarrow (Jc \times H)^{\frac{1}{q}} \propto \left(\frac{H}{H_{irr}}\right)^{\frac{p}{q}} \left(1 - \frac{H}{H_{irr}}\right)$$

$$\Rightarrow \boxed{(Jc)^{\frac{1}{q}}(H)^{\frac{1-p}{q}} \propto (1-h)} \qquad (3)$$

The final relation shows that $(Jc)^{\frac{1}{q}}(H)^{\frac{1-p}{q}}$ is proportional to h. The p and q values of Kramer plot represent 0.5 and 2 respectivily. Then the form of Kramer relation is given as follows $(Jc)^{0.5}(H)^{0.25} \propto (1-h)$. In fact, values of p and q are related to the type of pinning mechanism based on Dew Hughes classification. For example, in MgB_2 the dominant pinning mechanism occurs by grain boundaries where p and q value equal to 0.5 and 2 respectively [63]. Fig. 5.8 and Fig. 5.9 show the $(Jc)^{0.5}(H)^{0.25}$ quantity versus

H for all samples of MgB_2 pure and doped at annealing temperatures of 750°C and 850°C for a temperature range of (4,10, 20and 30K). There are clear linear parts of Kramer plots for each sample. We can benefit from these linear lines in detemination of the type of the pinning mechanism and the irreverivle magnetic field H_{irr}^{K} by the extrapolating these linear lines to the magnetic field axis. When the linear lines are parallel, i.e, have the same slope for the whole temperature range, the pinning mechanism in the sample obeys one type of the pinning and any change in the pinning means appearance of another pinning or occurrence of deviation in the dominant pinning. In our samples, we will investigate the dominant type of pinning and its deviation and extract the irreversible filed H_{irr}^{K} .

MB00 sample in Fig. 5.8 represents the parallel linear lines for the whole range of (4,10,20, and 30) K and indicates that the dominant pinning has been done by the grain boundary. As that H_{irr}^{K} decreases with increasing temperature from 4K to 30 K. On the other hand, MB26 pure sample annealed at 750°C exhibits the parallel linear lines for 4,10, and 20K except the linear line of 30K which shows a different slope and indicates the change in the dominant pinning mechanism. As seen that $(Jc)^{0.5}(H)^{0.25}$ and H_{irr}^{K} quantities are lower after annealing temperature in comparison with MB00. This lowering can be attributed to the contamination occurring in MgB_2 phase, according to XRD results, because of the annealing effects. In addition, H_{irr}^{K} reduces with increasing temeraure from 4K to 30K.

As that MB27 sample in Fig. 5.8 shows the effect of Mg excess in enhancement of $(Jc)^{0.5}(H)^{0.25}$ and irreversible magnetic field H_{irr}^{K} under the annealing temperature of 750°C. It is clear that Mg excess improves both previous quantities, $(Jc)^{0.5}(H)^{0.25}$ and

H_{irr}^{K} , but however the pinning mechamism follows the same behaviour of MB26 sample. The linear lines are parallel for 4, 10 and 20K while the linear line of 30K does not parallel them. This indicates a change in the pinning mechanism and an appearance of another dominent pinning at high temperature namely 30K. Kramer plots of MgB_2 phase doped with 2% CuF_2 at 750°C were studied in MB28 sample. We can clearly observe that all linear lines are almost parallel (the same slope) and follow the same dominent pinning mechanism. The irreversible field H_{irr}^{K} suffers a clear reduction in comparison with the previous samples.

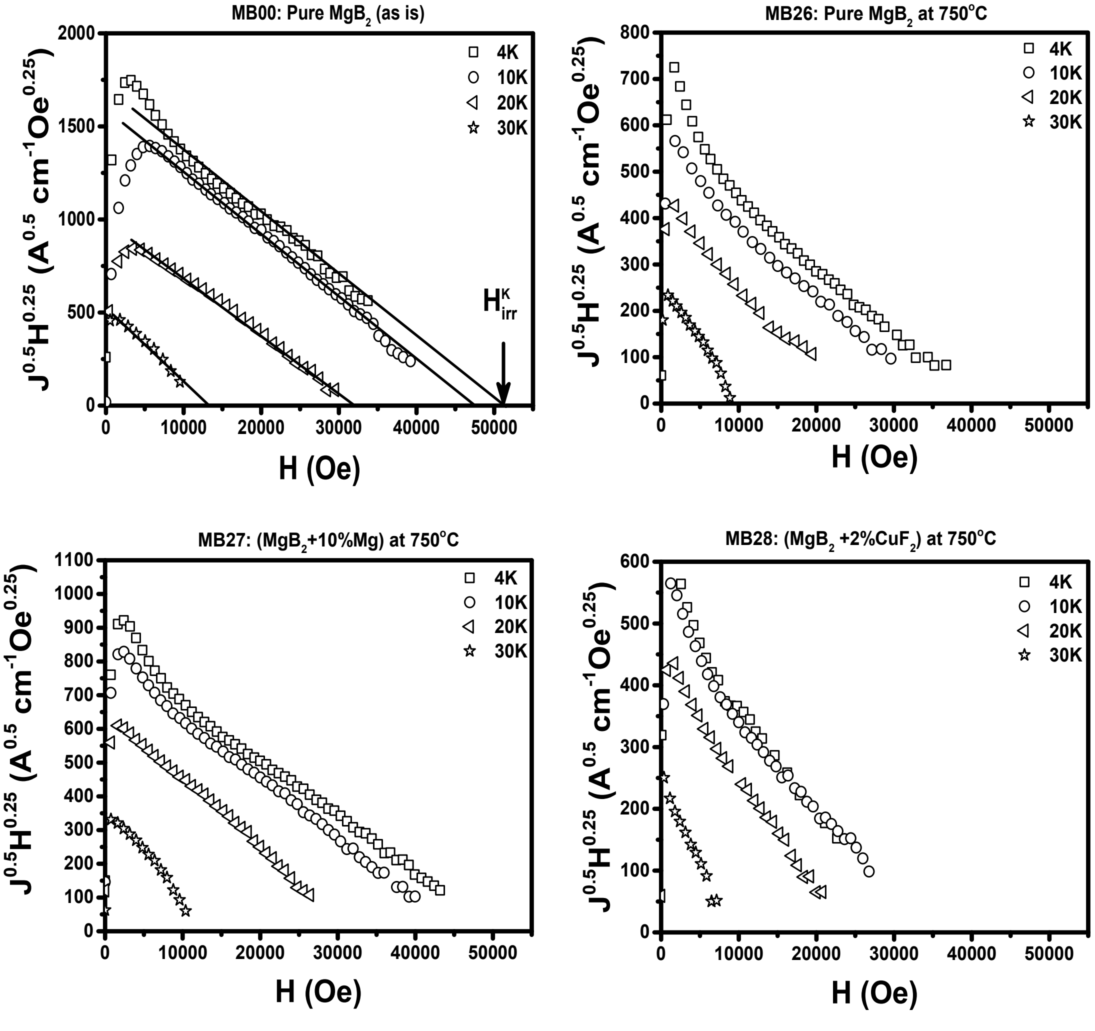

Fig. 5.8 Kramer plots of MB00, MB26, MB27 and MB28 samples for 4, 10, 20 and 30K

Fig. 5.9 shows effects of CuF_2 and excess of Mg on MgB_2. Three samples (MB8R, MB10 and MB21) were synthesized with two different concentrations of CuF_2 at annealing temperatures of 750ºC and 850ºC.

MB8R sample represents (MgB_2 +2%CuF_2+10%Mg) at 750ºC. This sample appears three linear lines belong to 4, 10 and 20K while the forth linear line at 30K is not parallel to them. This change in parallelism expresses about the change in the pinning mechanism at approaching toward the critical temperature, T_c .

As we can see that MB10 and MB21 samples exhibit (MgB_2 +5%CuF_2+10%Mg) and (MgB_2 +2%CuF_2+10%Mg) at 850ºC and 750ºC respectively. The behavior of both sample are similar with MB8R. However, the , $(\mathrm{Jc})^{0.5}(\mathrm{H})^{0.25}$ and $\mathrm{H}_{\mathrm{irr}}^{\mathrm{K}}$ are ligher values in MB8R which is ascribed to the purity of the MB8R from the contamination such MgO that can be formed on the grain boundaris of MgB_2 during its synthesis. MB8R and MB10 samples were synthesized at the same concentration of CuF_2 but different annealing temperature. The annealing temperaure of 850ºC produces a higher contamination in MB10 sample then $(\mathrm{Jc})^{0.5}(\mathrm{H})^{0.25}$ and $\mathrm{H}_{\mathrm{irr}}^{\mathrm{K}}$ quantities decreases more. This situation was repeated between MB10 and MB21. The concentration of CuF_2 (5%) in MB21 is higher than that in MB10 (2%) which in turn leads decreasing in $(\mathrm{Jc})^{0.5}(\mathrm{H})^{0.25}$ and $\mathrm{H}_{\mathrm{irr}}^{\mathrm{K}}$ quantities. We conclude from Kramer plots very important information about the nature of the dominant pinning in the superconductor and its changes assoscitaed with the annealing temperature, Mg excess and CuF_2 concentration.

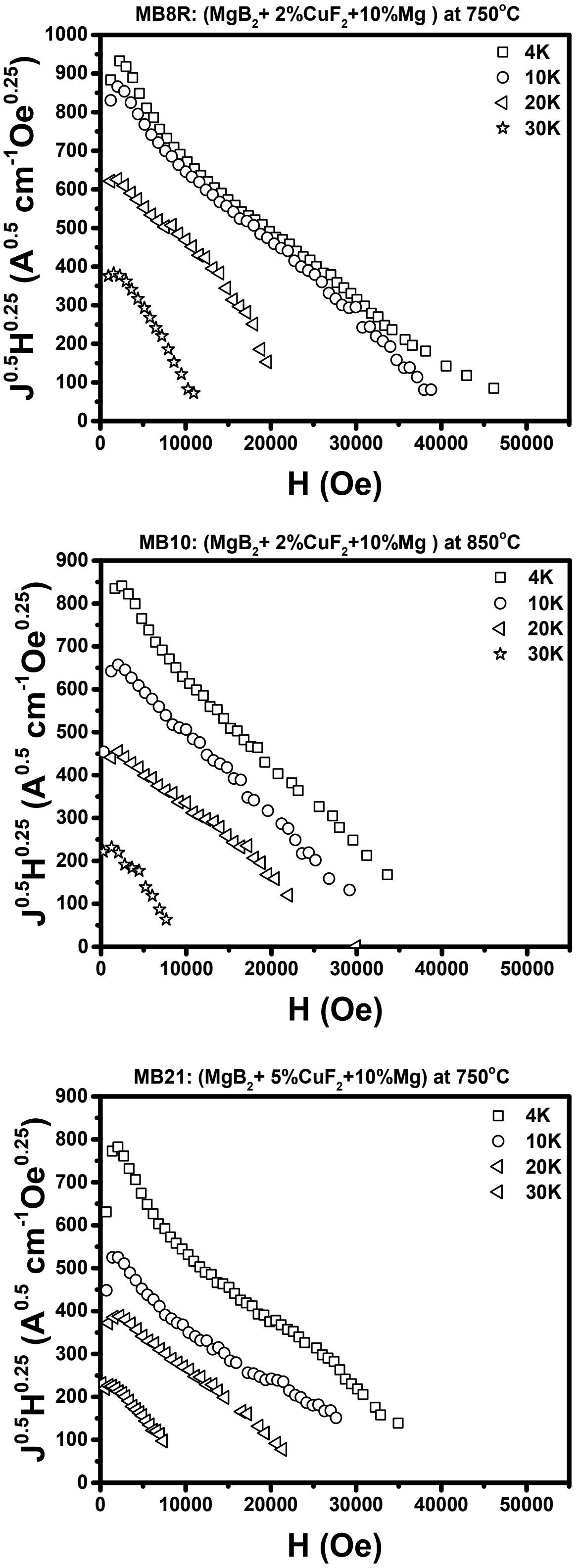

Fig. 5.9 Kramer plots of MB8R, MB10 and MB21 samples for 4, 10, 20 and 30K

CHAPTER 6

PINNING FORCE, F_P

6.1 Pinning Force, F_p Measurements

When an external magnetic field is applied to a type II superconductor at $T<T_c$, the field will be repeled from the superconductor interior as long as the applied magnetic field value does not exceed the lower critical field H_{c1}-it is called Meissner effect. When the external applied magnetic field exceeds $H_{c1,}$ its flux lines start threading through the superconductor forming normal regions surrounded by superconducting regions. The superconductor, in this case, becomes in the mixed state where the normal state and superconducting state coexist. The Lorentz force, F_L appears as result of interaction of the flux lines in the normal regions with vortices in the superconducting regions. This force drags these vortices through the superconductor giving rise to increasing thermal energy and the appearance of a resistance eventually destroying the superconducting state of the material. The superconductivity can be protected by preventing the vortices motion inside the superconductor by a reverse force called the pinning force, F_p. To stop motion of vortices, F_p must be larger than F_L. When F_p equals F_L, a current density J, can be carried by the superconductor, reaches to its maximum value. This maximum value is called the critical current density, J_c above which the te superconducting state is destroyed.

Fig. 6.1 shows the variation of the pinning force, F_p, with the applied magnetic field H for MB00 sample at various temperatures (4,10,15,20,25,30 and 32K). The pinning force, F_p was calculated by $F_p = J_c \times H$ with the help of M-H loops and the Bean's model. It is observed that Fp(AOe/cm^2) starts increasing to reach $F_{p,max}$ with increasing H(Oe) and then trends decreasing toward zero at H_{c2}.

In fact, F_p approaches to zero at a field is less than H_{c2} ,is called irreversible magnetic field, H_{irr} where the irreversible behavior disappears. At high fields and temperatures, a second peak, or a slower decrease in Fp is commonly observed. This is mainly due to thermally assisted flux flow (TAFF) [64], flux-shearing process of the flux line lattice (FLL) [65], and peak effects[66][57].

We also observed the presence of a tail at the end of some curves at high magnetic field may be ascribed to one of the causes mentioned above. For the data analysis; we extracted the magnetic field value, H* for the maximum pinning force peak ($F_{p,\ max}$) as well as the irreversible magnetic field H_{irr} from the extrapolation of the linear part of the pinning force curve to the field axis as shown in Fig. 6.1. H_{irr} indicates the field at which the pinning disappears.

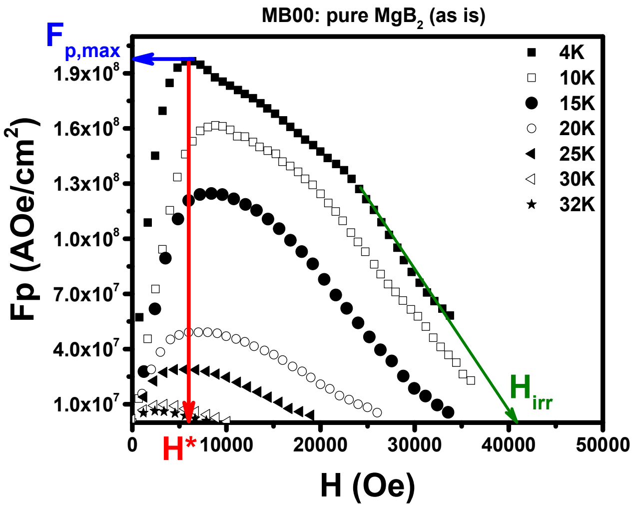

Fig. 6.1 The variation of the pinning force, F_p, with the applied magnetic field H for MB00 sample at various temperatures (4,10,15,20,25,30 and 32K).

- **Annealing of the pure samples (MB00, MB26 and MB01) for 4K:**

Error! Reference source not found. displays the variations of the pinning force, F_p vs. the applied magnetic field, H in MB00, MB26 and MB01 samples for 4K . It is observed that the pinning force, F_p of MB00 sample exhibits the highest pinning force curve and irreversible magnetic field in comparison with the annealed two samples. We can conclude that the annealing temperature plays a crucial role in degradation of the critical current density and the pinning force by producing unwanted contamination according to XRD analysis and resistivity measurements.

- **Excess of Mg-during preparation for 4K:**

Error! Reference source not found. also exhibits the F_p vs H measurements for MB27 and MB24 samples (MgB_2+10%Mg) which were annealed at 750°C and 850°C for 4K, respectively. The pinning force, F_p and irreversible field H_{irr} were enhanced by excess of 10% Mg if compared with F_p for MB26 and MB01samples (pure annealed at750°C and 850°C). We can attribute the enhancement of F_p and H_{irr} to improving the pinning centers by Mg atoms within the MgB_2 phase.

- **Effects of CuF_2 nanoparticles inclusion 4K:**

Error! Reference source not found. exhibits the F_p vs H measurements for MB28 and MB24 samples (MgB_2+2%CuF_2) for annealing temperatures of 750°C and 850°C for 4K, respectively. It is noticeable that the pinning force F_p and irreversible field H_{irr} of MB28 and MB24 seem much lower than that for pure MgB_2 samples annealed at 750°C and 850°C (MB26 and MB01). As it is observed the appearance of the second peak effect and fast degradation of Fp may be attributed to the collective motion of the vortices and deviation resulting from increasing H. Therefore, the doping by CuF_2 leads no improvement of the pinning force of MgB_2 sample.

- **Effects of CuF_2 and excess of Mg 4K**

As well **Error! Reference source not found.** represents the pinning force, F_p measured for two samples MB8R and MB10 (MgB_2+2%CuF_2+10%Mg) at annealing temperatures of 750ºC and 850ºC for 4K respectively. It is clearly observed that F_p and H_{irr} values are higher in MB8R followed by MB10. In the other samples doped with 5%CuF_2 (MgB2+5%CuF_2+10%Mg) at annealed at 750ºC and 850ºC for 4K, respectively, Fp and H_{irr} values show lower values indicating 5% CuF_2 is too much concentration in doping MgB_2. As it can be seen that the annealing temperature of 750ºC is better in enhancement of the pinning force Fp and H_{irr} . As we can see a tail at the ends of each curve in **Error! Reference source not found.** is attributed to deviations of F_p such as shearing the flux lines, collective motion pinning, or melting of the vortices lattice.

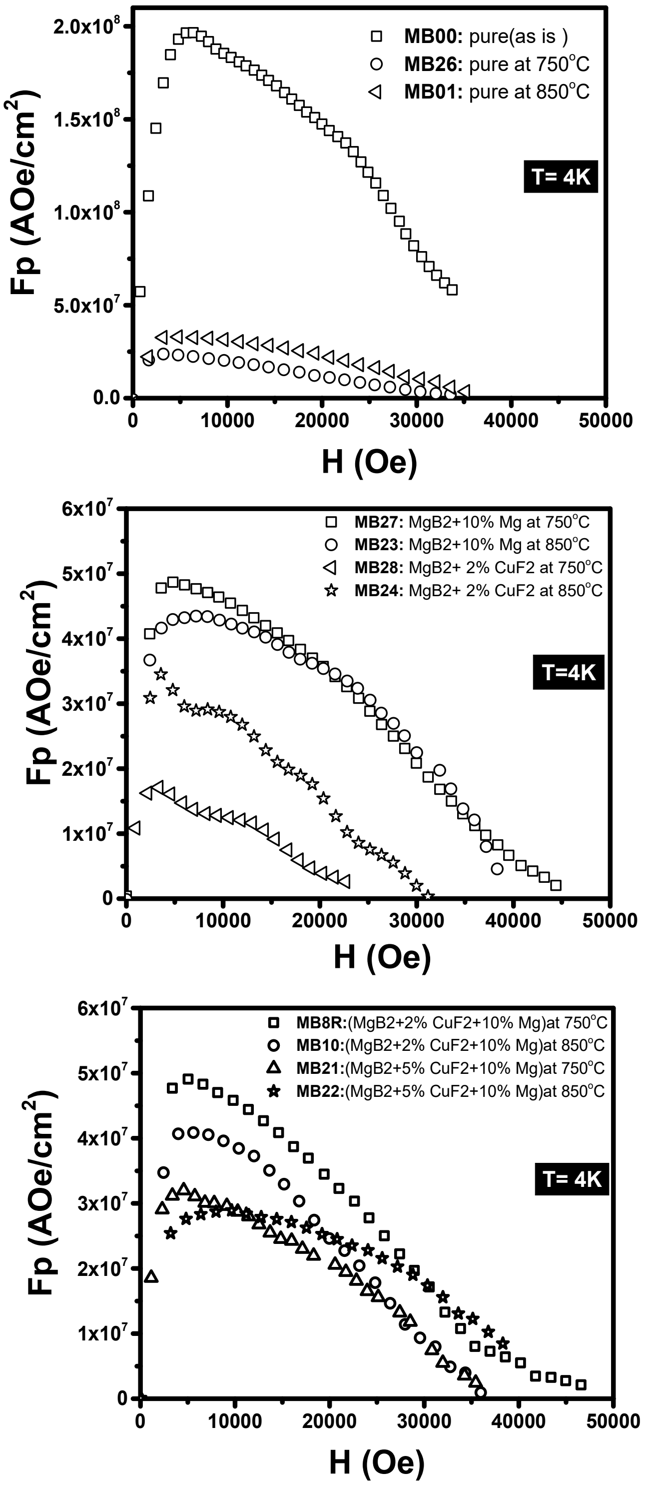

Fig. 6.2 The variations of the pinning force, F_p vs. the applied magnetic field, H in MB00, MB26 and MB01 samples for 4K.

6.2 Scaling of the pinning force, F_p

The shape similarity of the critical current density and pinning force curves at various temperature, suggests that they follow the similar behavior. This geometrical similarity suggests that they may follow a certain scaling behavior.

Several scaling procedures have been proposed since late 1960's. These are based on two scaling parameters on the geometrical similarities in the shapes of Fp vs. H curves at different temperatures. Fietz and Webb in 1969 were the first to introduced the scaling of Fp vs. H in dilute Nb-based alloys. They used two parameters $F_{p,max}$ and H_{C2}, namely, they represented the pinning force curves as $F_{p,}/F_{p,max}$ vs. H/H_{C2}, they found that all curves follow universal behavior[67],[68],[69].

The scaling behavior provides a useful relation which can be used to study the field and temperature dependence of volume pinning force F_p and critical current density J_c. It also provides useful information about the pinning mechanism. For example, the pinning force curves (with specific type of pinning) versus different temperatures and the magnetic field have similar shapes at various temperatures. This suggests using normalization procedures on these curves to obtain a universal behavior. The importance of scaling is attributed to two things; Firstly, its ability in prediction of the behavior of any property such as F_p or J_c. Secondly, extracting information about the type pinning force in the superconducting sample. Various scaling procedures have been developed for the pinning force F_p and critical current density J_c. The scaling in various superconductors has been achieved by conventional methods, i.e., by representing $(F_p/F_{p,max})$ vs (H/H_{c2}). The obtained curves followed a universal behavior of the pinning force. Conventionally the scaling by the upper critical field H_{c2} is used but not always successful for all materials. Later on Kramer found that $F_{p,max}$ is proportional to $(H_{c2})^2$ [68]

Near T_c or at high fields, it has been observed in several superconducting material that flux line lattice melting, and thermally activated flux flow and collective flux line motion lead to a difficulty in determination of H_{c2} and to large deviations from universal behavior [70]. Therefore several new scaling parameters have been introduced for example; the irreversible field H_{irr}, H* and the thermodynamic critical field Hc [71-73][2]. However, it should be mentioned that the scaling procedure does not have to depend on the geometry of curves or is achieved by two scaling parameters. In a study which has been first introduced by Ziq et al. [2] the thermodynamic critical field (H_c) was used as a single parameter to scale both the critical current density (J_c) and pinning force (F_p). As that Ziq et al.[70] introduced Hc as one parameter for scaling the pinning force Fp and critical current density Jc. They plotted $F_{p,max}$ vs H_c on a log-log scale for their samples and found the slope of the lines is 2 on this log-log plot showing that $F_{p,\ max}$ is proportional to the($H_c)^2$. By this scaling they calculated the free energy of the single line of vortex.

Thus, we can try to scale the pinning force first using log-log scale for $F_{p,max}$ vs. H_{irr}, H*(field at $F_{p,max}$) and H_p (full penetration field) which are shown in Fig. 6.3 for MB00 (as is) sample in temperature range of (4-32)K. It is expected that all procedures will generate a set of scalings or universal curves, but the physics behind that is not quite clear. In our case we find that F_p is proportional to $(Hirr)^{1.83}$, $(H^*)^{2.44}$ and $(Hp)^{2.31}$. However, the H powers may change from sample to sample so the scaling by this way is not practical, therefore we will use the conventional scaling with two parameters $F_{p,\ max}$ and H_{irr} to obtain the underlying pinning mechanism.

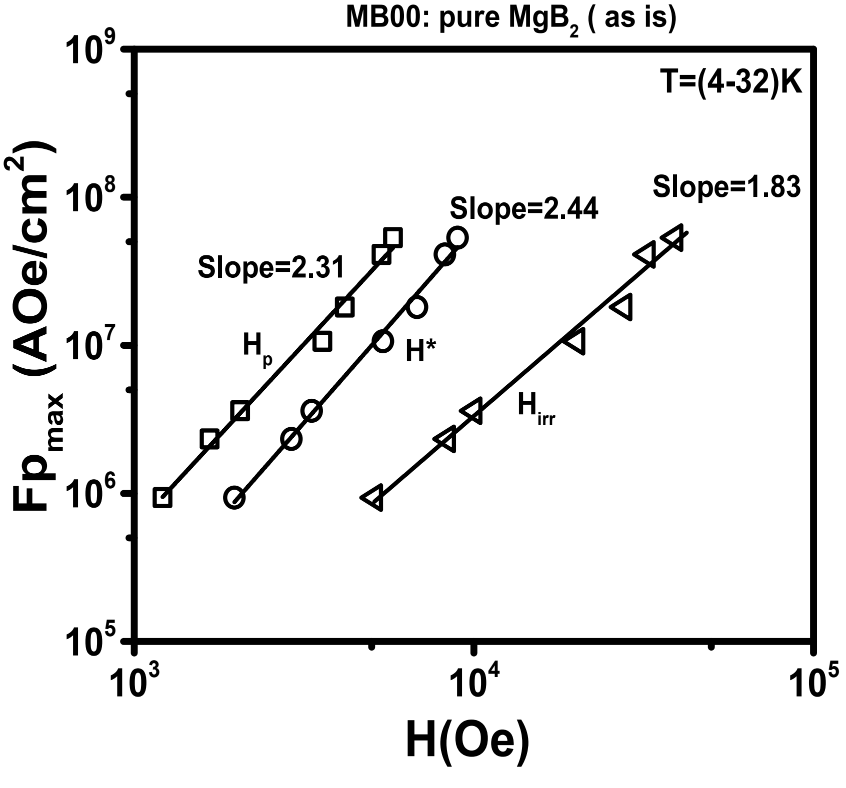

Fig. 6.3 $F_{p,max}$ **vs. H on log-log scale for** H_{irr}**, H* and** H_p **(MB00 sample).**

We use H_{irr} extracted from the linear parts of Kramer plots for the critical current density, J_c. As we denote to H_{irr} by the symbol H_{irr}^{K} to distinguish it about H_{irr} extracted from pinning force curve. We prefer H_{irr}^{K} because the linear part it is clear and large with little fluctuations then leads to more accurate irreversible magnetic field value. Fig. 6.4 shows that H_{irr}^{K} value is larger than H_{irr} value and proves that determination of irreversible field H_{irr}^{K} from Kramer plot is more accurate.

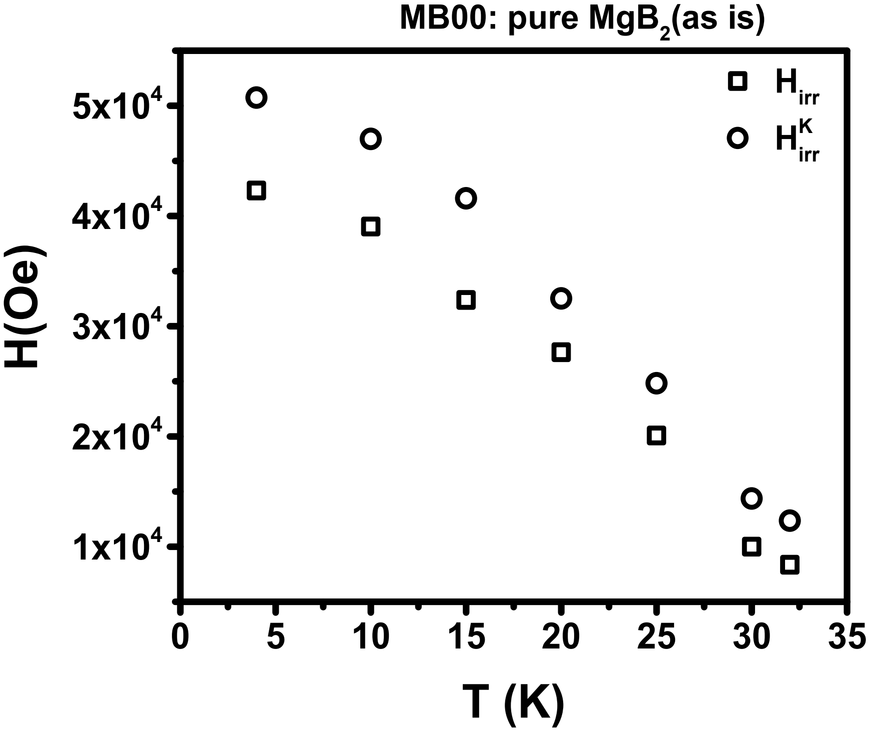

Fig. 6.4 Irreverible magnetic fields, H_{irr} and H_{irr}^{K} extracted from the direct pinning force measurement and Kramer plots respectively.

After that, we used the following Fietz and Webb relation which they introduced for scaling of pinning force F_p of niobium alloys using the following relation

$$f \propto h^p(1-h)^q$$

where ($f = F_p/F_{p,max}$) , $F_{p,max}$ is the maximum value of F_p and h being the reduced magnetic field, where ($h = H/H_{c2}$) and H_{c2} is the upper magnetic field [62]. Then Dew-Hughes suggested to categorize types of pinning mechanism based on the values of p and q [74]. The p and q values define the dominant type of pinning mechanism in the superconductor. The pinning mechanism can be (point, surface, or volume) defects and (core pinning or magnetic) interactions. Table 6.1 shows Dew-Hughes classification of the elementary types of pinning mechanism based on p and q values which can be calculated from Fietz and Webb relation [64]. However, there are other pinnings that are not classified or mentioned in Dew Hughes category such as vortex-vortex interaction, collective motion pinning, single-vortex, small bundle vortices, large bundle vortices and liquid vortices[75].

.

Table 6.1 Pinning mechanism classification based on Fietz and Webb relation[71] **by dew Hughes**

Interaction Type	Magnetic Interaction	Core Interaction					
Pinning Type	normal volume	normal			Δκ pinning		
		volume	surface	point	volume	surface	point
p	0.5	0	0.5	1	1	1.5	2
q	1	2	2	2	1	1	1

- **Annealing of the pure samples (MB00, MB26 and MB01)**

Fig. 6.5 shows three fitted groups of scaling for (MB00) sample; the first is for 4K, the second is related to (10-25) K and the third is for (30-32) K. The first group(4K) exhibits sharp peak at (h*~0.1), second group (10-25) K is localized at (h*~0.22) and the third group is shifted to (h*~0.24). These deviations of the h* mean that the pinning mechanism changes based on the changing temperature range. h* indicates the type of the pinning mechanism and is given by q/(p+q) for example, h* of 0.2 refers to the grain boundary pinning whereas 0.33 refers to the normal point pinning. The fitted scaling of the first group produces the p and q values of 0.22 and 1.45 which are not available within Dew Hughes classification but like this scaling may result from the single vortex pinning[76]. The second group shows a wider peak with (p=0.62 and q=2.17) which are closed to the grain boundary mechanism (p=0.5 and q=2). This mechanism becomes dominant and however, it is possible that there is an additional pining mechanism. The pinning mechanism of the third group (p=0.80 and q=2.51) may be mixed from grain boundary (p=0.5 and q=2) and point (p=1 and q=2).

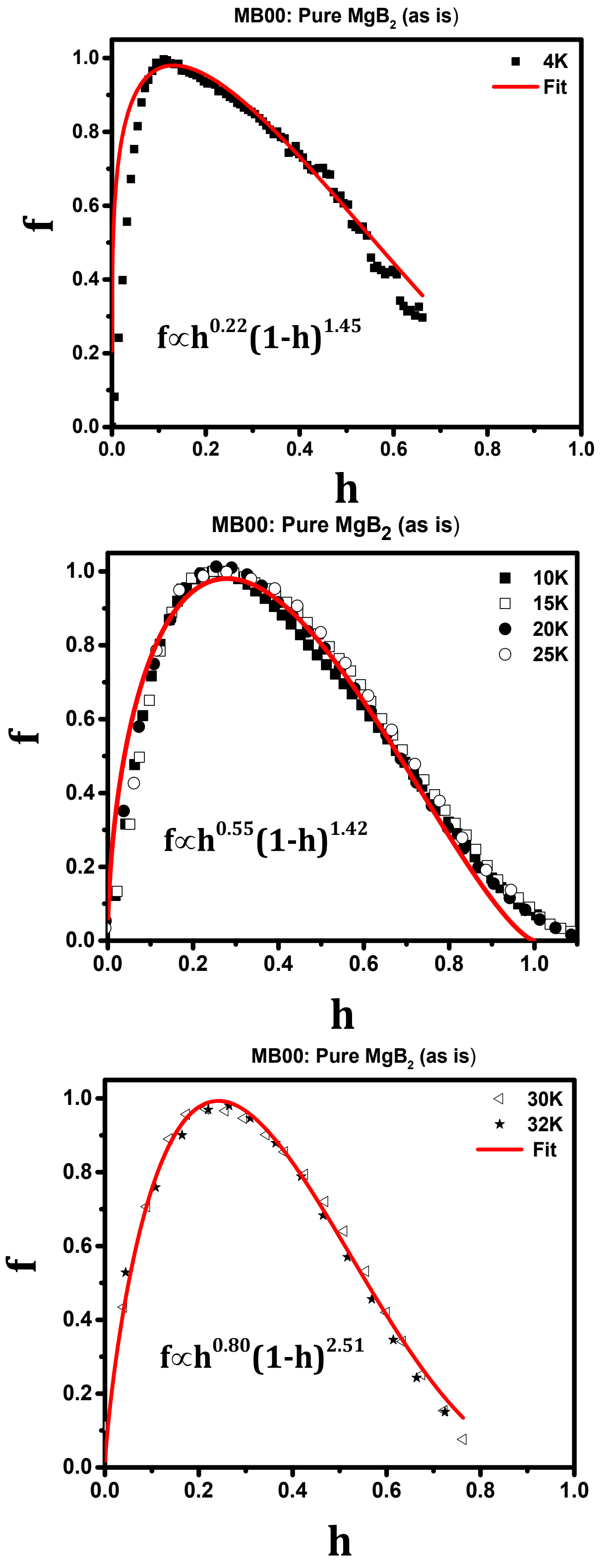

Fig. 6.5 Scaling of the pinning force, F_p and the magnetic field, H using $F_{p,max}$ and H_{irr}^{K} parameters respectively in MB00 sample for temperature ranges,4K , (10-25)K and (30-32)K.

Fig. 6.6 shows three fitted groups of scaling for the annealed pure MgB_2 sample at 750°C(MB26); (4-15) K, (20-25) K and (30-32) K respectively. In the first group(4K) exhibits a sharp single peak at (~0.1) and two peaks for (10-15) K at (0.13~0.16), the second group (10-25) K peaks are localized at (~0.18) and the third group peaks are shifted to (~0.21). Thus, values p and q for the three groups are (p=0.34, 0.46 and 0.64 and q=1.86,1.77 and 2.11) respectively. The pinning mechanism of the first group is controlled

by the single vortex pinning while the two groups, the grain boundary mechanism is dominant as shown for p and q values which are closed to p and q of the grain boundary pinning according to Dew Hughes classification. p values which are lesser than 0.5 may indicate the presence of contribution from another pinning such as normal points pinning while q values which are larger than 2 this means that pinning force suffers a weakness where there are channels for threading the flux lines through grain boundary of the sample[71]. As we think that the annealing temperature plays a cruitial role in enhancement of the grain boundary pinning mechamism.

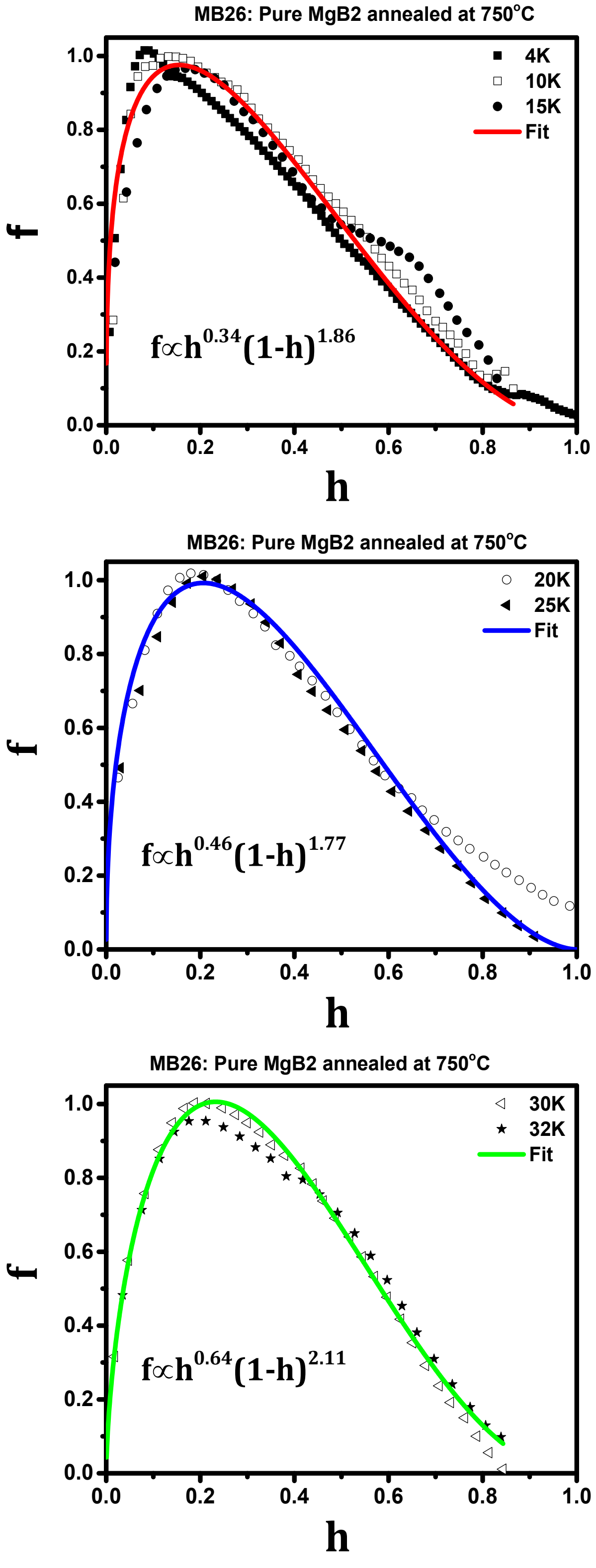

Fig. 6.6 Scaling of the pinning force, F_p and the magnetic field, H using $F_{p,max}$ and H_{irr}^{K} parameters respectively in MB26 sample for temperature ranges,(4-15)K , (20-25)K and (30-32)K.

- **Excess of Mg-during preparation**

Fig. 6.7 show three fitted groups of scaling for (MgB_2+ 10%Mg) sample annealed 750ºC (MB27) ; the first group for (4-15)K where the single vortex pinning mechanism is dominant with p=0.24 and q=1.55 whereas the second group for (20-25)K, p and q become 0.58 and 2.2 respectively which in turn indicate the dominant grain boundary pinning mechanism in this group. The third group for (30-32) K represents an additional pinning mechanism beside the grain boundary pinning mechanism according to p and q values (0.71 and 2.33). It is clearly noticeable the Mg extra enhances the point pinning mechanism if compared to pure MgB_2 sample annealed at 750ºC (MB26) in Fig. 6.6

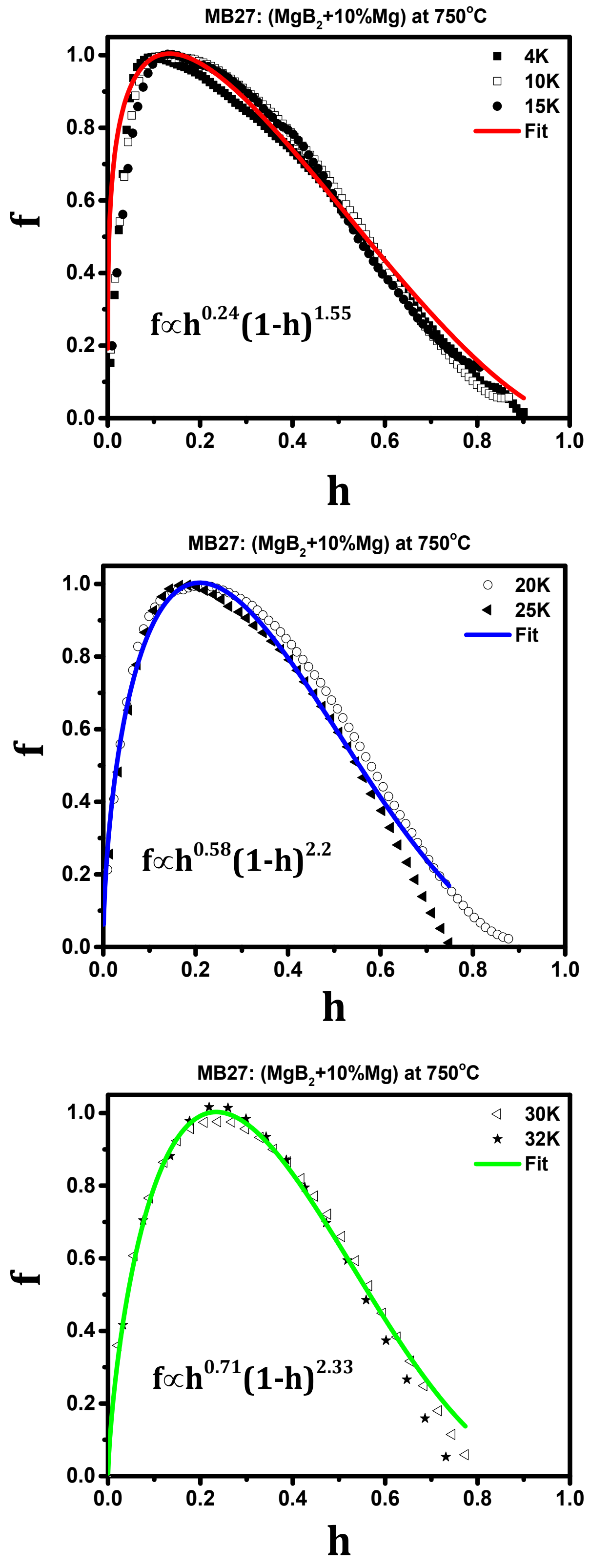

Fig. 6.7 Scaling of the pinning force, F_p and the magnetic field, H using $F_{p,max}$ and H_{irr}^{K} parameters respectively in MB27 sample for temperature ranges,(4-15)K , (20-25)K and (30-32)K.

- **Effects of CuF_2 nanoparticles inclusion**

Fig. 6.8 shows three fitted groups of scaling for (MgB_2 + 2% CuF_2) sample annealed 750^{o}C (MB28); the first group for (4-10) K and the second group for (15-25) K provide (p=0.22 and 0.39) and (q=1.50 and q=1.82) respectively to confirm the dominance of the single vortex pinning mechanism. The third group for (30-32) K represents the grain boundary pinning mechanism for p and q values (0.57 and 2.2). We think that 2% CuF_2 nanoparticles are localized between the grain boundaries, thus the effect of grain boundary pinning is reduced while the single vortex pinning is dominant in the first and second groups when we compare them with the pure sample annealed 750^{o}C (MB26).

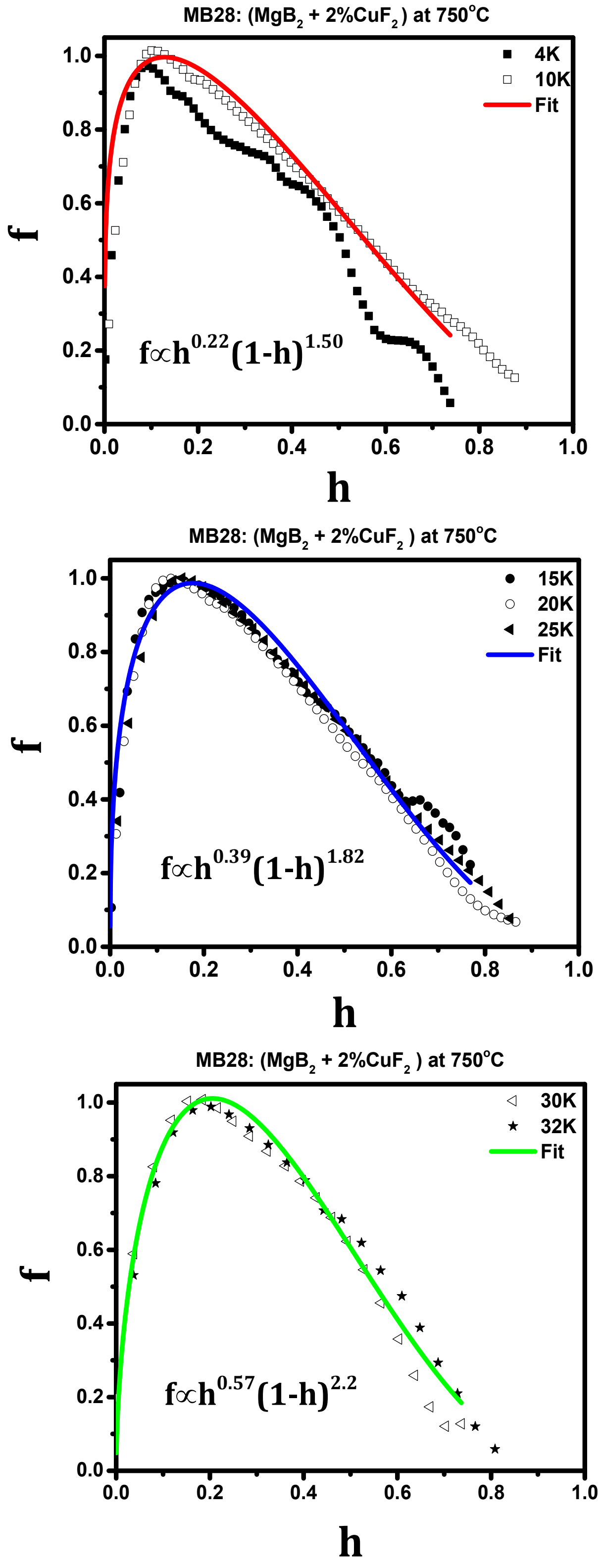

Fig. 6.8 Scaling of the pinning force, F_p and the magnetic field, H using $F_{p,max}$ and H_{irr}^{K} parameters respectively in MB28 sample for temperature ranges,(4-10)K , (15-25)K and (30-32)K.

- **Effects of CuF_2 and excess of Mg**

Fig. 6.9 epresents three groups of fitted scaling of MB8R sample (MgB_2+10%Mg+2%CuF_2 at 750^{o}C). They are distributed respectively for single vortex pinning (p=0.37 and q=1.93), grain boundary (p=0.56 and q=2.1) and point pinning (p=0.82 and q=2.2). As we can see that the peak of h* becomes wider and shifts to a larger new value of h*. This change in h* from single vortex pinning to point pinning refers to an enhancement of pinning centers into the sample.

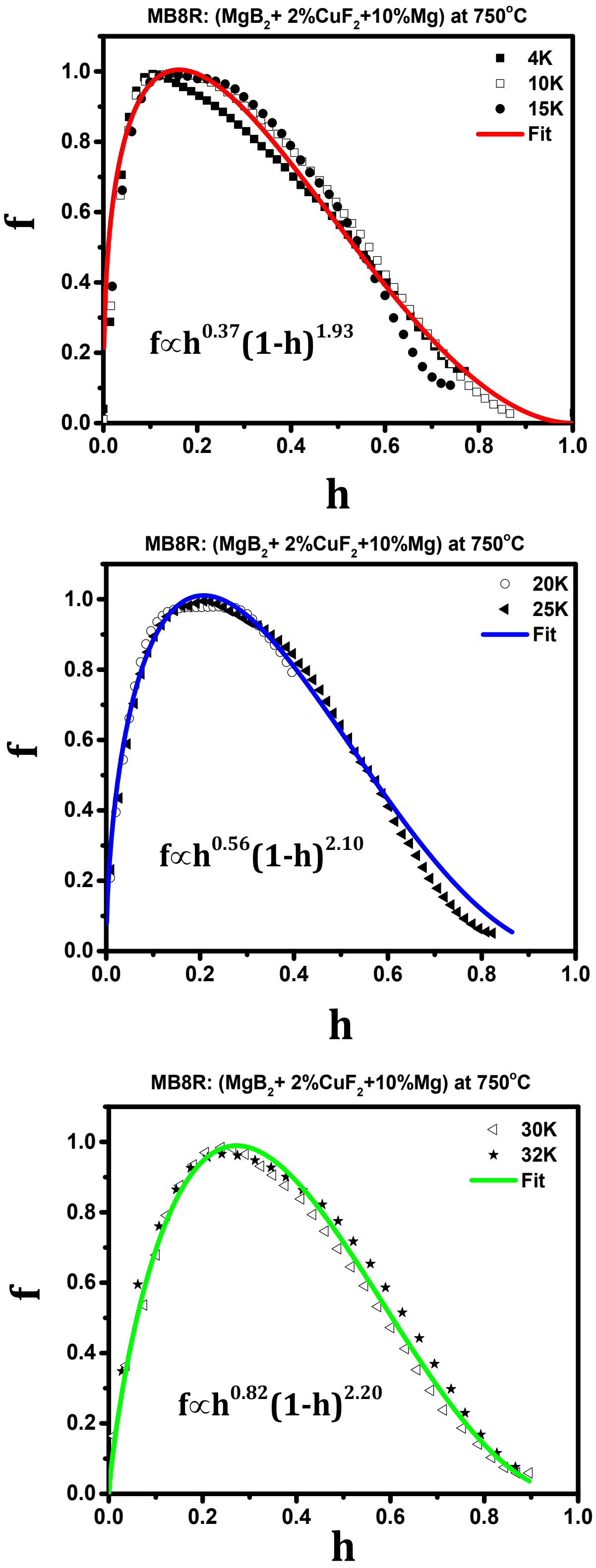

Fig. 6.9 Scaling of the pinning force, F_p and the magnetic field, H using $F_{p,max}$ and H_{irr}^{K} parameters respectively in MB8R sample for temperature ranges.(4-15)K , (20-25)K and (30-32)K.

Fig. 6.10 shows three groups of fitted scaling of MB10 sample (MgB_2+10%Mg+2%CuF_2 at 850°C). show grain boundary pinning due to (p=0.45 and q=1.8) and (p=0.56 and q=1.9) sequentially while the third group almost obeys the point pinning mechanism where p=0.81 and q=2.

We can conclude that the annealing temperature of 850°C makes a shift of the single vortex pinning to the grain boundary pinning where the grain boundaries may be highly produced at 850°C If compared with MB8R sample annealed at750°C.

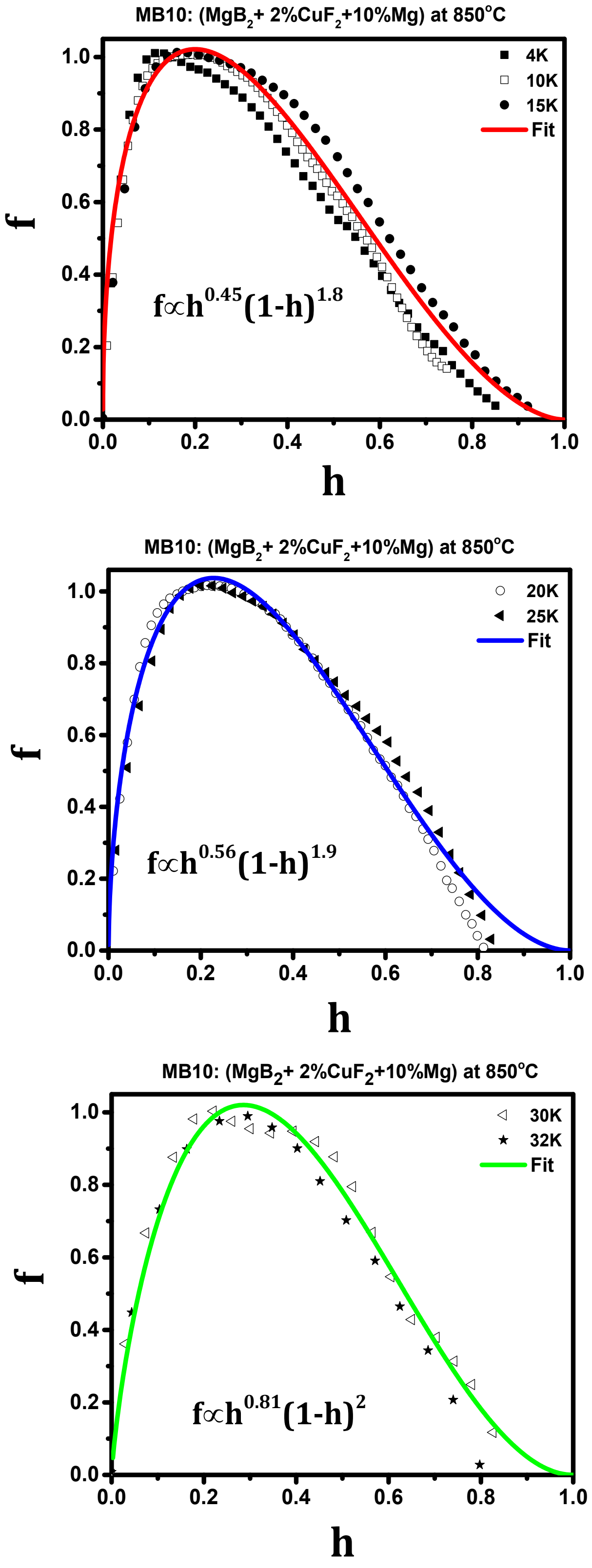

Fig. 6.10 Scaling of the pinning force, F_p and the magnetic field, H using $F_{p,max}$ and H_{irr}^{K} parameters respectively in MB10 sample for temperature ranges,(4-15)K , (20-25)K and (30-32)K.

Fig. 6.11 exhibits the fit of the scaling MB21 sample prepared from (MgB_2+10%Mg+5%CuF_2 at annealing temperature of 750°C to three groups according to p and q values define the kind of the pinning mechanism. The pinning mechanisms in the sample include the single vortex pinning, the grain boundary pinning and point pinning. Each of them appears as dominant pinning mechanism in a certain range of temperature based on p and q values. The first group of pinning mechanism for (4-15) K is for the single vortex pinning where p=0.28 and q=1.81. The second group displayed for (20-25K) range enhances the grain boundary pinning mechanism (p=0.48 and q=2.05) but the third group of (30-32K) range indicates to dominance of the point pinning mechanism (p=0.71and q=2.22). Of course, in each range, there remains contributions from other pinning mechanisms beside the dominant pinning mechanism. Therefore, this causes the deviation of p and q about Dew Hughes classification of the pinning mechanism.

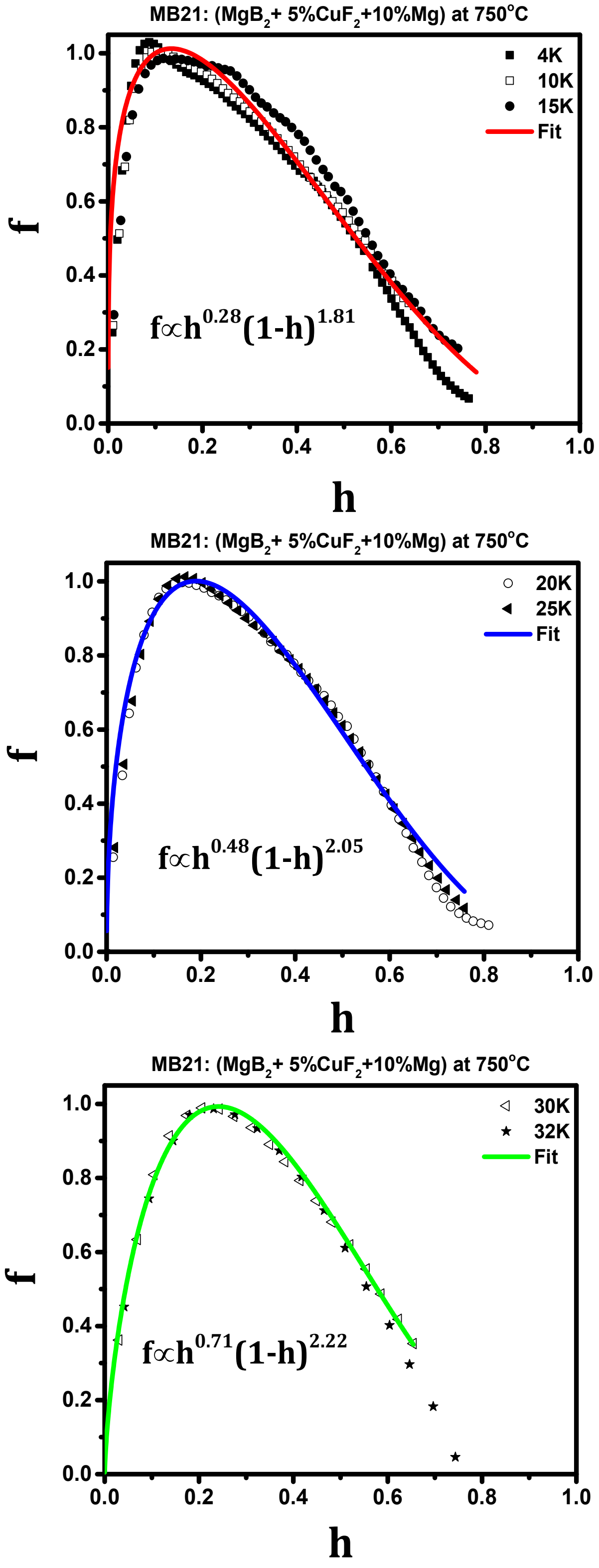

Fig. 6.11 Scaling of the pinning force, F_p and the magnetic field, H using $F_{p,max}$ and H_{irr}^{K} parameters respectively in MB8R sample for temperature ranges,(4-15)K , (20-25)K and (30-32)K.

Table 6.2 Values of p and q which were calculated from fitting $F/F_{p,max}$ vs H/H_{irr}^{K}

Sample	T (K)	p	q	Pinning type
MB00 MgB_2 (as is)	4	0.28	1.81	Single vortex
	10-25	0.48	2.05	Grain boundary
	30-32	0.71	2.22	Point + Grain boundary
MB26 MgB_2 (750ºC)	04-15	0.34	1.86	Single vortex
	20-25	0.46	1.77	Grain boundary
	30-32	0.64	2.11	Point + Grain boundary
MB27 MgB_2 +10% Mg (750ºC)	04-15	0.24	1.55	Single vortex
	20-25	0.58	2.2	Grain boundary
	30-32	0.71	2.33	Point + Grain boundary
MB28 MgB_2 + 2%CuF_2 (750ºC)	04-10	0.22	1.5	Single vortex
	15-25	0.39	1.82	Single vortex
	30-32	0.57	2.2	Grain boundary
MB8R MgB_2 +2%CuF_2 +10%Mg (750ºC)	04-15	0.37	1.93	Single vortex
	20-25	0.56	2.1	Grain boundary
	30-32	0.82	2.2	Point + Grain boundary
MB10 MgB_2 +2%CuF_2+10%Mg (850ºC)	04-15	0.45	1.8	Single vortex
	20-25	0.56	1.9	Grain boundary
	30-32	0.81	2	Point + Grain boundary
MB21 MgB_2 +5%CuF_2+10%Mg (750ºC)	04-15	0.28	1.81	Single vortex
	20-25	0.48	2.05	Grain boundary
	30-32	0.71	2.22	Point + Grain boundary

CONCLUSION

We investigated the effects of CuF_2 nano-particle inclusions on various properties of MgB_2 superconductor. CuF_2 nanoparticles inclusion on the MgB_2 grains played a dual significant role; first; reducing MgO commonly found on the grain boundaries and the second improving the grains connectivity. Both improved properties are highly important for practical applications of MgB_2. XRD results revealed significant reduction in MgO content in the MgB_2 matrix. Resistivity measurement revealed a very sharper superconducting transition and sizable reduction in the normal state resistance in all MgB_2 samples with various CuF_2 concentrations. The ac-susceptibility measurement also confirmed the improvement in the transition temperature and transition with in samples prepared under optimal conditions (2% CuF_2, annealing at 750C and 10% Mg excess).

The critical current density and the pinning force were estimated using Bean's model from the hysteresis loop. The optimal sample showed the better J_c *and* F_p among all the annealed samples. Scaling of the normalization of the pinning force, $f=F_p/ F_{p.max}$ and H_{irr}^{K} has been achieved. Curves of the pinning force collapsed to be three curves for three ranges of low temperature(4-15K), intermediate temperature(20-25K) and temperature (30-32K). The Fietz-Webb scaling procedure was used in analyzing the mechanism of pinning force. This scaling showed three pinning mechanisms; single vortex pinning, grain boundary pinning and normal point pinning in corresponding to low, intermediate and high ranges of temperature respectively.

REFERENCES

[1] v. V. Schmidt, *The Physics of Superconductors*. Moskau: Springer, 1982.

[2] Ah. F. A. A. Salem, “Effect of doping on some superconducting properties of MgB2,” Al-Azhar Uni, 2009.

[3] J. . B. K. K.H. Bennemann, *The Physics of Superconductors Vol.I. Conventional and High-Tc Superconductors*. Berlin: Physics, Chemical, 2003.

[4] W. Buckel and R. Kleiner, *Superconductivity, Fundamentals and Applications*, Second Edi. WILEY-VCH Verlag GmbH & Co. KGaA, Weinheim, 2004.

[5] “http://www.open.edu/openlearn/science-maths-technology/engineering-and-technology/engineering/superconductivity/content-section-4.3,” 2016. .

[6] A. C. Rose-Innes and E. H. Rhoderick, *Introduction to Superconductivity*, Second Edi. PERGAMON, 1994.

[7] “J. Jin, ‘High Temperature Superconductivity in the Past Twenty Years Part 2 – Towards to Practical Applications,’ vol. 6, no. 2, pp. 237–254, 2008.”

[8] A. Charnukha, *Charge Dynamics in 122 Iron-Based Superconductors*. Springer, 2014.

[9] C. Buzea and T. Yamashita, “‘Review of superconducting properties of MgB2,’” *Supercond. Sci. Technol.*, vol. 11, no. 14, pp. R115–R146, 2001.

[10] J. Nagamatsu, N. Nakagawa, T. Muranaka, Y. Zenitani, and J. Akimitsu,

“Superconductivity at 39 K in magnesium diboride.,” *Nature*, vol. 410, no. 6824, pp. 63–64, 2001.

[11] and J. K. D. Kaczorowski, A. J. Zaleski, O. J. ˙Zogal, “Incipient superconductivity in TaB2,” pp. 1–8, 2014.

[12] “D. P. Young, P. W. Adams, J. Y. Chan, and F. R. Fronczek, ‘Structure and Superconducting Properties of “BeB_2,”’ vol. 38, no. 7, pp. 1–7, 2001.”

[13] “R. R. Da Silva, J. H. S. Torres, and Y. Kopelevich, ‘Indication of superconductivity at 35 K in graphite-sulfur composites,’ Phys. Rev. Lett., vol. 87, no. 14, 2001.”

[14] “J. Nagamatsu, N. Nakagawa, T. Muranaka, Y. Zenitani, and J. Akimitsu, ‘Superconductivity at 39 K in magnesium diboride.,’ Nature, vol. 410, no. 6824, pp. 63–64, 2001.”

[15] “D. Tzeli and A. Mavridis, ‘Ab Initio Investigation of the Electronic and Geometric Structure of Magnesium Diboride ,’ pp. 10663–10674, 2005.”

[16] “M. Jones and R. Marsh, ‘The preparation and structure of magnesium boride, MgB2,’ J. Am. Chem. Soc., vol. XI, no. 1936, pp. 1434–1436, 1954.”

[17] C. Buzea and T. Yamashita, “Review of superconducting properties of,” *cond-mat*, no. 1, pp. 1–35, 2001.

[18] D. C. Larbalestier *et al.*, “Strongly linked current flow in polycrystalline forms of the superconductor MgB2.,” *Nature*, vol. 410, no. 6825, pp. 186–189, 2001.

[19] W. A. F. A. W. W. WEBB, “Magnetic Properties of Some Type-II Alloy Superconductors near the Upper Critical Field,” *Phys. Rev.*, vol. 161, no. 2, p. 11, 1967.

[20] “S. L. Bud’ko, C. Petrovic, G. Lapertot, C. E. Cunningham, P. C. Canfield, M.-H. Jung, and a. H. Lacerda, ‘Magnetoresistivity and Hc2(T) in MgB2,’ vol. 63, pp. 3–5, 2001.”

[21] “P. C. Canfield, D. K. Finnemore, S. L. Bud’ko, J. E. Ostenson, G. Lapertot, C. E. Cunningham, and C. Petrovic, ‘Superconductivity in dense MgB2 wires,’ Phys. Rev. Lett., vol. 86, no. 11, pp. 2423–2426, 2001.”

[22] “D. K. Finnemore, J. E. Ostenson, S. L. Bud’ko, G. Lapertot, and P. C. Canfield, ‘Thermodynamic and transport properties of superconducting Mg10B2,’ Phys. Rev. Lett., vol. 86, no. 11, pp. 2420–2422, 2001.”

[23] “S. L. Li, H. H. Wen, Z. W. Zhao, Y. M. Ni, Z. a. Ren, G. C. Che, H. P. Yang, Z. Y. Liu, and Z. X. Zhao, ‘Lower Critical Field at Odds with A S-Wave Superconductivity in The New Superconductor MgB2,’ vol. 64, p. 4, 2001.”

[24] “Y. Takano, H. Takeya, H. Fujii, H. Kumakura, T. Hatano, K. Togano, H. Kito, and H. Ihara, ‘Superconducting properties of MgB2 bulk materials prepared by high-pressure sintering,’ Appl. Phys. Lett., vol. 78, no. 19, pp. 2914–2916, 2001.”

[25] M. Bhatia, M. D. Sumption, E. W. Collings, and S. Dregia, “Increases in the irreversibility field and the upper critical field of bulk MgB 2 by ZrB 2 addition,” *Appl. Phys. Lett.*, vol. 87, no. 4, pp. 14–17, 2005.

[26] K. H. B. and J.B.Ketterson, *Superconductivity Conventional and Unconventional Superconductors*, vol. I. Springer, 2008.

[27] B. B. Sinha, M. B. Kadam, M. Mudgel, V. P. S. Awana, H. Kishan, and S. H. Pawar, “Synthesis and characterization of excess magnesium MgB2 superconductor under inert carbon environment,” *Phys. C Supercond. its Appl.*, vol. 470, no. 1, pp. 25–30, 2010.

[28] A. S. Shashwati Sen, D.K. Aswal, J. C. V. T.V.C. Rao, K.P. Muthe, and S. K. G. and V. C. S. and L. C. G. And, “Preparation and Characterization of MgB 2 Superconductor,” *BARC Newsl.*, no. 133, pp. 133–151.

[29] J. Ishiwata, M. Muralidhar, N. Koshizuka, K. Inoue, and M. Murakami, “Effect of sintering time on the optimal synthesis condition in MgB 2,” *Phys. Procedia*, vol. 58, pp. 102–105, 2014.

[30] a. Berenov *et al.*, “Enhancement of Critical Current Density in low level Al-doped MgB2,” *Supercond. Sci. Technol.*, vol. 17, p. 17, 2004.

[31] M. Mustapić, J. Horvat, M. S. Hossain, Ž. Skoko, and S. X. Dou, “Enhancing superconducting properties of MgB2 pellets by addition of amorphous magnetic Ni–Co–B nanoparticles,” *Supercond. Sci. Tech.*, vol. 26, p. 75013, 2013.

[32] J. H. and S. X. D. R. Zeng*, L. Lu, J L Wang, W. X. Li, D.Q. Shi, “Improvement of Jc and Hc2 in MgB2 superconductor with citric acid addition,” *J. Phys. Conf. Ser.*, vol. 97, pp. 16–20, 2008.

[33] N. Rogado *et al.*, "Low Temperature Fabrication of MgB 2," *J. Appl. Phys.*, vol. 91, no. 1, 2002.

[34] D. K. Singh, B. Tiwari, R. Jha, H. Kishan, and V. P. S. Awana, "Role of MgO impurity on the superconducting properties of MgB2," *Phys. C Supercond.*, vol. 505, pp. 104–108, 2014.

[35] M. Maeda *et al.*, "Fabrication of highly dense MgB_2 bulk at ambient pressure," *Supercond. Sci. Technol.*, vol. 21, no. 3, p. 32004, 2008.

[36] Y. Hishinuma, A. Kikuchi, Y. Iijima, Y. Yoshida, T. Takeuchi, and A. Nishimura, "Superconducting Properties of Mg 2 Cu-Doped MgB 2 Wires With Several Metal Sheath for Fusion Reactor Application," vol. 17, no. 2, pp. 2798–2801, 2007.

[37] D. G. Hinks, J. D. Jorgensen, H. Zheng, and S. Short, "Synthesis and stoichiometry of MgB 2," *Phys. C*, vol. 382, pp. 166–176, 2002.

[38] R. J. Cava, H. W. Zandbergen, and K. Inumaru, "The substitutional chemistry of MgB2," *Phys. C Supercond. its Appl.*, vol. 385, no. 1–2, pp. 8–15, 2003.

[39] "Y. Zhao, Y. Feng, C. H. Cheng, L. Zhou, Y. Wu, T. Machi, Y. Fudamoto, N. Koshizuka, and M. Murakami, 'High critical current density of MgB2 bulk superconductor doped with Ti and sintered at ambient pressure,' Appl. Phys. Lett., vol. 79, no. 8, pp. 1154–11."

[40] "M. Mudgel, V. P. S. Awana, H. Kishan, and G. L. Bhalla, 'Significant improvement of flux pinning and irreversibility field in nano-carbon-doped MgB2

superconductor,’ Solid State Commun., vol. 146, no. 7–8, pp. 330–334, 2008.”

[41] “C. Cheng and Y. Zhao, ‘Significant improvement of flux pinning and irreversibility field of nano-Ho2O3 doped MgB2,’ Phys. C Supercond. its Appl., vol. 463–465, no. SUPPL., pp. 220–224, 2007.”

[42] “H. L. Xu, Y. Feng, Y. Zhao, G. Yan, M. H. Pu, H. X. Lu, R. Zhang, and Z. Xu, ‘Investigation on MgB2 superconductor doped by nano-Al powder,’ Phys. C Supercond. its Appl., vol. 449, no. 1, pp. 53–56, 2006.”

[43] “C. H. Cheng, Y. Yang, C. Ke, and H. T. Lin, ‘Iron doping effect on superconducting properties of MgB2,’ Phys. C Supercond. its Appl., vol. 470, no. 20, pp. 1092–1095, 2010.”

[44] “I. a. Ansari, M. Shahabuddin, N. S. Alzayed, K. a. Ziq, a. F. Salem, V. P. S. Awana, and H. Kishan, ‘Enhancement of critical current density for nano (n)-ZnO doped MgB 2 superconductor,’ Phys. C Supercond. its Appl., vol. 495, pp. 208–212, 2013.”

[45] Y. Takano, *, and K. T. , Nobutaka Oguro, Yoshinari Kaieda, “Superconducting properties of combustion synthesized MgB 2,” *Phys. C*, vol. 414, pp. 125–129, 2004.

[46] A. K. K. Przybylskia , L. Stobierskia, J. Chmistb, “Synthesis and properties of MgB2 obtained by SHS method,” *Phys. C Supercond.*, vol. 387, no. 1–2, pp. 148–152.

[47] V. N. Narozhnyi *et al.*, “Comparative Study of Dense Bulk MgB2 Materials Prepared by Different Methods,” *J. Supercond.*, vol. 15, no. 6, pp. 599–601, 2002.

[48] A. Vajpayee *et al.*, “‘The effect of synthesis temperature on the superconducting properties of n-SiC added bulk MgB 2 superconductor,’” *Supercond. Sci. Technol.*, vol. 24, no. 4, p. 45013, 2011.

[49] M. Nikolo, “Superconductivity: A guide to alternating current susceptibility measurements and alternating current susceptometer design,” *Am. J. Phys.*, vol. 63. pp. 57–65, 1995.

[50] S. Yonezawa, T. Higuchi, Y. Sugimoto, C. Sow, and Y. Maeno, “Compact AC susceptometer for fast sample characterization down to 0.1 K,” *Rev. Sci. Instrum.*, vol. 86, no. 9, pp. 1–6, 2015.

[51] P. Vanderbemden, “Design of an A.C. susceptometer based on a cryocooler,” *Cryogenics (Guildf).*, vol. 38, no. 8, pp. 839–842, 1998.

[52] D. Martien, “Introduction to: ac susceptibility,” *Quantum Des.*, p. 4, 1994.

[53] “https://en.wikipedia.org/wiki/Vespel.” .

[54] C. W. Lo Oney, E. Kline, N. Hillier, N. Forouzani, and J. Song, “http://physics.wustl.edu/~jss/HeGas_2014_August.pdf,” 2014. .

[55] “http://www.sardarsinghsir.com/MSc/MSc%20-pdf%20files/Four-Probe-Method.pdf.” .

[56] S. D. B. E.W. Collings, M. D. Sumption, M. Bhatia* M. A. Susner, “Prospects for

Improving the Intrinsic and Extrinsic Properties of Magnesium Diboride Superconducting Strands," *Supercond. Sci. Technol.*, vol. 21, no. 10, p. 103001, 2008.

[57] A. V. Narlikar, *Superconductors*, First Edit. Oxford University Press, 2014.

[58] B. R. Lehndorff, *High - Tc Superconductors for Magnet and Energy Technology*, vol. 171. Springer, 2001.

[59] K. Arutyunov, "Nanoscale Superconductivity: Physics and Applications," in *Physics, Chemistry and Applications of Nanostructures*, World Scientific, 2013, pp. 191–194.

[60] R. S. T. and O. N. S. Chandra Shekhara*, Rajiv Giri and S. K. Malik, "Enhancement of flux pinning and high critical current density in graphite doped MgB 2 superconductor," *J. Appl. Phys.*, vol. 102, no. 9, pp. 1–6, 2007.

[61] H. Zhang, Y. Zhao, and Y. Zhang, "The Effects of Excess Mg Addition on the Superconductivity of MgB2," *J. Supercond. Nov. Magn.*, vol. 28, no. 9, pp. 2711–2714, 2015.

[62] W. A. Fietz and W. W. Webb, "Hysteresis in superconducting alloys temperature and field dependence of dislocation pinning in niobium alloys," *Phys. Rev.*, vol. 178, no. 2, pp. 657–667, 1969.

[63] C. H. Jiang, T. Nakane, and H. Kumakura, "Superior high-field current density in slightly Mg-deficient MgB 2 tapes," *Appl. Phys. Lett.*, vol. 87, no. 25, pp. 1–3,

2005.

[64] L. Niel, "Scaling laws for the volume pinning force in high-temperature superconductors," *Cryogenics (Guildf).*, vol. 32, no. 11, pp. 975–978, 1992.

[65] R. Wördenweber, "A modified flux-line shear model: a possible mechanism of flux-line motion in high temperature superconductors," *Cryogenics (Guildf).*, vol. 32, no. 11, pp. 1098–1103, 1992.

[66] A. K. Ghosh, Y. Hiraoka, M. Tokunaga, and T. Tamegai, "Anisotropic vortex pinning in the layered intermetallic superconductor CaAlSi," *Phys. Rev. B*, vol. 68, no. 13, p. 134503, 2003.

[67] H. Ullmaier, *"Irreversible Properties of Type II Superconductors."* Springer-Verlag Berlin Heidelberg New York 1975, 1975.

[68] "E. J. Kramer, 'Scaling Laws for Flux Pinning in Hard Superconductors.,' J. Appl. Phys., vol. 44, no. 3, pp. 1360–1370, 1973."

[69] "N. Chiao, 'of Tl-Ba-Ca-Cu-0 J. J.,' vol. 46, no. 2, pp. 1188–1192, 1992."

[70] K. Ziq, P. Canfield, J. Ostenson, and D. Finnemore, "Scaling of flux pinning with the thermodynamic critical field," *Phys. Rev. B*, vol. 60, no. 5, pp. 3603–3607, 1999.

[71] L. S. S. Md. Matin, Chandra, M. K. Chattopadhyay, R. K. Meena, and R. Kaul, "Magnetic irreversibility and pinning force density in the Ti-V alloys," *J. Appl. Phys.*, vol. 113, pp. 163903-1-163903–11, 2013.

[72] D. Tripathi and T. K. Dey, “A new scaling relation for n-AlN doped superconducting MgB2,” *J. Appl. Phys.*, vol. 114, no. 9, 2013.

[73] M. Shahabuddin, I. A. Ansari, N. S. Alzayed, K. A. Ziq, and A. F. Salem, “Effect of nano ZnO doping on the nature of pinning of MgB2 superconductors,” *J. Supercond. Nov. Magn.*, vol. 26, no. 5, pp. 1547–1552, 2013.

[74] D. Dew-Hughes, “Flux pinning mechanisms in type II superconductors,” *Philos. Mag.*, vol. 30, no. 2, pp. 293–305, 1974.

[75] J. L. Wang, R. Zeng, J. H. Kim, L. Lu, and S. X. Dou, “Effects of C substitution on the pinning mechanism of MgB2,” *Phys. Rev. B - Condens. Matter Mater. Phys.*, vol. 77, no. 17, 2008.

[76] T. Matsushita, *FluxPinning in Superconductors*, 2nd ed. Springer.

[77] “http://dc.edu.au/hsc-physics-ideas-to-implementation/.” .

VITAE

Name : Esam Gunaid Abdo Al-Nahari

Nationality : Yemeni

Date of Birth : 5/27/1975

Email : isamesc2000@gmail.com

Address : Dhahran, KFUPM

Academic Background : Superconductivity and nanomaterials

Call for Paper :

1. Kh. A. Ziq, M Abu Baker, M Faiz and E Al-Nahari “On the phase diagram of CrAs1-xSbx”, IOP Conf. Series: Journal of Physics: Conf.Series 869 (2017) 012044. (Doi :10.1088/1742-6596/869/1/012044)

2. Abdel-Latif, A. M. Ahmed, H. F. Mohamed, S. A. Saleh, J. A. Paixão, Kh A Ziq, M. Kh. Hamad, E G Al-Nahari, M. Ghoza, S. Allam “Magnetocaloric Effect, Electric and Dielectric Properties of Nd0.6Sr0.4MnxCo1-xMnxO3 Nanocomposites” Journal of Magnetism and Magnetic Materials 457,DOI. 10.1016/j.jmmm.2018.02.087